

NETWORK-WIDE TRAFFIC STATE ANALYSIS:  
ESTIMATION, CHARACTERIZATION, AND EVALUATION

By

Ramin Saedi Gerami

A DISSERTATION

Submitted to  
Michigan State University  
in partial fulfillment of the requirements  
for the degree of

Civil Engineering—Doctor of Philosophy

2020

## **ABSTRACT**

### **NETWORK-WIDE TRAFFIC STATE ANALYSIS: ESTIMATION, CHARACTERIZATION, AND EVALUATION**

By

Ramin Saedi Gerami

The Network Fundamental Diagram (NFD) represents dynamics of traffic flow at the network level. It is exploited to design various network-wide traffic control and pricing strategies to improve mobility and mitigate congestion. This study presents a framework to estimate NFD and incorporates it for three specific applications in large-scale urban networks. Primarily, a resource allocation problem is formulated to find the optimal location of fixed measurement points and optimal sampling of probe trajectories to estimate NFD accounting for limited resources for data collection, network traffic heterogeneity and asymmetry in OD demand in a real-world network. Using a calibrated simulation-based dynamic traffic assignment model of Chicago downtown network, a successful application of the proposed model and solution algorithm to estimate NFD is presented. The proposed model, then, is extended to take into account the stochasticity of day-to-day fluctuations of OD demand in NFD estimation.

Three main applications of NFD are also shown in this research: network-wide travel time reliability estimation, network-wide emission estimation, and real-time traffic state estimation for heterogeneous networks experiencing inclement weather impact. The main objective of the travel time reliability estimation application is to improve estimation of this network-wide measure of effectiveness using network partitioning. To this end, a heterogeneous large-scale network is partitioned into homogeneous regions (clusters) with well-defined NFDs using directional and non-directional partitioning approaches. To estimate the network travel time reliability, a linear relationship is estimated that relates the mean travel time with the standard deviation of travel time

per unit of distance at the network level. Partitioning and travel time reliability estimation are conducted for both morning and afternoon peak periods to demonstrate the impacts of travel demand pattern variations.

This study also proposes a network-level emission modeling framework via integrating NFD properties with an existing microscopic emission model. The NFDs and microscopic emission models are estimated using microscopic and mesoscopic traffic simulation tools at different scales for various traffic compositions. The major contribution is to consider heterogeneous vehicle types with different emission generation rates in the network-level model. Non-linear and support vector regression models are developed using simulated trajectory data of thirteen simulated scenarios. The results show a satisfactory calibration and successful validation with acceptable deviations from underlying microscopic emission model, regardless of the simulation tool that is used to calibrate the network-level emission model.

Finally, the NFD application for real-time traffic state estimation in a network experiencing inclement weather conditions is explored. To this end, the impacts of weather conditions on the NFD and travel time reliability relation are illustrated through a scenario-based analysis using traffic simulation. Then, the real-time traffic state prediction framework in the literature is adjusted to capture weather conditions as a key parameter. The extended Kalman filter algorithm is employed as an estimation engine to predict the real-time traffic state. The results highlight the importance of considering weather conditions in the traffic state prediction model.

Copyright by  
RAMIN SAEDI GERMI  
2020

*To my wife, Arezoo, for her  
endless and unconditional love, support, and encouragement*

## **ACKNOWLEDGEMENTS**

Sincere thanks go in particular to my advisor Dr. Ali Zockaie for his help and support in conducting my doctoral research at Michigan State University. I would also like to express my gratitude to my doctoral committee members: Drs. Gates, Ghamami, Savolainen, and Biswas for their time and valuable feedback. Special thanks to my lab mates who helped me a lot to conduct outstanding researches in Transportation Sustainability Lab of Michigan State University. Last but not least, my very special appreciation should go to my wife, Arezoo, for her support, patience and encouragement.

Ramin Saedi Gerami

2020

## TABLE OF CONTENTS

<b>LIST OF TABLES .....</b>	<b>x</b>
<b>LIST OF FIGURES .....</b>	<b>xi</b>
<b>KEY TO SYMBOLS .....</b>	<b>xv</b>
<b>CHAPTER 1 –Introduction .....</b>	<b>1</b>
1-1- Overview and Objectives.....	1
1-2- Knowledge Gap and Research Motivation.....	4
1-3- Research Significance and Contributions.....	6
1-4- Research Methods and Dissertation Outline .....	9
<b>CHAPTER 2 –State of the Art Review .....</b>	<b>12</b>
2-1- Overview .....	12
2-2- The Concept of Network Fundamental Diagram .....	12
2-3- Traffic State Estimation.....	14
2-4- Traffic State Prediction.....	16
2-5- Applications of Network-wide Traffic Flow Relationships .....	18
2-5-1- Network Partitioning .....	19
2-5-2- Travel Time Reliability Analysis .....	19
2-5-3- Vehicular Emission Estimation .....	20
2-5-4- Urban Traffic Control.....	22
2-5-5- Public Transportation Planning .....	24
2-6- Weather Impact on Traffic Flow .....	25
<b>CHAPTER 3 –A Resource Allocation Problem to Estimate Network Fundamental Diagram .....</b>	<b>28</b>
3-1- Overview .....	28
3-2- Model Formulation.....	30
3-3- Solution Algorithm.....	34
3-4- Numerical Results.....	38
3-4-1- Study Network.....	39
3-4-2- Optimal Locating of Fixed Measurement Points and Sampling of Probe Trajectories .....	41
3-4-3- Sensitivity to the initial solution.....	51
3-4-4- Sensitivity to the availability of trajectories.....	52
3-5- Practical Insights.....	55
3-6- Summary.....	58
<b>CHAPTER 4 –Traffic State Estimation in Heterogeneous Networks with Stochastic Demand and Supply.....</b>	<b>60</b>
4-1- Overview .....	60
4-2- Model Formulation.....	64

4-3- Solution Algorithm .....	69
4-4- Numerical Results.....	74
4-4-1- Study Network.....	76
4-4-2- Results .....	77
4-5- Summary.....	83
<b>CHAPTER 5 –Network-wide Travel Time Reliability Analysis .....</b>	<b>85</b>
5-1- Overview .....	85
5-2- Methodology.....	85
5-2-1- NFD estimation.....	86
5-2-2- Network partitioning.....	87
5-2-3- Network travel time reliability estimation.....	89
5-3- Data Description and Study Area .....	92
5-4- Partitioning the Heterogeneous Network .....	96
5-5- NFD and Travel Time Reliability Estimation .....	105
5-6- Summary.....	113
<b>CHAPTER 6 –Estimating Large-Scale Vehicular Emission .....</b>	<b>115</b>
6-1- Overview .....	115
6-2- Background and Modeling Tools .....	116
6-2-1- Traffic Flow Simulation .....	116
6-2-2- Traffic Composition .....	117
6-2-3- Micro-Emission Model.....	118
6-3- Modeling Framework .....	119
6-4- Numerical Experiment.....	123
6-4-1- Study Area and Traffic Scenarios.....	123
6-4-2- Model Calibration.....	125
6-4-3- Model Validation.....	129
6-5- Network Emission Diagram .....	131
6-6- Summary.....	135
<b>CHAPTER 7 –Real-Time Network-Wide Traffic State Prediction Considering Inclement Weather Impact .....</b>	<b>137</b>
7-1- Overview .....	137
7-2- Data Intuition.....	138
7-3- Theory.....	141
7-3-1- Network Dynamics.....	141
7-3-2- Extended Kalman Filter (EKF).....	141
7-4- Methodology.....	142
7-4-1- Nonlinear Dynamic System.....	143
7-4-2- Real-time EKF Traffic State Prediction .....	144
7-4-3- Exit Flow Function Incorporating Weather Variables .....	146
7-4-4- Optimal Limited Measurement Configurations.....	147
7-5- Numerical Results.....	148
7-6- Summary.....	157
<b>CHAPTER 8 –Concluding Remarks and Future Research .....</b>	<b>160</b>

8-1- Concluding Remarks .....	160
8-2- Future Research .....	163
<b>REFERENCES.....</b>	<b>165</b>

## LIST OF TABLES

Table 3-2- Objective function values of the initial and optimal solutions for three different initial solutions.....	52
Table 3-3- Summary statistics of the Base, 50%, 25% and 10% cases; when $a=b=0.6$ .....	54
Table 5-1- Estimation of the Reliability Coefficient for PM-Peak Directional Partitioning .....	110
Table 6-1 Parameters of the proposed macro-emission model for the pollutants considered ....	129

## LIST OF FIGURES

Figure 3-1- Illustration of the Chicago network and its downtown sub-network.....	40
Figure 3-2- Comparison of estimated NFD, initial NFD, and ground-truth NFD for different proportions of ODs $b=\{0.2, 0.4, 0.6, 0.8\}$ with a constant proportion of fixed detectors $a =\{0.2\}$ .....	41
Figure 3-3- Comparison of estimated NFD, initial NFD, and ground-truth NFD for different proportions of fixed detectors $a = \{0.2, 0.4, 0.6, 0.8\}$ with a constant proportion of ODs $b=\{0.2\}$ .....	42
Figure 3-4- Selected locations for optimal estimation of NFD for different proportions of ODs and fixed detectors.....	44
Figure 3-5- Selected ODs for optimal estimation of NFD for different proportions of ODs $b=\{0.2, 0.4, 0.6, 0.8\}$ with a constant proportion of fixed detectors $a =\{0.2\}$ and for different proportions of fixed detectors $a =\{0.2, 0.4, 0.6, 0.8\}$ with a constant proportion of ODs $b=\{0.2\}$ ; for all ODs .....	45
Figure 3-6- Convergence pattern for different proportions of ODs $a = \{0.2, 0.4, 0.6, 0.8\}$ with a constant proportion of fixed detectors $b=\{0.2\}$ .....	45
Figure 3-7- Initial and optimal objective values as a function of $a$ and $b$ .....	49
Figure 3-8- Comparison of estimated and actual NFD a) base scenario with $a=0.6, b=0.2$ , b) decreased-demand scenario with $a=0.6, b=0.2$ , c) increased-demand scenario with $a=0.6, b=0.2$ , d) base scenario with $a=0.6, b=0.6$ , e) decreased-demand scenario with $a=0.6, b=0.6$ , f) increased-demand scenario with $a=0.6, b=0.6$ .....	50
Figure 3-9- (a) Initial and (b) optimally estimated NFDs for three different initial solutions.....	52
Figure 3-10- Optimal estimation of NFD for the base case (all trajectories available), 50% case (50% of trajectories available), 25% case (25% of trajectories available) and 10% case (10% of trajectories available); when $a=0.6$ and $b=0.6$ . .....	55
Figure 3-11- Normalized frequency of OD pair distances for $a=b=0.6$ , (b) Frequency percentage of link types for $a=b=0.6$ , (c) Evolution of the spatial center of the links in the initial and optimal solutions compared to the spatial center.....	58
Figure 4-1- Estimated NFDs of the AM-peak period for Chicago downtown network on two days with different observed operational conditions .....	61

Figure 4-2- The proposed solution framework based on the SA algorithm .....	71
Figure 4-3- Chicago network and its CBD area considered for the NFD estimation .....	76
Figure 4-4- Estimated NFDs for two randomly selected scenarios A and B using three methods: simulation (ground-truth), the stochastic solution, and the deterministic solution based on scenario A .....	78
Figure 4-5- Convergence pattern for different budget scenarios .....	79
Figure 4-6- Location of the links selected to be equipped with loop detectors for different budget configurations .....	80
Figure 4-7- Comparison of stochastic objective values with cumulative deterministic objective values for different traffic scenarios (sorted) and different budget configurations .....	82
Figure 4-8- Ratio of the maximum, average, and minimum objective function values for the deterministic approach relative to the stochastic method .....	83
Figure 5-1- Extracted observations from vehicle trajectories for (a) Trajectory and (b) Sub- trajectory approaches to estimate travel time reliability measure .....	92
Figure 5-2- (a) Schematic sketch of the Chicago metropolitan network, the study network including 9,915 links, and Chicago CBD; (b) Chicago metropolitan network 24-hour loading profile.....	93
Figure 5-3- (a) NFD, (b) Reliability graph estimated by the trajectory approach, and (c) Reliability graph estimated by the sub-trajectory approach for the study network over the 24-hour simulation horizon .....	94
Figure 5-4- Density temporal and spatial distributions for the PM peak period .....	97
Figure 5-5- Partitioning results: (a) Two clusters for AM peak and non-directional approach, (b) Speed and density descriptor of partitioning quality during the AM peak, (c) Average density for the AM peak, and (d) Average space-mean-speed for the AM peak .....	101
Figure 5-6- Partitioning results: (a) Three clusters for PM peak using directional approach, (b) Speed and density descriptor of partitioning quality during the PM peak, (c) Average density for the PM peak, and (d) Average space-mean-speed for the PM peak .....	102
Figure 5-7- Partitioning results: (a) 3 clusters for the Entire day using non-directional approach, (b) Speed and density descriptor of partitioning quality during the entire day, (c) Average density for the entire day, and (d) Average space-mean-speed for the entire day .....	104

Figure 5-8- Minimum (lower graph) and average (upper graph) values of TVN over various time intervals (AM peak, PM peak, and entire day) for different partitioning approaches with 2 and 3 clusters [in each X-Y-Z scenario in horizontal axis, X represents AM or PM peak period or the entire day (ED), Y represents directional (D) or non-directional (ND) partitioning, and Z represents the number of clusters (2C or 3C)].....	105
Figure 5-9- NFDs over the PM peak period for the directional partitioning approach for (a) study network; (b) cluster 1 with 19.1 veh/mile average density; (c) cluster 2 with 84.3 veh/mile average density; (d) cluster 3 with 151.5 veh/mile average density; and associated travel time reliability diagrams for trajectory (upper diagrams) and sub-trajectory (lower diagrams) approaches in (e) study network; (f) cluster 1; (g) cluster 2; and (h) cluster 3 .....	109
Figure 5-10- Correlation of the coefficient of reliability relation with different congestion measures and the number of clusters during (a) AM Peak Period, and (b) PM peak period .....	112
Figure 5-11- Correlation between the area of hysteresis loops in (a) NFD and (b) Reliability of travel time graph (values are presented in logarithmic scale) .....	113
Figure 6-1 Research framework to estimate a macro-emission model.....	121
Figure 6-2 (a) Specifications of the study area, (b) simulated demand profiles, and (c) network fundamental diagrams of the Chicago city road network and its CBD (diagrams are for the base calibration scenario C5).....	126
Figure 6-3 Variation of traffic flow characteristics across the different traffic scenarios: (a) Maximum Average Flow, (b) Maximum Average Density, and (c) Area of Hysteresis Loop in NFD Diagram .....	127
Figure 6-4 Scaling effect of vehicle type percentages on macro emission model in the loading phase of NFD – CBD Network, micro-simulation: (a) emission vs density for CO <sub>2</sub> (b) emission vs speed for CO <sub>2</sub> (c) emission vs density for NO <sub>x</sub> (d) emission vs speed for NO <sub>x</sub> for 10 traffic composition scenarios in the calibration scenario C1 .....	128
Figure 6-5 Mean absolute relative error in macroscopic emission estimation using the (a) NLR model for CBD, (b) NLR model for city network, (c) SVR model for CBD, and (d) SVR model for city network .....	131
Figure 6-6 The NED of CO <sub>2</sub> for the city network for traffic composition set TC25 in the base validation scenario V2 for the macro-emission models NLR and SVR, along with the base micro-emission model .....	134

Figure 6-7 (a) network fundamental diagram, (b) emission rates, and (c) cumulative emissions for two scenarios of C01 and C10 for the city network.....	134
Figure 7-1 Relationship between the precipitation rate and (a) network maximum density, (b) network maximum throughput, (c) area of hysteresis loop in NFD, and (d) coefficient of reliability relation. The vertical axes values are scaled from zero to one, where one stands for the maximum observed value over all weather scenarios.....	140
Figure 7-2 Real-time network-wide traffic state estimation with limited observations and incorporating inclement weather impacts.....	144
Figure 7-3 (a) Chicago city network, (b) Chicago CBD network, (c) morning demand profiles, (d) Chicago city network NFD, and (e) Chicago CBD network NFD .....	149
Figure 7-4 Real-time network-wide traffic state prediction results for a randomly selected scenario (a) network accumulation, (b) exogenous demand, and (c) network throughput .	152
Figure 7-5 MAPE for (a) network accumulation, (b) exogeneous demand, and (c) network throughput considering all scenarios (86 days) and prediction time intervals per scenario (84) for different resource availability levels of the network accumulation observations ..	153
Figure 7-6 Comparing the predicted accumulation values using the optimal set of links for correcting measurements versus a random set of links, in a particular scenario (out of 86 days) with different levels of resource availability for data collection (percentages of the network links equipped with sensors): (a) 5%, (b) 10%, (c) 15%, and (d) 20%.....	154
Figure 7-7 MAPE values of the predicted network accumulation over all scenarios (86 days) using the optimal set of links for correcting measurements versus a random set of links, with different levels of resource availability for data collection .....	155
Figure 7-8 Estimated exit flow function (network throughput) using SVM approach including versus excluding weather variables (a) for a clear day scenario and (b) for a snowy day scenario .....	156
Figure 7-9 Average MAPE values over all scenarios (86 days including various weather conditions) including and excluding weather variables in the exit function: (a) network accumulation, (b) exogenous demand, and (c) network throughput .....	157

## KEY TO SYMBOLS

$T$	Number of time intervals over the horizon for NFD estimation
$t$	Time interval index
$\zeta$	Weight factor in objective function for minimizing deviation of estimated average flow from the ground-truth average network flow
$\eta$	Weight factor in objective function for minimizing deviation of estimated average density from the ground-truth average network density
$Q_t$	Ground-truth average network flow at time interval $t$
$\hat{Q}_t$	Estimated average network flow by fixed detectors at time interval $t$
$K_t$	Ground-truth average network density at time interval $t$
$\hat{K}_t$	Estimated average network density at time interval $t$
$I$	Number of links in the network
$i$	Link number index
$q_i^t$	Flow at link $i$ at time interval $t$
$l_i$	Lane-length of link $i$
$s_i^t$	Space-mean speed at link $i$ at time interval $t$
$x_i$	Binary variable associated with fixed detection at link $i$
$J$	Number of origin-destination pairs in the network
$j$	Origin-destination pair index
$K(j)$	Number of trajectories available for origin-destination pair $j$
$k$	Trajectory index for origin-destination pairs
$p_{ijk}^t$	Binary parameter specifying if $k^{th}$ trajectory of origin-destination pair $j$ includes link $i$ at time interval $t$

$\tilde{t}_{ijk}^t$	Experienced travel time at link $i$ and time interval $t$ by $k^{th}$ trajectory of origin-destination pair $j$
$\hat{t}_i^t$	Experienced average travel time at link $i$ and time interval $t$ by available trajectory of selected origin-destination pairs
$\hat{s}_i^t$	Estimated space-mean speed from mobile probe trajectories at link $i$ at time interval $t$
$z_i^t$	Binary variable specifying if there is any trajectory from selected origin-destination pairs that includes link $i$ at time interval $t$
$M$	A large number
$w_i^t$	Binary variable specifying if estimated speed is available through at least one trajectory from selected origin-destination pairs including link $i$ at time interval $t$ , and estimated flow is available through the detector at link $i$
$y_j$	Binary variable associated with the probe trajectory data for origin-destination pair $j$
$c_i$	Data collection or acquisition cost if there is a fixed detector at link $i$
$f_j$	Data collection or acquisition cost for probe trajectory data of origin-destination pair $j$
$B$	Total available budget for data collection or acquisition

## CHAPTER 1 – Introduction

### 1-1- Overview and Objectives

Improving the mobility and reliability of transportation systems is the main objective of traffic state analysis. This analysis can be conducted at segment- (street), node- (intersection), facility- (traffic corridors), traffic zone-, and network-level. Traffic state estimation is the first step to identify the characteristics of a traffic stream such as stability and travel time variability. Speed, density and flow are the three main characteristics describing the state of the traffic flow. Incorporating these three elements establishes the concept of fundamental diagram (FD) of a traffic stream. This reproducible diagram illustrates the different stages of a traffic condition at facility level. It is broadly used to describe the macroscopic behavior of a traffic link segment. Exploiting FD facilitates characterization and analysis of concepts such as the shockwave theory, speed oscillation phenomenon, and oversaturated flow regime in a traffic stream.

Aggregating link FDs at the network level by averaging the traffic flow elements over all links of a network gives rise to a new concept, which is referred to as Network Fundamental Diagram (NFD) or Macroscopic Fundamental Diagram (MFD). This concept initially introduced by Godfrey in 1969, elaborated by Mahmassani et al. in 1984, and revisited by Geroliminis and Daganzo in 2008 under the MFD terminology. NFD incorporates the main traffic flow characteristics at the network level and is a representative of the network-wide traffic state. It can be used to design and implement specific control and pricing strategies to improve mobility at the network level (Geroliminis et al., 2012; Haddad and Geroliminis, 2012; Ramezani et al., 2015; Yildirimoglu et al., 2015a). NFD is well-defined and has low scatter, when congestion distribution in the network is homogenous (Gayah and Daganzo, 2011; Geroliminis and Sun, 2011; Mahmassani et al., 2013; Zockaie et al., 2014b). Analytical methods to estimate NFD based on

variational theory are developed previously by Daganzo and Geroliminis (2008), and later refined by Geroliminis and Boyacı (2012) and Leclercq and Geroliminis (2013). These methods are limited to urban corridors in stationary conditions and cannot be applied to large-scale heterogeneous networks. Estimating NFD in real-world networks, when data collection budget is limited and network traffic is heterogeneous and initiated from an asymmetric and time-varying origin-destination (OD) demand matrix, is a challenging task that is addressed in this study.

Characterization of NFD facilitates the estimation of different performance indexes of transportation networks. Network travel time reliability, which can be represented by a relationship between network space-mean travel time and the standard deviation of network travel time per unit of distance (Herman and Lam, 1974; Mahmassani et al., 2012a) is one of the main network performance measures. In a large-scale network, estimating the travel time reliability is always associated with some inaccuracies, due to the heterogeneity that is imposed to the network by congestion distribution.

Characterizing NFD and its connection with variability of travel time can be utilized to develop more efficient routing strategies (Briganti et al., 2014) and urban planning activities (Cirianni et al., 2013). Considering the application of heterogeneous network partitioning in traffic control strategies (see for example (Haddad and Mirkin, 2017; Kouvelas et al., 2017)), this study intends to explore impacts of the network clustering on travel time reliability measures. The main objective is to improve estimation of the network travel time reliability with network partitioning.

NFD can also be utilized to assess the environmental impacts of transportation systems. The environmental impacts of vehicular traffic in urban transportation networks have been extensively studied. It is widely accepted that pollutants emitted from on-road vehicles constitute a majority of air pollution in urban environments (Cen et al., 2016), and have deleterious

consequences on human health and climate change (Grote et al., 2016; Jiang et al., 2015). In 2012, poor quality of air, due to vehicular emissions, was estimated to cause about 3.7 million premature deaths worldwide (Kumar Pathak et al., 2016). This number is expected to rise considerably in the next few decades. A systematic manner of investigation and policy making would therefore require fast and accurate estimates of emission at the aggregate level. Since accurate measurements in real networks are cumbersome, empirical estimation and modeling of vehicular emissions has become an important research topic in the disciplines of urban planning and transportation management.

The existing body of work on estimation of vehicular exhaust emissions can be broadly categorized into three types of techniques – macroscopic, microscopic, and mesoscopic modeling. For large networks, macroscopic models are usually preferred over microscopic and mesoscopic models because of their simplicity, though they often do not take into account the dynamics of traffic flow that can significantly affect emissions. This study is an attempt to constructively bridge this gap by employing NFD. While existing research advocates the use of NFD in improving transportation management of an urban network, there is no sufficient literature on its potential in estimating air pollution over the network, or the influence of the aforementioned properties of NFD on it.

Finally, the application of network-wide traffic flow relationships in the real-time traffic state estimation within a network that experiences inclement weather conditions is illustrated. The evaluation of in-field deployment and experimental analyses indicate that macroscopic traffic flow relationships are affected by changes in network supplies, such as climate change, signal coordination, number of accidents, and changes in the specifications of roadways and intersections. This study first aims to explore the impacts of weather conditions on network-wide fundamental diagram and travel time reliability relation through a scenario-based analysis using traffic

simulation. Then, it imbeds weather condition factors in a real-time traffic state prediction framework. The extended Kalman filter algorithm is employed as an estimation engine of this traffic state prediction framework. Note that this framework provides real-time prediction of traffic state which is different from the earlier application of NFD for traffic state estimation.

## **1-2- Knowledge Gap and Research Motivation**

Despite the growing number of studies on the NFD estimation problem, there is still a need to further develop methods to properly estimate NFD, when network loading is not homogenous, data from fixed detectors and mobile probes are combined, and data collection resources are constrained. Data from fixed detectors are not always available uniformly throughout an urban network. Similarly, availability of trajectory data from mobile probes is usually geographically limited and yet expensive to acquire. Therefore, this study formulates a resource allocation problem as a mathematical model to estimate NFD, using a combined sample of vehicle trajectories and fixed detector data in a large-scale real-world network accounting for traffic heterogeneity and asymmetry in OD demand. Furthermore, this study extends this concept to take into account the stochasticity of day-to-day fluctuation of the OD demand and network supply.

In addition to addressing the existing limitations in the NFD estimation studies, three significant applications of NFD are also presented in this research: network-wide travel time reliability estimation, network-wide emission estimation, and real-time traffic state estimation for heterogeneous networks experiencing inclement weather conditions. Estimation of NFD for homogeneous subnetworks of a partitioned large-scale heterogeneous network facilitates the reliability of travel time estimation. Heterogeneity due to congestion should be taken into account to reflect the errors of aggregating the mean and standard deviation of travel time across the network. In order to mitigate the scatter in NFD shape and improve the reliability of travel time

estimation, this study investigates how clustering of a heterogeneous network may result into presenting a more robust travel time relationship for different subnetworks.

Network-wide emission estimation is the second application of NFD discussed in this study. Estimation of vehicular emissions is a prominent issue in transportation planning and management of urban areas, especially large cities that struggle with traffic congestion. Modeling is an effective means of estimating emissions, broadly categorized as macroscopic and microscopic. For large networks, macroscopic models are usually preferred over microscopic models because of their simplicity, though they often do not take into account the dynamics of traffic flow that can significantly affect emissions. In this study, a modeling framework is proposed for the estimation of emissions at the network level based on the macroscopic traffic flow characteristics of the network commonly summarized in the form of NFD. This is achieved by integrating the macroscopic properties of a set of NFDs with an existing microscopic emission model through traffic micro-simulation for different traffic compositions.

Lastly, the real-time traffic state prediction in the large-scale networks experiencing inclement weather conditions is another gap in the literature, which is aimed to be addressed in this research. The growing emergence of traffic congestions has imposed many direct and indirect expenses on roadway users. Therefore, an efficient traffic management and control system is an indispensable need for large-scale networks. Traffic state estimation is an important part of the real-time closed-loop traffic control framework. Although several methodologies have been developed regarding network-wide traffic state estimation, there is still the need in the literature to focus on the strategies that are applicable to networks experiencing inclement weather conditions. To this end, this research studies the problem of real-time traffic state estimation for networks with varying weather conditions.

Overall, the existing limitations in deterministic and stochastic approaches of NFD estimation, besides the necessity for three main applications of it are the knowledge gaps that this research aims to fill.

### **1-3- Research Significance and Contributions**

The core objective of this study is to provide mathematical frameworks to estimate and predict the traffic state for heterogeneously congested large-scale networks that experience fluctuating demand and supply. Several novel techniques are presented based on the network-wide traffic flow relationships to address some of the existing gaps in the literature of the mobility studies in large-scale networks. The main contributions of this study are as follows:

#### *NFD estimation subject to a limited budget*

- This study presents a mathematical model and solution algorithm to find the optimal location of fixed measurement points and sampling of probe trajectories in a resource allocation problem framework to estimate NFD in a large-scale heterogeneous network with asymmetric demand.
- The objective is to minimize the discrepancy between the estimated NFD and ground-truth NFD subject to a limited budget for data collection given that the availability of fixed detectors and probe trajectories are not always uniformly distributed across a network.
- The main contribution of the proposed method is that it does not require any priory known penetration rate for probe trajectories.

#### *Traffic state estimation in heterogeneous networks with stochastic demand and supply*

- The proposed framework for NFD estimation is modified to capture the stochasticity due to day-to-day changes in the network demand and supply.
- The robustness of the model including different scenarios with various demand levels, weather conditions, and other influential factors in the NFD estimation problem is the main advantage of this approach.

#### *Improving travel time reliability estimation with network partitioning*

- This study explores the impacts of partitioning a heterogeneous network on the estimated travel time reliability measure.
- This study also demonstrates an application of partitioning on an actual large-scale network, exploring the impacts of different congestion patterns in the morning and afternoon peak periods and comparing two partitioning approaches (directional vs. non-directional), and two methodologies for the network travel time reliability estimation.
- Moreover, different clustering approaches employing density and space-mean speed of the network elements are utilized to propose the best clustering strategy.

#### *Incorporating NFD into large-scale emission estimation*

- A general framework to produce a network-wide emission estimation model that can be easily and reliably used by urban transportation planners and agencies is proposed. The presented framework is flexible with respect to modeling parameters, such as the choice of the base micro-emission model and traffic simulation tool, which can be determined at the system planners' discretion. This framework can be applied in the real-time traffic management and urban planning to control network emission level using incentivizing policies for alternative fuel vehicles or congestion management.

- This study addresses some key issues associated with current macro-emission estimation techniques: (a) It demonstrates the effectiveness of the mesoscopic traffic simulation in estimating emissions at a large scale with significantly low resource consumption compared to microscopic models. (b) It offers a way to include different vehicle classes without the loss of generality for generating NFD by considering their fuel type. (c) It allows for the inclusion of an array of road network elements in simulation and emission estimation, including freeways, arterial roads, signalized intersections, and interchanges.
- The relationship between NFD and macro-emission is also discussed in the form of a three-dimensional diagram, hereby called the network emission diagram (NED). This presents a qualitative interpretation of the network emission production process at different stages of the network loading cycle.

*Network-wide Real-time Traffic State Estimation Considering Inclement Weather Impact*

- Exploring impacts of weather conditions on network-wide traffic flow relationships (network fundamental diagram and network-wide travel time reliability)
- Imbedding weather condition measures in predicting real-time traffic state for an urban network by modeling the network exit flow as a function of not only the network accumulation but also the weather variables such as visibility (in mile), snow precipitation rate (in inch/hour) and rain precipitation rate (in inch/hour).
- Utilizing Support Vector Machine (SVM) algorithm to model the network exit flow considering the weather condition factors.
- Solving a resource allocation problem for collecting the network accumulation data by equipping only an optimal subset of network links by loop detectors (instead of assuming

that the entire accumulation data is available). This decreases the data collection cost significantly and improves the algorithm performance with a limited budget.

#### **1-4- Research Methods and Dissertation Outline**

This dissertation includes eight chapters. The first two chapters provide the description of the concept and objectives of the study, as well as a comprehensive background review on the dissertation topic. Chapter 3 presents a resource allocation problem to find the optimal location of fixed measurement points and optimal sampling of probe trajectories to estimate NFD accounting for limited resources for data collection, network traffic heterogeneity and asymmetry in OD demand in a real-world network.

In order to estimate the NFD for a heterogeneous large-scale network, data from fixed detectors are used to estimate flows and data from probe trajectories passing through the links with fixed detectors are used to estimate space-mean speed. The problem is formulated as a mixed integer program with non-linear constraints, which is known to be NP-hard including possible local optimal solutions. Therefore, an SA algorithm is used to solve the proposed model using a dynamic network model of Chicago. The proposed methodology incorporates the ground-truth NFD as an input to find a subset of links and trajectories to estimate NFD for traffic state monitoring. As the ground-truth NFD may not always be available, a surrogate needs to be obtained analytically or using simulation. Assuming that this surrogate provides the ground-truth NFD, the proposed methodology finds the optimal configuration of links and trajectories for data collection and to estimate the NFD given a limited budget.

Chapter 4 extends the concept and formulation of the NFD estimation presented in Chapter 3 to capture the stochasticity due to the day-to-day fluctuations in the traffic demand and network supply. Stochastic variations due to weather conditions, incidents, special events, work zones, and

service interruptions may significantly affect the approximation of an estimated NFD. This chapter aims to propose a modified and robust framework to estimate network traffic states and observe NFD, while capturing the stochasticity in transportation networks.

Chapter 5 discusses an application of NFD in assessing one of the transportation networks performance measures – network-wide reliability of travel time. Network travel time reliability can be represented by a relationship between network space-mean and standard deviation of travel time. The primary objective of this chapter is to improve estimation of the network travel time reliability with network partitioning. A heterogeneous large-scale network is partitioned into homogeneous regions (clusters) with well-defined NFDs using directional and non-directional partitioning approaches. To estimate the network travel time reliability, a linear relationship is estimated that relates the mean travel time with the standard deviation of travel time per unit of distance at the network level. The impacts of different partitioning approaches, as well as the number of clusters, on the network travel time reliability relationships are also explored in Chapter 5. To estimate individual vehicle travel times, two distinct approaches are utilized to allocate vehicle trajectories to different time intervals, namely trajectory and sub-trajectory methods. The proposed framework is applied to a large-scale network of Chicago using a 24-hour dynamic traffic simulation. Partitioning and travel time reliability estimation are conducted for both morning and afternoon peak periods to demonstrate the impacts of travel demand pattern variations.

Chapter 6 proposes a network-level emission modeling framework based on the network-wide fundamental diagram, via integrating NFD properties with an existing microscopic emission model. The NFDs and microscopic emission models are estimated using microscopic and mesoscopic traffic simulation tools at different scales for various traffic compositions. The major contribution is to consider heterogeneous vehicle types with different emission generation rates in

the network-level model. This framework is applied on a large-scale network of Chicago as well as its CBD area. Non-linear and support vector regression models are developed using simulated trajectory data of 13 simulated scenarios. The proposed model is also used to demonstrate the relationship between macroscopic emission and flow characteristics in the form of a network emission diagram.

Chapter 7 studies the problem of real-time traffic state prediction for large-scale urban networks experiencing inclement weather conditions. Note that this study extends the earlier discussions on traffic state estimation towards the traffic state prediction to be used proactively in developing control strategies, rather than traffic estimation that can be used passively. First, it explores the impacts of weather conditions on the network-wide fundamental diagram and travel time reliability relations through a scenario-based analysis. Then, a mathematical framework based on the supervised learning algorithms is presented to estimate the real time traffic state for a large-scale network capturing impacts of the inclement weather conditions.

Chapter 8 provides a summary of the finding of this study besides the potential future research directions.

## **CHAPTER 2 – State of the Art Review**

### **2-1- Overview**

A comprehensive review of the previous studies on network-wide traffic flow relationships is presented in this chapter. The concept and characterizations of the network wide fundamental diagram (NFD) besides the influencing factors are discussed first. It is followed by a review of different methodologies and tools presented for the network-wide traffic state estimation. Then, some applications of network-wide traffic flow relationships in addressing some of the major traffic related issues are presented.

### **2-2- The Concept of Network Fundamental Diagram**

Simulation-based and empirical studies in the literature confirm the existence of a consistent and well-defined network-wide relationship between flow and density known as Network Fundamental Diagram (NFD), also known as Macroscopic Fundamental Diagram (MFD) (Godfrey, 1969; Mahmassani et al., 1984; Williams et al., 1985; Mahmassani et al., 1987; Geroliminis and Daganzo, 2008; Buisson and Ladier, 2009). NFD is an important indicator of the network-wide traffic state and is used to compare the performance, stability, travel time reliability and congestion characteristics of urban networks (Castrillon and Laval, 2017; Daganzo and Geroliminis, 2008; Geroliminis and Daganzo, 2008; Mahmassani et al., 2013a; Mahmassani et al., 2013b; Saedi et al., 2018a). The indicators and properties of NFD are naturally important for studying and analyzing transportation management strategies. Ji et al. (2010) investigated the factors that influence the shape of an NFD and concluded the influence of factors such as weather conditions, demand variation, proportion of heavy trucks, and proportion of ‘well-informed’ users.

The heterogeneous spatiotemporal distribution of congestion across real networks often creates scatter and hysteresis in the NFD (Gayah and Daganzo, 2011; Geroliminis and Sun, 2011; Knoop and Hoogendoorn, 2013; Zockaie et al., 2014a). Network performance has been shown to be affected by spatial variability of congestion throughout the network (Knoop et al., 2015; Mazlounian et al., 2010). Moreover, at a certain level of congestion, heterogeneous networks undergo a bifurcation, which causes multivaluedness in the NFD (Daganzo et al., 2011).

Studies in the literature have mostly used microscopic simulation models (e.g. Mühlich et al., 2015), empirical data (e.g. Geroliminis and Sun, 2011; Saberi et al., 2014a; Saberi et al., 2014b), and simulation-based dynamic traffic assignment tools (e.g. Mahmassani et al., 2013) to study the factors affecting the shape and scatter in the NFD. Few studies have also explored the network travel time reliability in connection with NFD to further capture network dynamics and day-to-day variations in network traffic (Kim and Mahmassani, 2015; Mahmassani et al., 2012a). More specifically, Gayah et al. (2014) proposed an analytical model representing the day-to-day variability of travel time in a network. Boyacı and Geroliminis (2010) characterized the NFD for a network with variable link lengths and signal specifications, including variations caused by turning movements and heterogeneous drivers.

NFD, generally, is not a new concept, but the relevant research on this topic is quite recent. Estimation of NFD in real transportation networks and the application of network-wide traffic flow relationships, which have been broadly studied during the last decade, are the main subjects to be discussed in the next sections.

### 2-3- Traffic State Estimation

Three main approaches for the traffic state estimation have been proposed in the literature: analytical methods (e.g. Daganzo and Geroliminis, 2008; Ramezani et al., 2015), empirical experiments (e.g. Geroliminis and Daganzo, 2008; Saberi and Mahmassani, 2012), and simulation-based approaches (e.g. Keyvan-Ekbatani et al., 2012; Saedi et al., 2018a; Zheng et al., 2012). Analytical methods to estimate NFD based on variational theory developed previously by Daganzo and Geroliminis (2008) and later refined by Geroliminis and Boyacı (2012) and Leclercq and Geroliminis (2013) are limited to urban corridors in stationary conditions and cannot be applied to large-scale heterogeneous networks. A recent study by Leclercq et al., (2014) evaluated existing estimation methods for NFD focusing only on homogenous network loading. They suggested that using the complete population of vehicle trajectories to estimate NFD is the only estimation method with no bias agreeing with recent findings of Saberi et al., (2014b). However, availability of the entire population of trajectories is still limited in urban networks and will continue to be limited even when connected vehicles are deployed in near future.

Gayah and Dixit (2013) proposed a method to estimate average network density using probe vehicles combined with NFD. Leclercq et al. (2014) suggested that combining information from probe vehicles and traffic loop detectors can also provide fairly accurate estimation of NFD in stationary conditions even for sample rates as low as 10%. Other studies by Ortigosa et al. (2014) and Nagle and Gayah (2014) estimate NFD using combined mobile probes and traffic loop detector data. Ortigosa et al. (2014) studied the optimal number and location of measurement points by minimizing the error in estimated average network density. However, they overlooked the potential of using probe trajectory data in the NFD estimation problem. Nagle and Gayah (2014) proposed a method to estimate the average network density and flow using data from

mobile probes, given a constant and known penetration rate of probes across the network. In a later study, Du et al. (2015) extended the method to varying penetration rates with heterogeneous demand in an idealized square grid network. A limitation of this method is that the penetration rate of probe vehicles must be known a priori. More recently, Ambühl and Menendez (2016) proposed a fusion algorithm that decomposes the network into two sub-networks and uses both loop detector data and floating car data to estimate NFD.

The findings of these studies are mostly limited to stationary conditions and homogeneous networks with the availability of all vehicle trajectories. Heterogeneity due to the spatiotemporal distribution of congestion across the network results in inconsistency and scattered NFDs across different days. Day-to-day demand and supply variation is one of the major sources of stochasticity in transportation networks that affect the traffic state and travel time reliability (Gayah et al., 2014a). Moreover, the complete population of trajectories may not be available in real-world urban networks due to various technological or privacy-related reasons. These factors necessitate considering stochasticity in NFD estimation. The number of studies considering the stochasticity in FD/NFD estimation is limited. At the facility level, Qu et al. (2017) proposed an optimization model using the theorem of total probability to obtain stochastic fundamental diagrams for freeway segments, which can be used to develop and assess various traffic control strategies. At the network level, Laval and Castrillón (2015) approximated the NFD of inhomogeneous corridors and networks using a probabilistic method. They considered stochastic corridors consisting of different segment length and signal coordination. Both studies concluded that stochasticity is an important factor in the estimation of facility and network level fundamental diagrams.

There are growing number of studies on the traffic state estimation problem both on deterministic and stochastic approaches, however, there still exists some significant limitations

due to simplifying assumptions in these studies. This dissertation aims to address some of these limitations.

## **2-4- Traffic State Prediction**

Traffic state prediction is the core section of a real-time closed-loop traffic management system. Prediction of traffic state denotes identifying the traffic flow variables required by a system controller as state feedback at the next time interval. For this purpose, it is assumed that some real-time measurements are available from the plant (system). Due to the restrictions in number of the data collecting sensors, data dropouts and other communication problems, the complete real-time traffic state variables are not easy to predict. However, for a large-scale urban network, a complete picture of the network should be represented by some traffic state variables. This makes the prediction frameworks design more complicated. In addition to the complexity in identifying accurate approximation of the unknown traffic state variables, it should be noted that the available measurements are associated with some noises. Minimizing deviations between the predicted state values from the ground-truth observations is the essential contribution of developing prediction frameworks.

A recent study (Ampountolas and Kouvelas, 2015) presented an algorithm with the main objective of maximizing the network throughput. For this purpose, the critical accumulation of the network is predicted and utilized as a set-point in feedback controllers. In a similar study, Saeedmanesh et al. (2019) presented a framework established on the concept of Extended Kalman Filter (EKF) algorithm to predict the traffic state in real-time. Kalman filter is an optimal state estimator utilized in linear dynamic systems that incorporates random (Gaussian) noise and contains a limited amount of noisy real-time measurements. The EKF algorithm, which is applicable for nonlinear systems, will be discussed in detail in Chapter 7. The application of this

framework is shown for a large-scale urban network partitioned in multiple clusters in Saeedmanesh et al. (2019). It is assumed that the sensor measurements (to correct the predicted states) are available from the entire network. This assumption, however, is not always authentic in large scale networks. It requires a massive resource availability to collect the measurements on every segments of a road network.

In addition to EKF, the Bayesian approach is also utilized in dynamic state prediction (Herring et al., 2010; Hofleitner et al., 2012). In this method the state probability density function at every time interval is created based on the historical data (previous state values up to the end of the current time interval). The Bayesian approach consists of two stages: prediction and correction (based on available measurements) similar to the EKF approach. In the prediction stage, the state probability distribution is predicted based on the transition probabilities. Then, utilizing the Bayes theorem, the available measurements are incorporated to update the state probability distribution. Recursive implementation of Bayesian filter establishes another method called Particle Filter, which is also a powerful prediction engine (Arulampalam et al., 2002). Monte Carlo simulation is exploited to apply the recursive Bayesian filter in this algorithm. Particle Filter has extensive application in prediction problems for complex nonlinear systems. Particle filtering utilizes a set of particles to represent the posterior distribution of a stochastic process, where only limited noisy state measurements are available.

One of the main capabilities of the methods such as EKF and PF is that these algorithms can provide an accurate prediction of the states that no real-time measurements available for them. If an explicit (or even implicit) relationship with other state variables can be established, these algorithms can provide a prediction for the target variable (with no measurements available) with acceptable accuracy. Besides the prediction engines, simulation-based models are also developed

for real-time traffic state predictions. DYNASMART-X is a simulation-based real-time traffic state estimation and prediction tool that works based on dynamic traffic assignment (DTA) (Fei et al., 2009). Application of DYNASMART-X facilitates the conjunction of prediction and estimation procedures with real-time surveillance data to design multiple traffic management strategies and scenarios. Utilizing DYNASMART-X enables the traffic control centers to respond to unfolding situations, such as bottlenecks and incidents, by providing the real-time traffic information to road users. The time-consuming nature of the DTA methodology makes the prediction process very slow in comparison to the prediction engines. This is the main drawback of the simulation tools in the real-time traffic state prediction problem.

## **2-5- Applications of Network-wide Traffic Flow Relationships**

The concept of NFD has been extensively used in network-wide transportation and traffic flow analyses since 2008. Its applications have been identified in network congestion control, urban planning, real-time traffic estimation and prediction, emission estimation, etc. Employing an NFD stipulates the implementation of a new generation of traffic control schemes that enhance the mobility of transportation networks (Haddad and Mirkin, 2016; Mariotte et al., 2017; Ramezani et al., 2015; Yang et al., 2017; Yildirimoglu et al., 2015a; Zhong et al., 2017). Characterizing NFDs can also be used to model the uncertainty in urban network dynamics (Gao and Gayah, 2017), formulate the dynamic user equilibrium (Laval et al., 2017) and evaluate the environmental impacts of vehicular traffic in urban areas (Saedi et al., 2020). NFD is also an important factor in determining the long-term stability of networks (Geroliminis and Sun, 2011). This section discusses major applications of NFD.

### *2-5-1- Network Partitioning*

Congestion naturally induces heterogeneity in a transportation network. Geroliminis and Ji (2011) and Saeedmanesh and Geroliminis (2016) explored the properties of NFD in a heterogeneous network and suggested approaches to partition the network in regions to increase the homogeneity level in the spatial distribution of congestion and reduce scatter in the estimated NFD for each region. Partitioning a heterogeneous network into homogeneous clusters based on the spatial and temporal distribution of link densities is expected to improve estimation of well-defined NFDs. Along this line, Briganti et al. (2014) partitioned a heterogeneous transportation network based on the spatial distribution of urban activities and consequently estimated NFDs for partitioned sub-networks. Similarly, Huang and Gao (2014) reviewed existing heterogeneous network partitioning algorithms and evaluated different methodological approaches. The applications of partitioning of heterogeneous networks are also studied in developing traffic control strategies (Haddad and Mirkin, 2017; Kouvelas et al., 2017), travel time prediction (Lopez et al., 2017a), and speed estimation (Lopez et al., 2017b).

### *2-5-2- Travel Time Reliability Analysis*

In heterogeneous transportation networks the degree of uncertainty, due to the variability of travel time and the behavioral characteristics of travelers, is a contributing factor in the reliability of the system. Travel time reliability describes the performance of a transportation network from the users' perspective (Chen et al., 2002; Chen et al., 2003). In the literature, the distance-weighted standard deviation of travel time rate is considered as a measure of travel time variability (Herman and Lam, 1974), and it is suggested that there is a linear relationship between the mean and standard deviation of travel time per unit of distance (Mahmassani et al., 2012a).

Characterizing NFD and its connection with variability of travel time has been utilized to develop more efficient routing (Briganti et al., 2014) and urban planning (Cirianni et al., 2013) strategies.

### *2-5-3- Vehicular Emission Estimation*

The existing body of work on estimation of vehicular emissions can be broadly categorized into three types of techniques: microscopic, macroscopic, and mesoscopic modeling. Microscopic modeling is common in emission estimation at both vehicular and network levels (Ahn et al., 2002; Noland et al., 2004). These models invariably rely on vehicular motion state characteristics, such as speed and acceleration, rather than vehicle-specific characteristics such as engine specifications and drivers' behavior (Boulter et al., 2006; Ntziachristos and Samaras, 2000). While average speed models neglect the role of speed fluctuations (Boulter et al., 2006; Han et al., 2016), instantaneous speed models are more robust in capturing traffic flow dynamics. Several studies use speed and acceleration profiles of individual vehicles to calculate vehicle performance measures such as vehicle specific power, which in turn are used to build emission estimates (El-Shawarby et al., 2005; Qi et al., 2004; Zegeye et al., 2013). Normally, these detailed profiles are created by using an equivalent microscopic traffic assignment model and used simultaneously to generate the values of emission (El-Shawarby et al., 2005). CMEM and MOVES Lite are two of the main software packages that work on this principle. Alternatively, detailed vehicle trajectories are generated using traffic micro-simulators like PTV Vissim, Paramics, and Aimsun (Barceló and others, 2010; Int Panis et al., 2006), which are then used to estimate emission on a second-by-second basis (Sun et al., 2015). This process, however, is resource intensive and is therefore not preferred for larger systems such as urban road networks.

Macroscopic emission models, on the other hand, are used on relatively larger scales such as the zone or network level. They typically use aggregate properties such as traffic flow and

density to estimate network-wide emissions without capturing variations of traffic and emission variables at the individual level (Dia et al., 2006). Popular packages like MOBILE (User's Guide to MOBILE6.1 and MOBILE6.2: Mobile Source Emission Factor Model, 2002), EMFAC (CARB, 2007) and COPERT (Ntziachristos et al., 2009) make use of macroscopic emission models. While macroscopic models can be used to approximate emissions on large scales, they systematically ignore important actions and interactions such as vehicle acceleration and braking that are integral parts of the more accurate microscopic models. As a macroscopic tool, a simplified method of NFD application in emission estimation is shown by Shabihkhani and Gonzales (2013) in an ideal ring model, but has not seen an application on large real urban road networks.

Mesoscopic models lie between microscopic and macroscopic models in both scope and utility. They typically operate on presumably homogeneous platoons within the network based on traffic characteristics, and therefore present a somewhat reasonable approximation of microscopic effects of traffic dynamics without significant addition to the resource complexity. The VT-Meso modeling framework proposed by Zegeye et al. (2013), for example, requires using a micro-emission model – VT-Micro (Ahn, 1999) on such homogeneous platoons, which are computed based on the unrealistic assumption of absolute homogeneity of traffic composition. Despite the apparent advantages of the mesoscopic models, the application of such hybrid approaches in emission estimation is currently limited to basic isolated networks, such as freeways (Zegeye et al., 2013), signalized intersections (Gori et al., 2013), and simple theoretical networks (Jamshidnejad et al., 2017). The lack of effective tools, therefore, necessitates the development of quick and effective techniques for large-scale emission approximation, such as in large cities that consist of different types of roadways and intersections.

#### *2-5-4- Urban Traffic Control*

NFD has also been exploited to propose an efficient control strategy to ameliorate traffic congestions and delay in urban networks (Haddad and Mirkin, 2016; Mariotte et al., 2017; Yildirimoglu et al., 2015b; Zheng et al., 2012). Several studies employed NFD for traffic control purposes of single and multi-region networks (Aboudolas and Geroliminis, 2013a; Daganzo, 2007; Geroliminis et al., 2012; Haddad and Geroliminis, 2012; Haddad and Shraiber, 2014; Keyvan-Ekbatani et al., 2012). Although many traffic signal control strategies have been developed, there is still the need for designing a framework to be applicable to heterogeneous large-scale networks. The required strategy entails considering the traffic congestion and propagation, especially in over-saturated traffic flow conditions.

The background of traffic signal control is traced back to 1980s by introducing strategies such as SCOOT and SCATS (Hamilton et al., 2013; Hunt et al., 1982; Robertson and Bretherton, 1991; Sims, 1979; Yagar and Dion, 1996). Given that these strategies are not efficient under saturated traffic flow conditions, researchers have come up with advanced responsive strategies, which are unduly complex to be applied to real-time network-wide applications (Lo et al., 2001; Putha and Quadrifoglio, 2010). A feasible strategy for saturated traffic flow conditions is Traffic-responsive Urban Control (TUC), which seeks to minimize the oversaturation and spill-back of link queues (Dinopoulou et al., 2006). This strategy makes use of a gating component to limit the inflow of the links before overloading. However, these strategies may lead to sub-optimal solutions when they are applied to heterogeneous networks with multi-centric congestion patterns.

Gating is one of the most common used strategies in urban traffic control in which the inflow to a protected network (PN) is metered and the traffic is held back upstream. This strategy prevents the PN from over-saturation. The majority of the studies in this area concentrate on only

the control of the urban region borders, called perimeter control, using NFD. This type of control has been proposed for single-region networks in various studies (Daganzo, 2007; Haddad and Shraiber, 2014; Keyvan-Ekbatani et al., 2012). Different control approaches have been utilized so as to propose an algorithm for perimeter control strategies. Ramezani et al. (2015) and Zhou et al. (2016) pursued a hierarchical control approach named model-predictive control to solve the optimal control problem. Using the current state of plant feedback, the model-predictive control approach acquires the current control variables of each step by solving an open-loop control problem (Haddad and Geroliminis, 2012). Keyvan-Ekbatani et al. (2012, 2014) proposed a feedback-based gating strategy that makes use of urban NFD to propose an efficient traffic control plan with an application to the urban network of Chania, Greece. However, these approaches may lack practicability in that they require precise models. Furthermore, the aforementioned perimeter control strategies might be suboptimal in the presence of heterogeneity in the congestion distribution. To address these drawbacks, Keyvan-Ekbatani et al. (2013) presented a multiple concentric-boundary feedback-based control strategy, which takes into account the heterogeneity of congestion in transportation networks.

Several studies exploited partitioning strategies in order to split the heterogeneous network into multiple homogenous regions with different individual NFDs as mentioned earlier (Aboudolas and Geroliminis, 2013b, 2013a; Geroliminis et al., 2012; Haddad and Geroliminis, 2012; Hajiahmadi et al., 2013). This multiple-region strategy adds another layer of aggregated control approach to the previously implemented single-region perimeter control method.

Given the significant impacts of signal timing on the existence and shape of NFD, several researches have been conducted to evaluate the influence of signal coordination and network irregularities on the shape and existence of NFD. Zhang et al. (2013) investigated the effects of

adaptive signal controls on the shape of NFD. They considered multiple realistic signal timing scenarios and compared them with a pre-designed highly adaptive traffic signal system. This study concludes that the NFD of a self-organizing adaptive system is situated above the realistic systems in terms of the performance. Similarly, Gayah et al. (2014b) and Girault et al. (2016) examined the impacts of adaptive traffic signal systems as well as their endogenous parameters such as cycle length on the network and NFD stability.

To overcome the limitations of previous studies (Haddad, 2017; Kouvelas et al., 2017, 2015) a hybrid signal timing strategy is suggested by Hajiahmadi et al. (2015, 2013). The proposed signal timing strategy is composed of a switching signal timing plan in addition to the perimeter control. This method showed a better performance in comparison to previous perimeter control strategies. Similarly, Keyvan-Ekbatani et al. (2016) examined the efficiency of a combined strategy including an adaptive traffic signal strategy and a perimeter control. This study concludes that the combined perimeter and signal timing control creates a network with lower delays and shorter boundary queues. However, the mentioned studies consider limited fixed timing scenarios for the inter-regional signal timings. Therefore, there is still a gap in the literature to propose an optimal signal coordination control strategy using NFD that considers the split of all signalized intersections in the network.

#### *2-5-5- Public Transportation Planning*

Analysis and evaluation of public transportation system performance is another application of NFD. The concept of passenger network fundamental diagram (p-NFD) is recently introduced in Chiabaut (2015) to create a unified relationship capturing the traffic flow of cars and buses. The main objective is to evaluate of the efficiency of a global transport system consisting cars and buses. This research shows that the p-NFD characteristics highly depend on the ratio of different

modes. Optimal transit strategies are proposed utilizing the introduced concept in this study. Exploiting simulated data, a three-dimensional NFD (3D-NFD) relating the traffic flow characteristics of cars and buses is presented in Zheng et al. (2013). They derived an analytical function for 3D-NFD of passenger network flows and suggested the presented model applications in monitoring traffic performance and designing optimal traffic management strategies in bi-modal networks. Similarly, Geroliminis et al. (2014) developed a three-dimensional vehicle NFD (3D-vNFD) relating cars and buses network-wide accumulation and flow. They proposed a parsimonious model to estimate a three-dimensional passenger NFD (3D-pNFD). The presented framework shows a different perspective of traffic flow characteristics in bi-modal networks assuming that buses transport more passengers.

Utilizing the data gathered by fixed loop detectors and automatic vehicle location devices (AVL) of public transport vehicles, Loder et al. (2017) presented an empirical estimation tool for 3D-NFD. The application of the proposed framework is investigated in identifying the share of public transport users in maximizing trip speeds in an urban network. In a similar research, vehicle and passenger network fundamental diagrams (vNFD and pNFD) are employed to evaluate the performance of a multimodal network experiencing various traffic states (Hemdan et al., 2017). The reviewed studies in this section are important steps toward designing proper strategies for public transportation system employing the NFD concept.

## **2-6- Weather Impact on Traffic Flow**

Inclement weather conditions, defined based on its type (rain, snow, etc.), duration, and intensity, affect the driving behavior and consequently the traffic flow characteristics (Hou et al., 2013). Depending on the network size and specification, the network-wide traffic flow relationships are influenced by the fluctuation in weather indexes. According to Maze et al. (2006),

traffic demand, safety and flow relationships are all affected by the prevailing weather conditions. Drastic increase in the collision rate is reported for the networks experiencing inclement weather in comparison to clear weather condition (Andrey et al., 2003; Eisenberg and Warner, 2005; Khattak et al., 2000). The network average speed also reduces as a result of harsh weather conditions (Maze et al., 2006). The adverse weather has a direct impact on traffic demand volume. Based on the adversity type, e.g. snow versus rain (Ibrahim and Hall, 1994), trip type, e.g. commute versus recreational (Datla and Sharma, 2008), and hour of the day, e.g. off-peak versus peak periods (Datla and Sharma, 2008), the severity of the impact is different. Using the traffic data collected on freeways, it has been shown that the slope of the flow-occupancy curve is reduced by inclement weather conditions (Hall and Barrow, 1988). Highways maximum flow rate also decreases by adverse weather conditions (Ibrahim and Hall, 1994).

In order to control the detrimental impacts of inclement weather on traffic flow and safety characteristics, different efforts have been made. Several statistical models are created to quantify the impacts of adverse weather on traffic flow specifications (Hranac et al., 2006). These models are then exploited in developing decision support systems and weather-responsive traffic management strategies with the main objective of system control for different scenarios of weather severity (Hou et al., 2013; Mahmassani et al., 2009). In order to characterize this in greater depth (Hou et al., 2013) presented a systematic framework to consider the weather impact in the traffic state estimation problem. Traffic flow models are initially calibrated for different weather scenarios. Then, the calibrated models are incorporated in a mesoscopic dynamic traffic assignment (DTA) framework to estimate the weather-sensitive traffic flow measures.

Different statistical procedures are adopted to quantify the weather impacts on traffic flow relationships. Using the data collected by loop detectors in several metropolitan areas in the United

States, weather adjustment factors (WAFs) are developed to incorporate the impact of weather condition in traffic flow characteristics (Rakha et al., 2008). Calibrating weather sensitive DTA models for different specifications of road networks is another procedure adopted in the literature to capture the impacts of inclement weather conditions in the traffic flow estimation process (Dong et al., 2010; Mahmassani et al., 2012b).

## CHAPTER 3 – A Resource Allocation Problem to Estimate Network Fundamental Diagram

### 3-1- Overview

Despite the growing number of studies on the NFD estimation, there is still a need to further develop methods to properly estimate NFD when network loading is not homogenous, data from fixed detectors and mobile probes are combined, and data collection resources are constrained. Data from fixed detectors are not always available uniformly throughout an urban network. Similarly, availability of trajectory data from mobile probes is usually geographically limited and yet expensive to acquire. Therefore, in this chapter a resource allocation problem is formulated as a mathematical model to estimate NFD using a combined sample of vehicle trajectories and fixed detector data in a large-scale real-world network accounting for traffic heterogeneity and asymmetry in OD demand. Information from mobile probes provides an accurate space-mean network speed while information from fixed detectors provides an accurate mean network flow as shown in Leclercq et al. (2014) and Ambühl and Menendez (2016). Similarly, probe vehicles can be applied to estimate flow only when all trajectories are available or the penetration rate of probe vehicles are known a priori. Building upon recent studies by Leclercq et al. (2014) and Du et al. (2016), the proposed method finds the optimal location of measurement points and optimal set of trajectories associated to OD pairs in a heterogenous network required to estimate an NFD. The main contribution of this chapter is, therefore, formulating NFD estimation as a resource allocation problem and the presented solution algorithm that facilitates estimation of NFD by optimally locating fixed measurement points and sampling of probe trajectories. Note that unlike some of the previous studies, this research takes advantage of both fixed and mobile data sources without the need for an aggregate pre-known penetration rate for probe vehicles.

The proposed mathematical model minimizes the deviation between the NFD and estimated network average flows and densities using the optimal configuration of detectors and set of trajectories from OD pairs. The optimal configuration considers a budget constraint for detector installation and trajectory data acquisition. In the proposed formulation, flows are estimated from links selected to be equipped with the detectors. However, traffic flow can only be used in NFD estimation, if at least a single trajectory is available to measure the link space mean speed. The proposed methodology incorporates the ground-truth NFD as input to find a subset of links and trajectories to estimate NFD, and it does not rely on the ground-truth NFD calculation method. Evidently, the ground-truth NFD may not be available or might just be measured for certain conditions. Here, the objective is the estimation of NFD in general conditions considering variability of demand and day-to-day traffic patterns. Therefore, a surrogate is necessary to provide this input such as analytical methods or traffic simulation. Assuming that this surrogate provides the ground-truth NFD, the proposed methodology finds the optimal configuration of links and trajectories to collect data and estimate the NFD considering the available budget for data collection. To demonstrate the performance of the proposed framework based on a certain ground-truth NFD, the estimated NFD by the selected detectors and trajectories are compared with the ground-truth NFD, under a range of different demands. This comparison confirms applicability of the model various conditions. Note that the presented approach also contributes to estimation of network traffic state any given time  $t$ . Even when the ground-truth NFD is known, there is still the need to estimate network traffic state for traffic control purposes; in other words, where on the NFD the network is at any time  $t$ .

The proposed model is a mixed integer problem with non-linear constraints. Mixed integer linear problems are known to be NP-hard, and non-linear constraints add more complexity by

providing local optimal solutions for the formulated problem. As a result, no exact solution method exists for large-scale network applications. Therefore, a heuristic solution algorithm, Simulated Annealing (SA), is implemented to solve the problem. The method starts with an initial solution that is randomly selected as the current solution. Then, the current solution is perturbed iteratively to a neighbor solution (selected randomly) and is substituted by the neighbor solution, when the objective function is improved. The neighbor solution is also probabilistically accepted when the objective function is not improved to avoid local optimal solutions. This probability needs to be reduced by the iteration number to ensure convergence of the algorithm. This study shows that how different combinations and variations in the proportion of fixed detection points and OD trajectories affect the estimated NFD. The focus of the chapter is not on the implemented solution algorithm. Therefore, no comparison with other possible solution methodologies is made. The study mainly focuses on the problem formulation and numerical results from a real-world network. The successful implementation of the SA algorithm in the numerical results section for a case study with large-scale network application confirms suitability of this heuristic method for the proposed mathematical model. The SA algorithm is a proper methodology for problems in which evaluation of the objective function is intuitive for a given solution of decision variables. This is the case for the proposed model, where average flows and densities need to be calculated for a given detector and set of trajectories.

### **3-2- Model Formulation**

Here, the NFD estimation problem is formulated as a resource allocation problem to find the optimal locations of fixed measurement points and the optimal set of trajectories associated with OD pairs given a fixed data acquisition budget. For this purpose, the presented mathematical model finds a subset of candidate links for fixed detectors in order to estimate an NFD with the

maximum possible precision. Moreover, the mathematical model finds a subset of OD pairs in which their associated trajectory data are needed to improve NFD estimation. The optimal combination of the fixed detectors and OD pairs provides an accurate estimation of both network-wide space-mean speeds and average flows, when a sufficient fixed data acquisition budget is provided. Using the space-mean speeds estimated by trajectories and estimated flows by fixed detectors, densities can be calculated using the traffic flow fundamental identity  $q=k.v$ . Both flow and space-mean speed are estimated at the link level to be later incorporated in estimation of network-wide averages.

The constraints of the model limit the total number of detectors to be deployed and the total number of trajectories to be acquired. The optimal solution for the mathematical model includes the optimal measurement locations and OD pairs that provide an estimated NFD with minimum discrepancy from the case with no constraints on the number of loop detectors and trajectories. Here, a heuristic solution algorithm is also presented to estimate the optimal solution in a reasonable computational time frame for large-scale applications considering heterogeneous traffic demand distribution and asymmetric OD demand matrix. The proposed problem formulation is as follows.

$$\text{Min} \sum_{t=1}^T \left[ \zeta (Q_t - \hat{Q}_t)^2 + \eta (K_t - \hat{K}_t)^2 \right] \quad (3-1)$$

Subject to

$$Q_t = \frac{\sum_{i=1}^I (q_i^t l_i)}{\sum_{i=1}^I l_i} \quad \forall t = 1, \dots, T \quad (3-2)$$

$$K_t = \left[ \sum_{i=1}^I (l_i q_i^t / s_i^t) \right] / \sum_{i=1}^I l_i \quad \forall t = 1, \dots, T \quad (3-3)$$

$$\hat{t}t_i^t = \frac{[\sum_{j=1}^J \sum_{k=1}^{K(j)} (p_{ijk}^t \hat{t}t_{ijk}^t y_j)]}{[\sum_{j=1}^J \sum_{k=1}^{K(j)} (p_{ijk}^t y_j)]} \quad \forall t = 1, \dots, T, \forall i = 1, \dots, I \quad (3-4)$$

$$\hat{s}_i^t = l_i / \hat{t}t_i^t \quad \forall t = 1, \dots, T, \forall i = 1, \dots, I \quad (3-5)$$

$$\sum_{j=1}^J \sum_{k=1}^{K(j)} (p_{ijk}^t y_j) \leq z_i^t M \quad \forall t = 1, \dots, T, \forall i = 1, \dots, I \quad (3-6)$$

$$z_i^t \leq \sum_{j=1}^J \sum_{k=1}^{K(j)} (p_{ijk}^t y_j) \quad \forall t = 1, \dots, T, \forall i = 1, \dots, I \quad (3-7)$$

$$z_i^t + x_i - 1 \leq w_i^t \quad \forall t = 1, \dots, T, \forall i = 1, \dots, I \quad (3-8)$$

$$w_i^t \leq z_i^t \quad \forall t = 1, \dots, T, \forall i = 1, \dots, I \quad (3-9)$$

$$w_i^t \leq x_i \quad \forall t = 1, \dots, T, \forall i = 1, \dots, I \quad (3-10)$$

$$\hat{Q}_t = \left[ \sum_{i=1}^I (l_i q_i^t w_i^t) \right] / \left[ \sum_{i=1}^I l_i w_i^t \right] \quad \forall t = 1, \dots, T \quad (3-11)$$

$$\hat{R}_t = \left[ \sum_{i=1}^I \left( \frac{q_i^t}{\hat{s}_i^t} l_i w_i^t \right) \right] / \left[ \sum_{i=1}^I (l_i w_i^t) \right] \quad \forall t = 1, \dots, T \quad (3-12)$$

$$\sum_{i=1}^I c_i x_i + \sum_{j=1}^J f_j y_j \leq B \quad (3-13)$$

$$x_i = 0 \text{ or } 1 \quad \forall i = 1, \dots, I \quad (3-14)$$

$$y_j = 0 \text{ or } 1 \quad \forall j = 1, \dots, J \quad (3-15)$$

$$z_i^t = 0 \text{ or } 1 \quad \forall i = 1, \dots, I \quad (3-16)$$

$$w_i^t = 0 \text{ or } 1 \quad \forall j = 1, \dots, J \quad (3-17)$$

In the formulation,  $x$  and  $y$  are binary decision variables, specifying if a detector is located on a link ( $x_i=1$ ) or a specific OD pair is selected to acquire data trajectories ( $y_j=1$ ).  $z$  and  $w$  are binary state variables.  $z$  specifies if there is any crossing trajectory on link  $i$  at time  $t$  based on the decision variable  $y$  over OD pairs.  $w$  specifies if the link should be considered for the network-wide average value calculation or not based on availability of detectors (specified by  $x$ ) and trajectory data over the link (specified by  $z$ ). The latter is one for a specific link and time interval when both  $x$  and  $z$  are equal to one for that link and time interval.

Equation 3-1 lists the objective function as the weighted sum of squared deviations in network-wide average values of flow and density at different time intervals. In this equation, estimated network-wide average values by selected links and trajectories are compared with the NFD calculated by all links and trajectories. As the order of network-wide average values for flow and density are different, the two terms are weighted with different factors ( $\zeta$  and  $\eta$ ). Equations 3-2 and 3-3 present NFD using network-wide average flow and density for each time interval based on all link flows and space-mean speeds. Note that the weighted average values are calculated considering the lane-length of each link. Equation 3-4 calculates the average travel time on each link at each time interval using experienced travel times by crossing probe vehicles at the time interval of interest. The probe vehicles' travel times are considered in the average travel time, if the OD pair of the probe vehicle is selected in the optimal solution. This equation simply goes over all trajectories that can be observed (with  $y$  equal to 1) and adds the observed travel time for each link  $i$  along the trajectory with departure time interval of  $t$  to the total travel time for that link and time interval. Then, it divides the total observed travel time for each link and time interval by actual number of observed trajectories. Equation 5 calculates the space-mean speed for each link and time interval. Equations 3-6 and 3-7 specify if there is any crossing probe vehicle available that its origin and destination are among the selected OD pairs in the optimal solution (specifying  $z$  based on  $y$ ). When there is at least one trajectory that crosses link  $i$  at time interval  $t$ , which can be observed (with  $y$  equal to 1),  $z$  needs to be equal to 1 for that link and time interval to hold Equation 3-6. In this case, Equation 3-7 would not be binding. When there is no such trajectory, Equation 3-7 sets  $z$  for that link and time interval to zero and Equation 3-6 would not be binding. In this model, for simplicity of the presentation, it is assumed that when an OD pair is selected, all trajectories traveling between the origin and destination are available for NFD estimation. The

model formulation can be easily adjusted to consider other assumptions such as partial trajectory availability for OD pairs by considering an extra binary variable for each trajectory in these equations ( $u_{kj}$ ). Equations 3-8, 3-9, and 3-10 determine if a link and time interval should be considered in the network-wide average calculation based on the availability of both detector and crossing probe vehicles at that link and time interval (specifying  $w$  based on  $z$  and  $x$ ). Note that the three linear constraints in Equations 3-8, 3-9 and 3-10 can be replaced by a single non-linear constraint as  $w_i^t = x_i \times z_i^t$ . Equations 3-11 and 3-12 estimate the average flow and density at each time interval over the selected links in the optimal solution with positive  $w$ . Equation 3-13 enforces the budget constraint by limiting the number of selected links and OD pairs. Equations 3-14 to 3-17 are feasibility constraints for the binary variables. Note that the feasibility constraint for non-binary variables, which is positivity constraints, is not listed in the above formulation.

### **3-3- Solution Algorithm**

The proposed model, formulated as a Mixed Integer Non-Linear Program (MINLP), aims to minimize the deviation of the estimated NFD by a limited number of links and trajectories, due to the budget constraint for data collection or acquisition, and the calculated NFD using all the network links and trajectories. The location problems are known to be NP-hard, especially for the defined problem in this study where the non-linear constraints add to the problem complexity. Thus, a heuristic algorithm is developed to estimate NFD with optimal sampling of fixed detection points and OD pairs. Here, a Simulated Annealing (SA) algorithm (e.g. Černý, 1985; Davidovich and Mikhailovich, 1980; Kirkpatrick et al., 1983; Metropolis et al., 1953; Van Laarhoven and Aarts, 1987) is implemented to solve the proposed mathematical model. SA is a proper solving technique for the problem of interest in this study, as it can find the optimal solution without being trapped in local optimal solutions. Note that the problem of interest has non-linear constraints that

might lead to including many local optimal solutions. SA is an appropriate methodology for problems in which the objective function can be evaluated by simple calculations when the decision variables are known. This is the case for the formulated problem where given  $x$  and  $y$ , the objective function can be simply calculated.

The implementation of the SA method in this study is based on the Metropolis algorithm (Hejazi, 1999; Metropolis et al., 1953) and the more recent implementation in Zockaie et al. (2016) and Ghamami et al. (2016) is followed here. The algorithm derives its underlying idea from the heating and cooling phenomenon of solid materials. A solid at a liquid state cooled gradually will form a crystal, whereas rapid cooling from the same initial condition will lead to a frozen solid. Accordingly, the SA algorithm usually “simulates” the process of gradual temperature decreasing. At each temperature, an equilibrium state should be achieved before moving to a lower temperature. The final solution will be achieved at the minimum or final temperature.

The SA algorithm starts with a feasible initial solution. In each iteration, it picks a neighborhood solution through a local search and evaluates the objective values,  $C(.)$ , at the current,  $n$ , and previous,  $m$ , solutions. The algorithm will then decide whether to move to the new solution or to stay at the current solution as follows. It sets  $\Delta C_{mn} = (C(n) - C(m))/C(m)$ . If  $\Delta C_{mn} \leq 0$ ,  $n$  is selected as the new solution with probability 1, and if  $\Delta C_{mn} > 0$ ,  $n$  is selected as the new solution with the probability of  $\exp(\frac{-\Delta C_{mn}}{Temp})$ , where  $Temp$  is a control parameter interpreted as the “temperature” in the cooling process. This implies that a solution worse than the current one may be adopted with a non-zero probability. This specification provides the opportunity of not being trapped in a local optimal solution. The above process continues until an equilibrium state is reached at a certain temperature such as  $Temp$ . In each step,  $Temp$  is reduced and the system is equilibrated under a new temperature. The algorithm terminates at a small  $Temp$

such that any increase in the objective function value is prohibited (Zockaie et al., 2016). A description of the basic SA algorithm follows.

### *Simulated Annealing Algorithm*

**Step1:** Consider an initial solution  $m$  (which assigns variable  $x$  and  $y$  to 0 or 1 for different sets of  $i$  and  $j$  considering the budget constraint to maintain feasibility)

Set iteration index  $iter=0$ ; Set an initial  $Temp_0$ , the number of main iteration  $Iter$  and the number of inner iteration  $Inner-Iter$

**Step2:** Repeat Steps 3-5  $Inner-Iter$  times and afterwards go to Step 6.

**Step 3:** Select solution  $n$  close to  $m$  (finding a neighbor solution by changing one of  $x$  and  $y$  values for a particular  $i$  or  $j$  considering the budget constraint to maintain feasibility)

**Step 4:** Calculate  $\Delta C_{mn} = (C(n) - C(m))/C(m)$  (where function  $C(.)$  calculates the objective function)

**Step 5:** If  $\Delta C_{mn} \leq 0$ , then set  $m=n$ ;

Otherwise, if  $\exp\left(\frac{-\Delta C_{mn}}{Temp_k}\right) > \text{Random number} \in [0,1)$  then set  $m=n$ .

**Step 6:**  $iter = iter + 1$

**Step 7:** Reduce  $Temp$  using  $Temp_{iter+1} = f(Temp_{iter})$ , if  $iter \leq Iter$  go to Step 2, else stop.

Several remarks on implementation issues are in order here. The first has to do with the choice of control parameters, such as initial temperature, the number of inner iterations at each temperature, the temperature reduction function, and the number of main iterations. The second issue is related to the choice of initial solution and the third and perhaps the most important implementation question is how to get a neighbor solution by perturbing the current solution. In

this study, following Zockaie et al. (2016), the initial temperature is assumed to be 0.05. The temperature is decreased by the rate of 0.85 for each outer loop iteration. Therefore, the following relation at Step 7 of the algorithm is used:

$$Temp_{iter+1} = 0.85 * Temp_{iter} \quad or \quad Temp_{iter+1} = (0.85)^{iter} Temp_0 \quad (3-18)$$

To select the initial and neighbor solutions, random number generation is used, considering uniform distribution, to select specific  $x$ , and  $y$  to be included in the initial or neighbor solutions. The main challenge in the random selection strategy is how to move from current solution to a neighbor solution satisfying the budget constraint (Equation 3-13). For the simplicity, it is assumed that the costs associated with the fixed detection and trajectory data are uniformly distributed over the network and OD pairs. Therefore, the budget constraint is enforced through solving the problem for different proportions of both fixed detection points and OD trajectories. Furthermore, it is assumed that  $\zeta = 1$  and  $\eta = 1$ . Note that these assumptions do not affect the generality of the solution method and do not limit its applicability to the formulated problem. It is also assumed that the availability of trajectory data is linked to the OD pairs.

The algorithm uses proportion rates for available fixed detections,  $a$ , and trajectory OD pairs,  $b$ , as the main input. Note that parameters  $a$  and  $b$  do not represent the penetration rate of probe vehicles. They represent the proportion of employed fixed detection points and OD pairs, respectively. To further clarify, parameters  $a$  and  $b$  are only representative of the “estimation budget”. Given the proportions, a set of links and OD pairs are randomly selected as the initial solution and are stored as the current solution. To find the neighbor solution, first it is randomly decided to perturb the current solution, by choosing between modifying the location of fixed measurement points and modifying OD trajectories, to move to a neighbor solution. Then, based on this decision, one of the links or OD pairs in the current solution is randomly selected and

removed from the current solution. Also, one of the links or OD pairs that is not in the current solution is selected to be added in the neighbor solution. Note that by adding one link or OD pair, and removing another link or OD pair, the neighbor solution has exactly the same proportion rates as the current solution. Furthermore, for any given current and neighbor solutions, estimating the objective function is intuitive. At the selected locations of fixed measurements, the link flows are known, and crossing trajectories are used to estimate the space-mean speed. Knowing flow and space-mean speed, density can be calculated using the traffic flow fundamental identity. Finally, network-wide flow and density averages at each time interval can be calculated using Equations 3-11 and 3-12. Applying the random selection strategy to find the initial and neighbor solutions and estimating the objective function as explained earlier, the iterative steps of the algorithm can be implemented as discussed in Step 2 to Step 7 of the algorithm. In this study, 100 inner loop iterations are considered to reach an equilibrium state at each temperature for each of the outer loop iterations required iterations to decrease temperature and as a result decreasing probability of accepting worse neighbor solutions relative to the current solution. The temperature for 50 iterations as the outer loop is also modified.

### **3-4- Numerical Results**

Here, the proposed mathematical model is applied to a large-scale network of Chicago to estimate the NFD for downtown sub-network as illustrated in Figure 3-1. In the proposed framework, the ground-truth NFD is an input. As mentioned earlier, the actual ground-truth might not be available at all or it might be measured under specific conditions. In this study, a methodology is developed to estimate the ground-truth NFD using sampled observations from detectors and trajectories. Here, a surrogate of the ground-truth NFD is used as an input to optimize the sampling procedure. The surrogate NFD used here can be measured experimentally or

analytically for small networks. However, for large-scale network applications, a mesoscopic traffic simulation model can alternatively be used. Here, a calibrated simulation-based dynamic traffic assignment (DTA) model of Chicago is utilized to estimate the surrogate for the ground-truth NFD. Then, the optimal location of trajectories and detectors will be found. Observations made by the located detectors and trajectories under general conditions provide proper estimation of NFD. To examine the applicability of the proposed methodology under general conditions, this study also shows the performance of the estimation method for cases where ground-truth NFD is modified as a result of variation in demand and seed number for random number generations that are used for different purposes throughout the network simulation (demand generation, signal control, en-route users assignment, etc.).

#### *3-4-1- Study Network*

DYNASMART-P is employed to conduct the experiments and to obtain the ground-truth NFD using fixed measurements of density and flow at all links throughout the selected sub-network. DYNASMART-P is a simulation-based dynamic traffic assignment tool and it has the capability to find the dynamic user equilibrium in an iterative process. It also can distribute traffic over the network using the best current path, which can be changing during the simulation time depending on the congestion distribution across the network. In this study, the best current path, often known as zero shot simulation, is used. Modeled trajectory of all vehicles in the network during the simulation horizon is available. The Chicago downtown network, which is bound from West and East by O'Hare airport and Lake Michigan respectively, is considered as the large-scale case study. It includes downtown Chicago and some Western and Northern suburban cities of Chicago, and contains 1578 nodes, 4805 links, and 218 zones. The simulation horizon is the AM peak period between 5:00 AM and 10:00 AM. The static hourly demand is provided by the Chicago

Metropolitan Agency for Planning (CMAP) for the AM peak. The static demand is transformed into a time-dependent OD demand table through the OD-estimation techniques presented in Zockaie et al. (2014a) resulting in about 550,000 vehicles simulated in the network. In this case study, estimation of NFD for a sub-network located in Downtown Chicago is targeted. This sub-network, which is illustrated in Figure 3-1, includes 921 links and 7,212 OD pairs with positive demand. Chicago CBD is selected because it is the most congested part of the greater Chicago area network. The traffic distribution is more homogenous in this part of the network relative to the entire network. Also, the NFD for this portion of the network is more difficult to estimate relative to the entire network, where the congestion regime is phased out in the average value calculation by many uncongested links in other parts of the network. Generally speaking, the proposed method can be applied to any network, larger or smaller in size without any computational complexity issue. Note that the dynamic simulation is conducted for the greater Chicago area network. Therefore, the OD pairs counted and reported relate to the larger network. The simulation is run for the larger network, but the proposed method is only applied to the CBD sub-network for the NFD estimation.

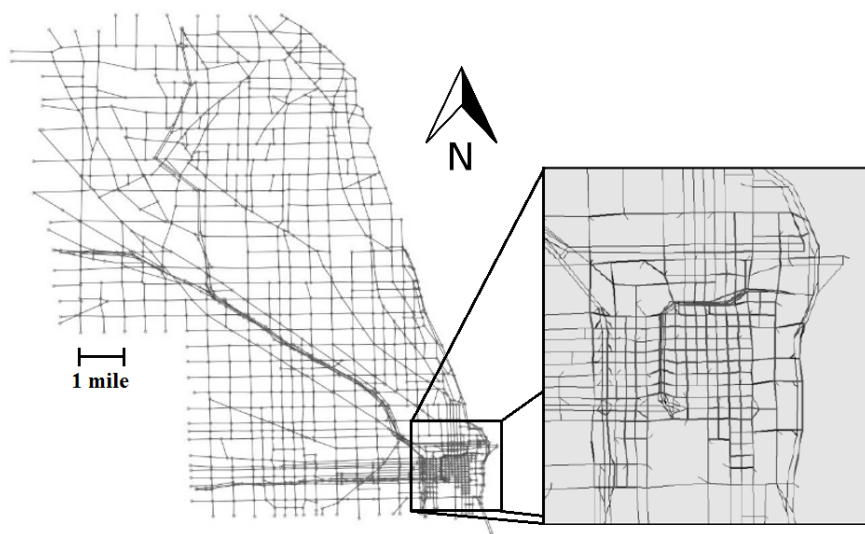


Figure 3-1- Illustration of the Chicago network and its downtown sub-network

### 3-4-2- Optimal Locating of Fixed Measurement Points and Sampling of Probe Trajectories

It is first examined that how different proportions of fixed detection points  $a = \{0.2, 0.4, 0.6, 0.8\}$  and OD pairs  $b = \{0.2, 0.4, 0.6, 0.8\}$  affect the initial and optimal objective values as a representation of discrepancy between the estimated and ground-truth NFD. All the  $4 \times 4$  combinations are tested, and the selected numerical results are reported to demonstrate the applicability of the proposed method in a large-scale heterogeneous network. Figures 3-2 and 3-3 show a comparison of the ground-truth, initial, and estimated NFDs for a combination of  $a$  and  $b$  values. First, the proportion of fixed detection points is set to a constant  $a=0.2$  and the proportion of OD pairs  $b=\{0.2, 0.4, 0.6, 0.8\}$  is changed as illustrated in Figure 3-2.

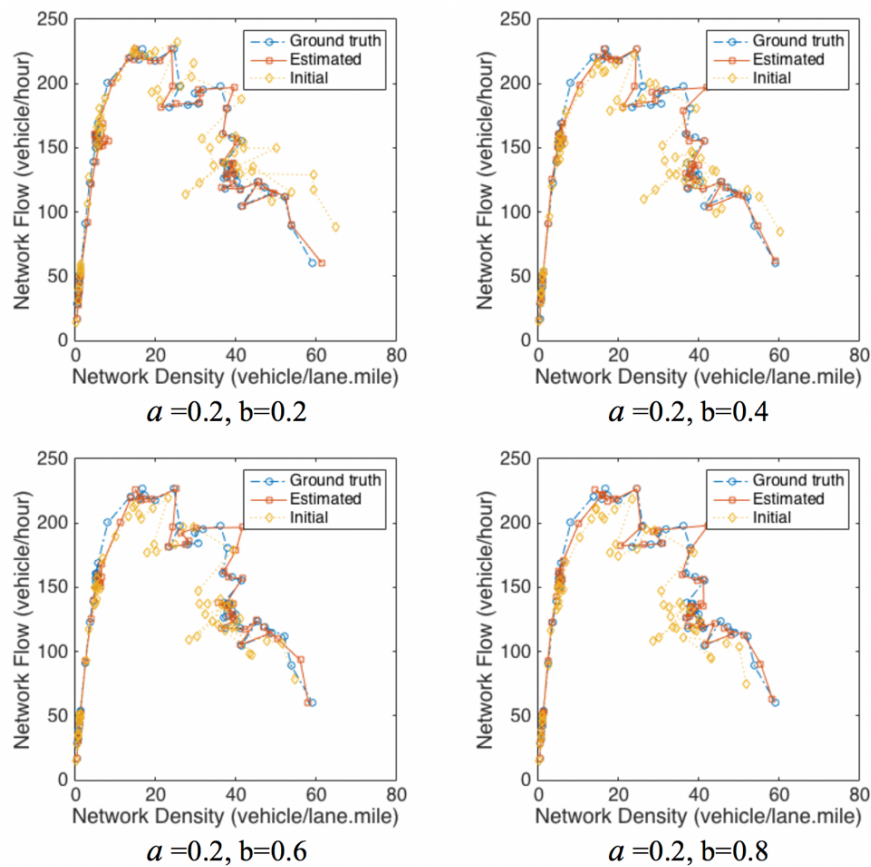


Figure 3-2- Comparison of estimated NFD, initial NFD, and ground-truth NFD for different proportions of ODs  $b=\{0.2, 0.4, 0.6, 0.8\}$  with a constant proportion of fixed detectors  $a=\{0.2\}$

The initial NFD is estimated from randomly selected links for fixed detection and randomly selected ODs for probe trajectories. The estimated NFDs obtained from optimally selected links and ODs are also shown. Then, the proportion of OD pairs is set to a constant  $b=0.2$  and the proportion of fixed detection locations  $a=\{0.2, 0.4, 0.6, 0.8\}$  is changed as illustrated in Figure 3-3. The comparison of NFDs demonstrates that the optimal estimated NFDs have smaller deviation from the ground-truth NFD compared to NFDs estimated from randomly selected initial solutions, as expected. Later, it will be shown that increasing the proportion of fixed detection points or increasing the proportion of OD pairs both improve the initial estimated NFD.

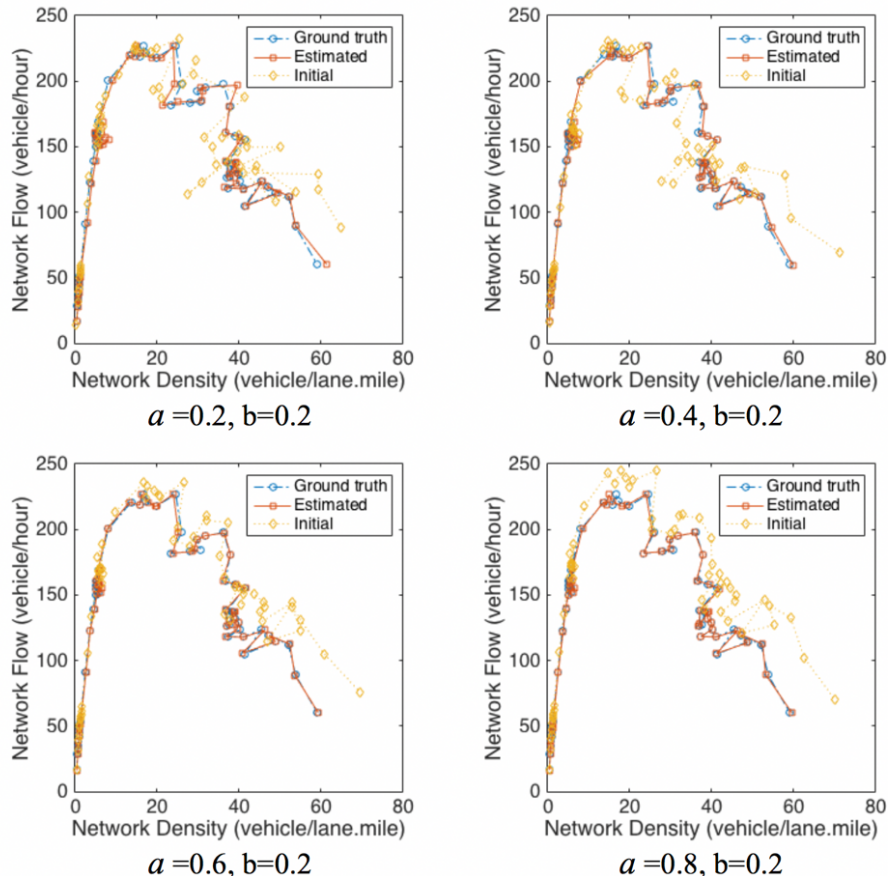


Figure 3-3- Comparison of estimated NFD, initial NFD, and ground-truth NFD for different proportions of fixed detectors  $a = \{0.2, 0.4, 0.6, 0.8\}$  with a constant proportion of ODs  $b=\{0.2\}$

Finally, it will be shown that for a constant proportion of detection points, increasing the proportion of trajectories does not affect the quality of the estimated NFD. However, for a constant proportion of OD pairs, increasing the proportion of detection points improves the estimated NFD with small deviation from the ground-truth NFD.

Figure 3-4 illustrates the location of the optimally selected fixed measurement points in the network for the same combination of  $a$  and  $b$  values. An interesting observation is the variation between the selected links across cases with the fixed  $a=0.2$ . Although the proportion of fixed detection points is constant, the locations of the detection points vary because of the changing proportion of ODs  $b=\{0.4, 0.6, 0.8\}$ . Figure 3-5 visualizes the selected OD pairs for the same combination of  $a$  and  $b$  values and for the entire network including all ODs using a schematic graph. Here, a circular graph is drawn with nodes on the circumference of the circle in order of node degree and links connecting nodes. A node pair is connected with a link if the OD pair is selected for estimating NFD. The graph showing all ODs represents the entire OD matrix of the Chicago network. The circular illustration here does not represent the links entering or exiting the CBD area. All traffic analysis zones with positive demand crossing the CBD area are located on the circle to show the connectivity between different OD pairs in the network. It is found that the selected ODs across the network vary even when the proportion of OD pairs is fixed (e.g.  $b=0.2$ ) because of varying proportion of fixed measurement points  $a = \{0.2, 0.4, 0.6, 0.8\}$ . Increasing detection points proportion for a fixed proportion of OD pairs results in more dispersed distribution of selected OD-pairs. This improves the network connectivity to cover the increased selected number of links.

Figure 3-6 shows the convergence pattern for the same combination of  $a$  and  $b$  values. The initial objective value, representing the deviation between estimated and ground-truth NFD, is as

large as 10,000. However, as the number of iterations increases, the SA algorithm significantly reduces the optimal objective value, demonstrating the convergence pattern of the algorithm. When the number of iterations is large enough, increasing the OD pair proportions does not improve the optimal objective value. In other words, when the link proportion is limited, there is no benefit in increasing the OD pair proportion to cover the entire network. However, increasing the OD pair proportion to a certain limit, ensures reliability of the optimal solution. Note that the number of iterations listed in this figure, includes both inner and outer loops. Iterations 1 to 100 are associated with the first outer loop and iterations 101 to 200 are associated with the second outer loop and so on.



Figure 3-4- Selected locations for optimal estimation of NFD for different proportions of ODs and fixed detectors

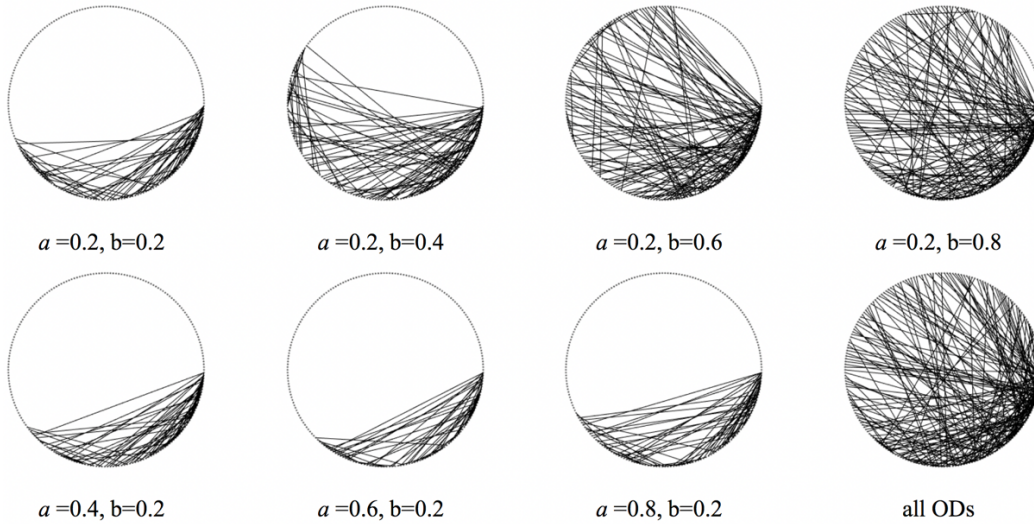


Figure 3-5- Selected ODs for optimal estimation of NFD for different proportions of ODs  $b = \{0.2, 0.4, 0.6, 0.8\}$  with a constant proportion of fixed detectors  $a = \{0.2\}$  and for different proportions of fixed detectors  $a = \{0.2, 0.4, 0.6, 0.8\}$  with a constant proportion of ODs  $b = \{0.2\}$ ; for all ODs

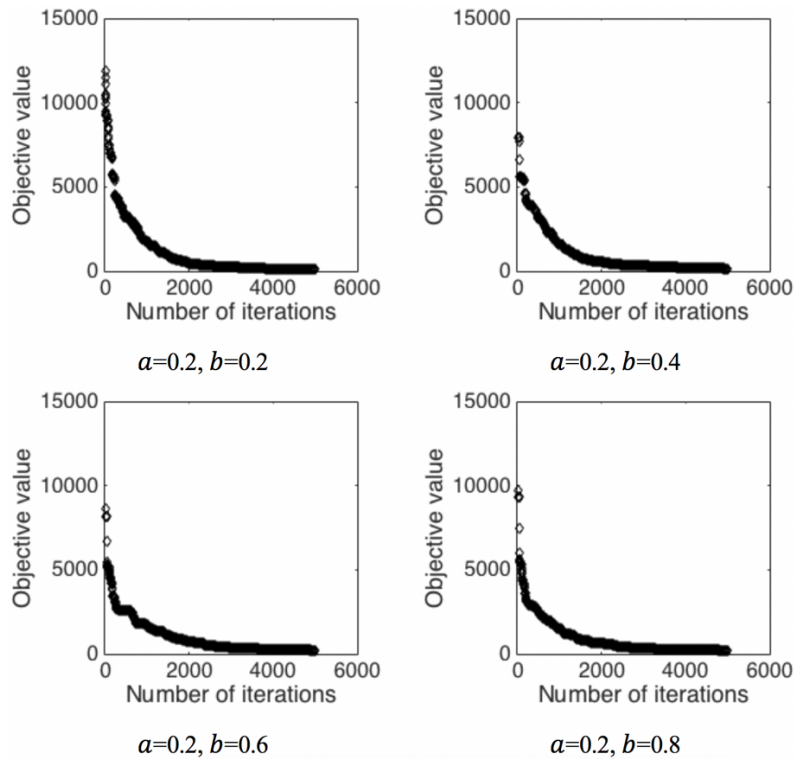


Figure 3-6- Convergence pattern for different proportions of ODs  $a = \{0.2, 0.4, 0.6, 0.8\}$  with a constant proportion of fixed detectors  $b = \{0.2\}$

Figure 3-7 shows the initial and optimal objective values as a function of  $a$  and  $b$ . Figure 3-7(a) illustrates the change in the initial and optimal objective values for a set of constant proportions of fixed measurements  $a$  while changing  $b$ . The initial objective values are relatively large and do not follow a specific pattern given that they are mainly based on a random selection of links and OD pairs for NFD estimation. Counter intuitively, the optimal objective value does not change monotonically with increase or decrease of  $b$  for constant link proportions  $a$ . However, the value of optimal objective function for different OD pair proportions decreases with increase of the link proportion. Figure 3-7(b), indicates the change in the initial and optimal objective values for a set of fixed proportion of OD pairs  $b$  while changing  $a$ . The initial objective values follow a decreasing pattern for all  $b$  when  $a$  increases (except  $b = 0.2$  due to the randomness of the methodology). The optimal objective values also follow a decreasing pattern when  $a$  increases.

Results suggest that for a fixed proportion of OD trajectories, the increase in the proportion of fixed detection points decreases the deviation from the ground-truth NFD as expected. However, when the proportion of fixed detection points is set to be constant, the increase in the proportion of OD trajectories does not necessarily improve the estimated NFD. This is due to the fact that for a certain link proportion, an optimal level of OD pair proportion can be found. Increasing or decreasing the level of OD pair proportion might lead to selection of some links in the optimal solution that increases the objective function value. To clarify why such pattern is observed in the numerical results, a simple example is presented to explain how increasing the OD pair proportion might increase the objective function value. Let's say a certain link proportion results in selecting  $n$  links among the  $m$  links of the network. The OD pair proportion is set to a certain value that exactly results in crossing probe vehicles in  $n-1$  of the links. Let's say the left-out link is the least similar link to the ground-truth NFD. Increasing the OD pair proportion results in selecting the

left-out link as the maximum link proportion is  $n$ . As this link has the minimum similarity to the ground-truth NFD, this addition would increase the deviation of the estimated NFD from the ground-truth NFD. Although increasing OD pair proportion might not improve the objective function value for a constant link proportion, it might improve the reliability of the estimated NFD under general conditions. In a rare case, there might be only a single link in the network with a fundamental diagram that matches the ground-truth NFD. Selecting this link alone, along with OD-pairs that include probe vehicles crossing this link, results in the objective function value of zero. However, this estimation is not reliable and with a minor change in the network conditions, the ground-truth NFD might deviate from the estimated NFD. Therefore, as far as the budget constraint allows, the link and OD pair proportions should be increased.

To understand the reliability of the solution found by the proposed methodology, the performance of NFD estimation by the selected detectors and trajectories under general conditions, with different ground-truth NFDs relative to the one that is used as the input to the model, is studied. To this end, three different ground-truth NFDs, all derived from the simulation, are considered. The first ground-truth NFD is the base scenario that is used as the input for the mathematical model to find the optimal set of detectors and trajectories as shown in Figure 3-8(a) and Figure 3-8(d). Decreasing the total simulated demand in the base scenario by 5 percent results in the second ground-truth NFD, shown in Figure 3-8(b) and Figure 3-8(e), and increasing the demand by 5 percent results in the third ground-truth NFD, shown in Figure 3-8(c) and Figure 3-8(f). In both scenarios, different seed numbers are used for generating random numbers to specify users who have access to en-route travel time information. Results show that changes in demand and route assignment create significant variations in the shape of the ground-truth NFD.

The proposed methodology is applied to the first scenario to find the optimal set of detectors and trajectories to estimate the NFD for two different cases. The proportion rate for detectors is considered as 0.6 for both cases ( $a=0.6$ ), while the proportion rate for OD pairs is 0.2 for the first case ( $b=0.2$ ) and 0.6 for the second case ( $b=0.6$ ). The actual NFD for the first scenario and the estimated NFDs by the proposed methodology for both cases are presented in Figure 3-8(a) and Figure 3-8(d). The OD pairs proportion of 0.2 seems to be as effective as of the OD pairs proportion of 0.6 to estimate the ground-truth NFD. However, the role of the additional proportion rate of OD pairs can be seen in the reliability of the NFD estimation in Figure 3-8(b), Figure 3-8(c), Figure 3-8(e) and Figure 3-8(f). In these figures, the selected detectors and subset of trajectories, as the optimal solution based on the ground-truth NFD in the first base scenario, are used to observe the NFD under decreased and increased demand scenarios, respectively. Figure 3-8(b) compares the observed NFD with the ground-truth NFD of the decreased demand scenario, where the proportion rates of detectors and OD pairs are 0.6 and 0.2. Figure 3-8(e) presents a similar comparison for the decreased demand scenario when the proportion rates of detectors and OD pairs are both equal to 0.6. Figure 3-8(c) and Figure 3-8(f) present similar comparisons for the increased demand scenario. In both scenarios, the observed NFDs better match with the ground-truth NFD in the second case, Figure 3-8(e) and Figure 3-8(f), where the proportion rate of the selected trajectories based on the first scenario is higher. This is unlike the similar performances of the two cases in the base scenario and demonstrates the importance of finding reliable optimal solutions. It shows the importance of considering stochasticity of the travel demand and supply in the NFD estimation, which is the subject of Chapter 4.

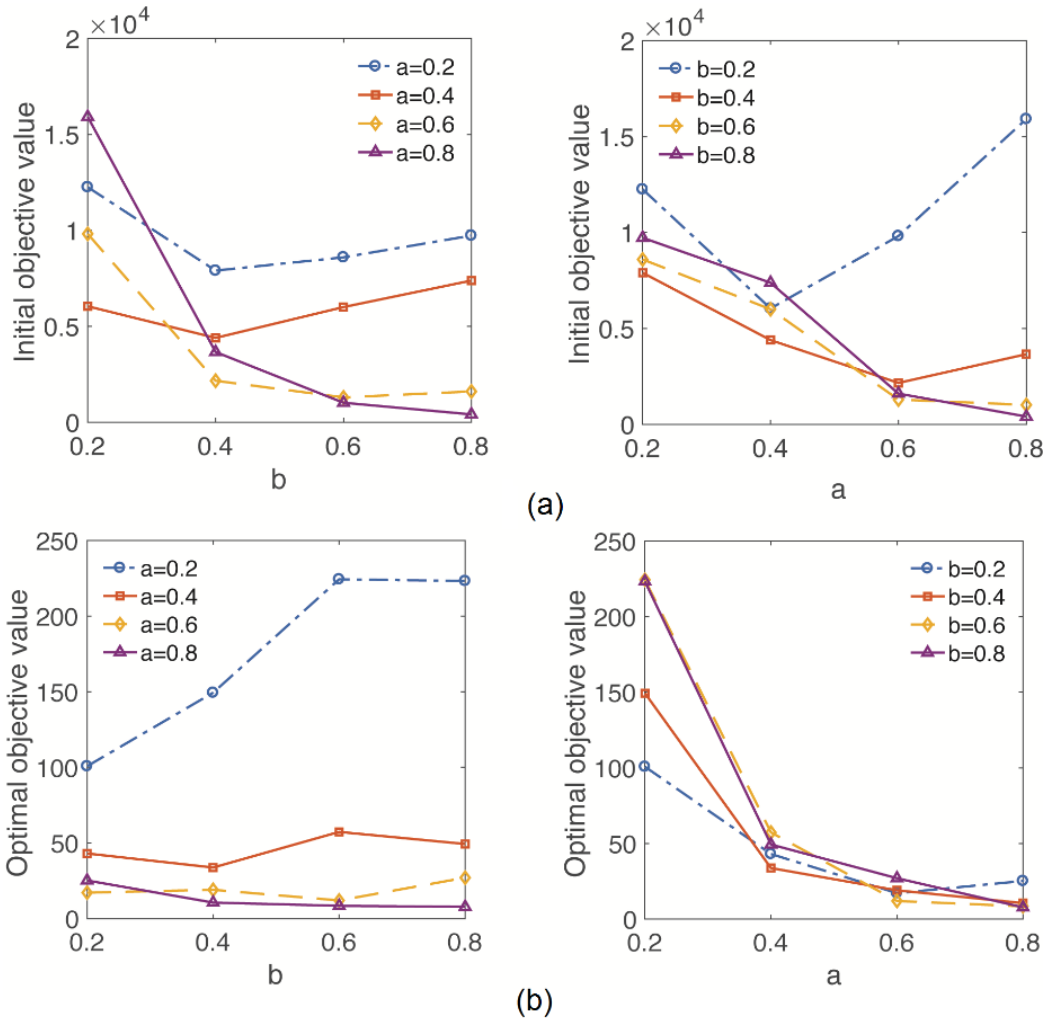


Figure 3-7- Initial and optimal objective values as a function of  $a$  and  $b$

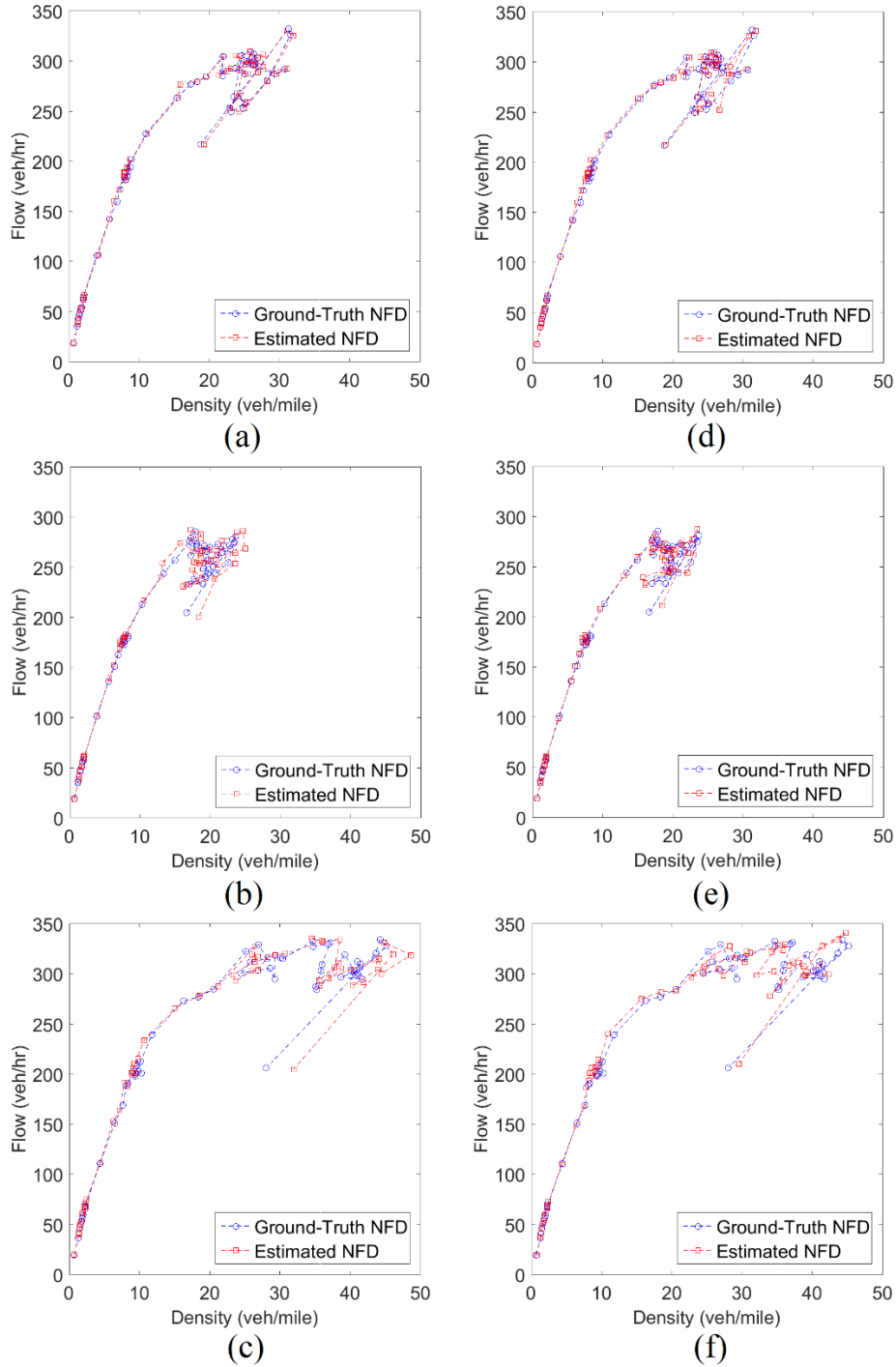


Figure 3-8- Comparison of estimated and actual NFD a) base scenario with  $a=0.6, b=0.2$ , b) decreased-demand scenario with  $a=0.6, b=0.2$ , c) increased-demand scenario with  $a=0.6, b=0.2$ , d) base scenario with  $a=0.6, b=0.6$ , e) decreased-demand scenario with  $a=0.6, b=0.6$ , f) increased-demand scenario with  $a=0.6, b=0.6$

### *3-4-3- Sensitivity to the initial solution*

The proposed methodology and the implemented SA algorithm are robust to the initial solution. To further demonstrate this, different initial solutions are used and the estimated NFDs are presented. In the SA algorithm, the initial solution can affect the number of required iterations to achieve an acceptable optimal solution. The number of iterations is related to the computational efficiency of the algorithm, which was not an issue for the large-scale proposed case study. Therefore, for any initial solution with a proper number of iterations, the optimal solution can be achieved. Here, the model is applied for three different initial solutions with link and OD proportions of  $a=b=0.6$  as an example and the results are compared to demonstrate the robustness of the methodology with respect to the initial solution. Note that the SA algorithm avoids local optimal solutions by accepting the worse solutions in the initial outer loop iterations.

The first and second initial solutions here are generated randomly with different seed numbers. The third initial solution is generated by considering a different distribution of link types relative to the other two initial solutions. Instead of considering a uniform distribution of link types, in this solution, all freeways and ramps are selected. The remaining links for the initial solution are selected randomly among the arterial links with a different seed number relative to the other two initial solutions. Results presented in Figure 3-9 suggest that having a different initial solution does not significantly change the estimated optimal NFD. The values of the objective function for all three initial solutions and their associated optimal objective function values are shown in Table 3-1. This shows that although the initial solutions are different, the estimated NFDs in all three cases are comparable.

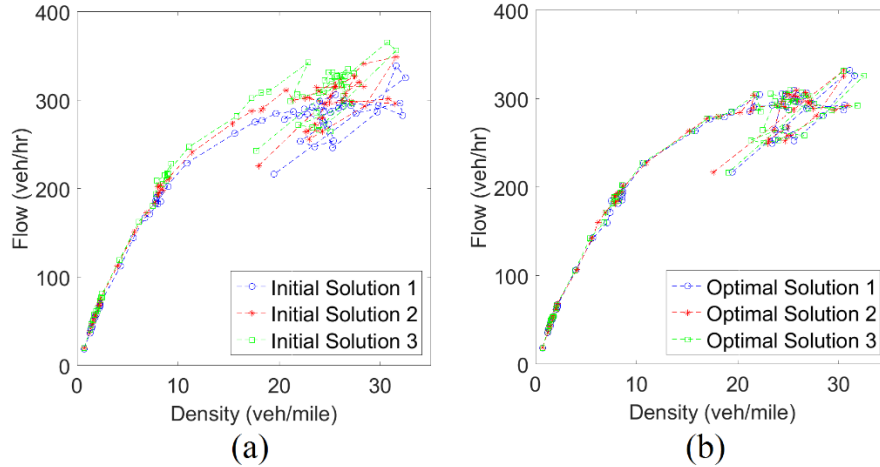


Figure 3-9- (a) Initial and (b) optimally estimated NFDs for three different initial solutions

Table 3-1- Objective function values of the initial and optimal solutions for three different initial solutions

	Objective function value	
	Initial	Optimal
<b>Initial solution 1</b>	2,074	13
<b>Initial solution 2</b>	6,764	22
<b>Initial solution 3</b>	28,506	31

#### 3-4-4- Sensitivity to the availability of trajectories

Here, it is demonstrated that the proposed method is implicitly sensitive to the proportion of trajectories available for each OD pair. The proposed mathematical framework does not optimize the proportions of trajectories for each OD pair as decision variables. Instead, selecting trajectories is based on their availability. Note that not all trajectories may be available for each OD pair. Using a portion of trajectories from each OD pair instead of all trajectories can indeed affect the quality of the space mean speed estimates. Without loss of generality, it is assumed that all trajectories are available for each selected OD pair. As mentioned earlier, the proposed formulation can be easily modified and extended to cases with less than 100% availability of trajectories. To demonstrate the impact of trajectory availability, a fraction of all trajectories is

randomly selected for each OD pair in the network (10%, 25%, and 50%) with a fixed link and OD proportion rates of  $a = 0.6$  and  $b = 0.6$ , and the results are compared with the original case where 100% of trajectories are available (called base case). Note that here, for simplicity, a fixed proportion of trajectory availability is considered for all OD-pairs to demonstrate sensitivity of the method to this parameter. In reality, different proportions might be available for different OD-pairs.

Figure 3-10 shows that the difference between the estimated NFDs for all examined cases is very small. The values of the objective function are significantly improved from initial values (see Table 3-2). This suggests robustness of the method to the proportion of available trajectories. Reducing the fraction of available trajectories has no impact on the number of selected OD pairs and link detectors selected in the estimation process as  $a=b=0.6$ . The optimal objective function value increases with the reduction of the available trajectories, as expected. However, the methodology successfully decreases the objective function value to an acceptable level even for the 10% case. This clearly indicates that the model amends the optimal solution when the availability of trajectories for each OD pair is different. Nevertheless, the estimated NFDs have low errors and good agreement with the ground truth NFD.

In another experiment, the optimal solution (configuration of links and OD pairs) of the base case is utilized to evaluate the objective function for the cases with 50%, 25% and 10% of trajectories available for each OD pair without running the optimization algorithm. The objective function values for each case are also presented in Table 3-2. Results suggest that considering a proportion of trajectories for each OD pair does not affect the objective function, while the solutions (selected links and OD pairs) are different. The formulated mathematical problem aims to find the optimal location of fixed measurement points and set of OD pairs in estimating NFD.

The model responds to the proportion of available trajectories for each OD pair implicitly and as a result, the optimal solution will differ when different proportions are used. However, the model does not explicitly find the optimal proportion of trajectories to be available. It is actually shown that the resulting estimated NFD when a lower proportion of trajectories is available may not affect the estimated NFD as long as there is at least one trajectory going through the links with detectors. Considering that, it is obvious that a greater availability of trajectories may result in higher quality and more reliable estimation.

Table 3-2- Summary statistics of the Base, 50%, 25% and 10% cases; when  $a=b=0.6$

	<b>Initial value of objective function</b>	<b>Optimal value of objective function</b>	<b>Shared OD Pairs with Base case</b>	<b>Shared Link Detectors with Base case</b>
<b>Base case</b>	2,074	29	100%	100%
<b>50% case</b>	3,307	47	70%	64%
<b>50% case using Base Solution</b>	1,654	-	100%	100%
<b>25% case</b>	17,329	73	69%	64%
<b>25% case using Base Solution</b>	16,043	-	100%	100%
<b>10% case</b>	129,905	137	67%	65%
<b>10% case using Base Solution</b>	131,262	-	100%	100%

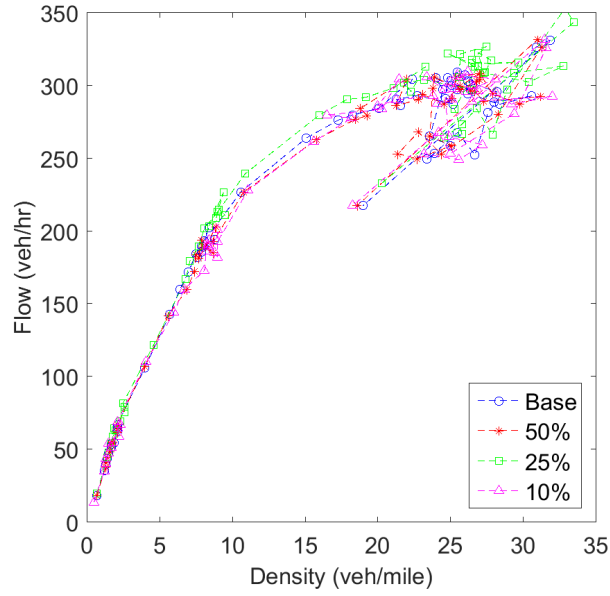


Figure 3-10- Optimal estimation of NFD for the base case (all trajectories available), 50% case (50% of trajectories available), 25% case (25% of trajectories available) and 10% case (10% of trajectories available); when  $a=0.6$  and  $b=0.6$ .

### 3-5- Practical Insights

Here, several insights on the distribution of links and OD pairs for a more accurate estimation of network traffic states (e.g. average network flow and speed) are presented. In real world networks, obtaining a ground truth NFD is almost impossible, given the complexity of network geometry, traffic control, turning movements, changing capacities and OD patterns. It is also almost infeasible to have loop detectors on all links and have access to detailed trajectory of every single vehicle in the network. Therefore, a more practical approach is to estimate NFD using a combination of loop detector and probe vehicle data.

The optimal solution is characterized with three measures: (i) distribution of OD pair distances, (ii) distribution of link types (arterial, freeway, and ramps), and (iii) spatial center of the links in the network. Three different initial solutions are also considered. In the first case, initial

solution is obtained from a synthesized distribution of the OD pair distances, which is different from the overall distribution in the network (Figure 3-11a). In the second case, the initial solution has a different distribution of link types relative to the overall link type distribution across the network (Figure 3-11b). Finally, in the third case, initial solution is obtained such that the spatial center of the selected links is located furthest away from the spatial center of all links in the network (Figure 3-11c). The spatial center of links is defined as the average of the center point of the links weighted by the link lane-length. This measure represents the extent that selected (optimal) links are spatially distributed. These initial solutions are selected to represent a different pattern relative to the original network. Following, specifications of the optimal solution relative to the initial solutions and network overall specifications are explored.

Figure 3-11a shows the normalized frequency of OD pair distances in the network, the synthesized initial solution, and the optimal solution for a fixed link and OD-pair proportions ( $a=b=0.6$ ). While the frequency of OD pair distances in the initial solution follows an almost triangular distribution, the proposed optimization framework results in an optimal solution that follows the overall distribution of OD pair distances in network more closely. The objective function values for the initial and optimal solution are 2038 and 23, respectively. Results further suggest that the proposed method is robust to the initial solution and reveal that the optimal OD pairs for estimating NFD should follow a similar distribution of OD pair distances in the network.

A similar pattern can also be observed from Figure 3-11b where the frequency percentage of link types in the optimal solution almost matches the frequency percentage in the network while the initial solution follows a completely different distribution. Also, Figure 3-11c illustrates the evolution of the spatial center of the links in the initial and optimal solutions compared to the spatial center of the links in the network when  $b=0.6$  and  $a$  varies between 0.2 and 0.8. Regardless

of the location of the initial solution and parameters  $a$  and  $b$ , the optimal solution moves towards the spatial center of all links in the network. The numbers next to the center points on the figure show the average distance of the selected links to the spatial center of the network weighted by the link lane-length as a dispersion measure for selected links. This value is equal to 1.1 km for the network and optimal solutions in all cases. This means that the distribution of the selected links (optimal solution) around the spatial center is similar to the distribution of all the links around the spatial center of the network, which is different for the initial solutions.

Overall, results suggest that for an accurate estimation of network density and flow, when combined loop detector and probe vehicle data are used, selected links and OD pairs should be distributed over the network such that it follows a similar spatial pattern to the network original links and OD pairs distribution. A previous study by Courbon and Leclercq (2011) suggested that loop detectors should be uniformly distributed within links across the network. Findings of this study suggest that the selection of an appropriate set of links with loop detectors and OD pairs are also important. It was shown that a uniform distribution across the network may not necessarily result in optimal solution. Instead, distribution of links and OD pairs should follow the same distribution of links and OD pairs in the network.

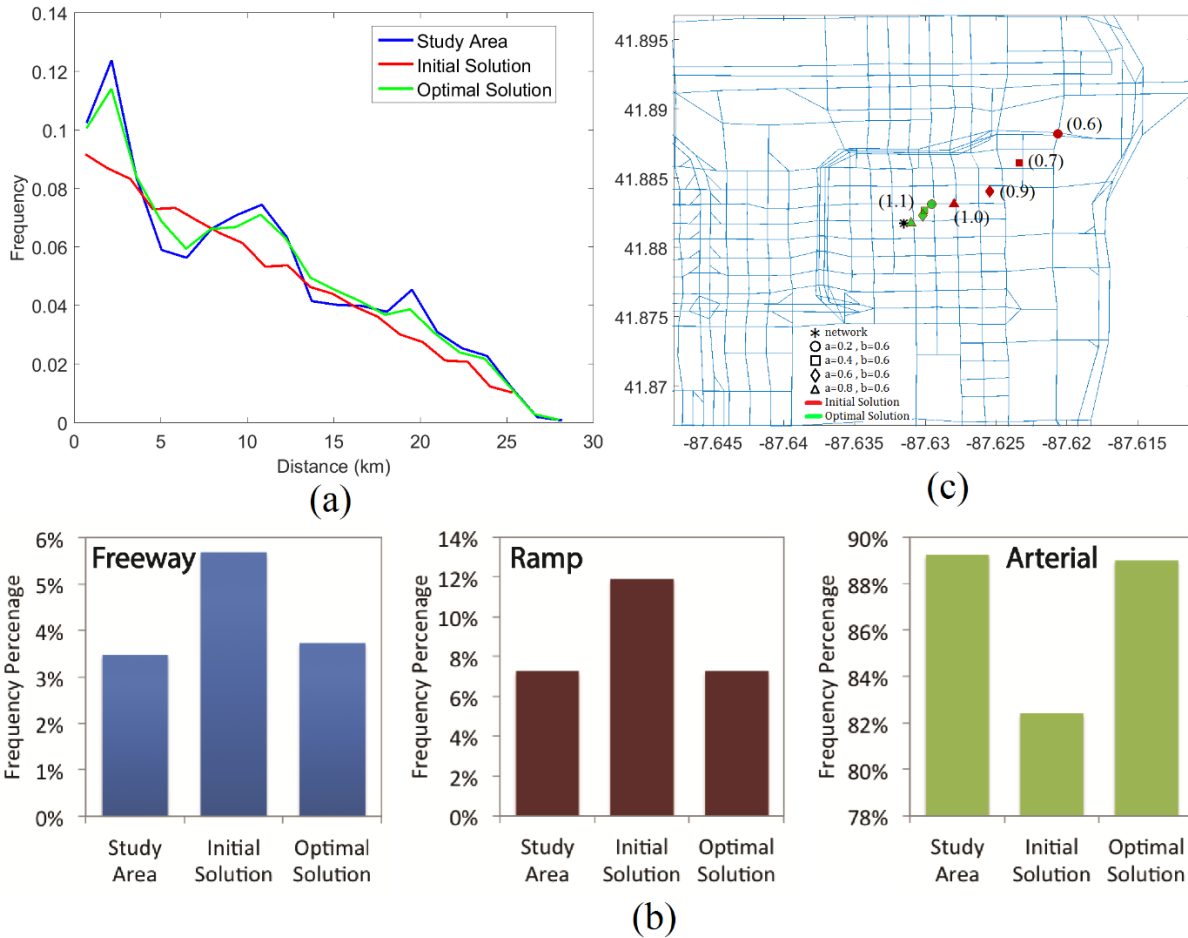


Figure 3-11- Normalized frequency of OD pair distances for  $a=b=0.6$ , (b) Frequency percentage of link types for  $a=b=0.6$ , (c) Evolution of the spatial center of the links in the initial and optimal solutions compared to the spatial center

### 3-6- Summary

This chapter presents a mathematical model and solution algorithm to find the optimal location of fixed measurement points and sampling of probe trajectories in a resource allocation problem framework to estimate NFD in a large-scale heterogeneous network with asymmetric demand. The major findings of the chapter are summarized below:

- A combination of fixed detectors and probe vehicles provides sufficient data to estimate NFD with minimal deviation from the ground-truth NFD in a heterogeneous network.

- When the proportion of fixed detection points is constant, increasing the proportion of probe trajectories does not necessarily improve the estimated NFD under the same conditions, however, it might improve reliability of NFD estimation under general traffic conditions.
- When the proportion of probe trajectories is constant, increasing the proportion of fixed measurement points improves the estimated NFD.
- The optimal locations of fixed measurement points are not only a function of the proportion rate of fixed measurement points; rather, it also changes when the proportion of probe trajectories varies.
- The optimal set of OD pairs is not only a function of the proportion rates of OD pairs; rather, it also changes when the proportion rates of fixed measurements varies.

## **CHAPTER 4 – Traffic State Estimation in Heterogeneous Networks with Stochastic Demand and Supply**

### **4-1- Overview**

Stochastic variations in network demand and supply due to weather conditions, incidents, special events, work zones, and service interruptions may significantly affect the approximation of an NFD. This chapter aims to propose a modified framework to estimate network traffic states to observe NFD while capturing the stochasticity in transportation networks. It actually presents a modified version of the previous chapter formulation. A mixed integer problem with non-linear constraints is formulated to address stochasticity in the NFD estimation problem. To solve this NP-hard problem, a solution algorithm based on the Simulated Annealing method is applied. The problem is formulated and the solution algorithm is implemented to find an optimal configuration of loop detectors and probe vehicles to estimate the NFD of the Chicago downtown network and capture its day-to-day variations, considering a given available budget. The main contribution of this chapter is to capture stochasticity in demand and supply sides to find a more robust subset of links and trajectories to be acquired for the NFD estimation.

Incorporating the data collected by probe vehicles, known as the Lagrangian approach, and fixed loop detectors, known as the Eulerian approach, facilitates the estimation of an NFD (Leclercq et al., 2014; Nagle and Gayah, 2014; Ortigosa et al., 2014). To overcome the limitations of recent studies, the previous chapter proposed a resource allocation formulation to estimate an NFD using a mixed Lagrangian-Eulerian approach. In Chapter 3, the NFD estimation was facilitated with an optimal fusing of fixed measurement points data and sample vehicle trajectories based on the available budget without requiring any assumption on the penetration rate of probe vehicles on each link.

Although the proposed model in the previous chapter addressed the main limitation of several previous studies, it does not capture the impacts of the day-to-day variations in network demand and supply on the optimal configuration of loop detectors and probe trajectories. So, there is a need to further explore the effect of stochasticity due to demand variation in observation and estimation of an NFD. Figure 4-1 establishes this need by showing NFDs associated with the AM-peak period of two different weekdays for the Chicago downtown network. The NFDs are estimated based on complete data from a dynamic traffic simulation for the selected two days where the input of the simulation model varies based on the observed weather conditions, incidents, and demand level (estimated using total observed counts at all available loop detectors). The figure shows that the fluctuation in network input can significantly alter the shape and characteristics of the NFD.

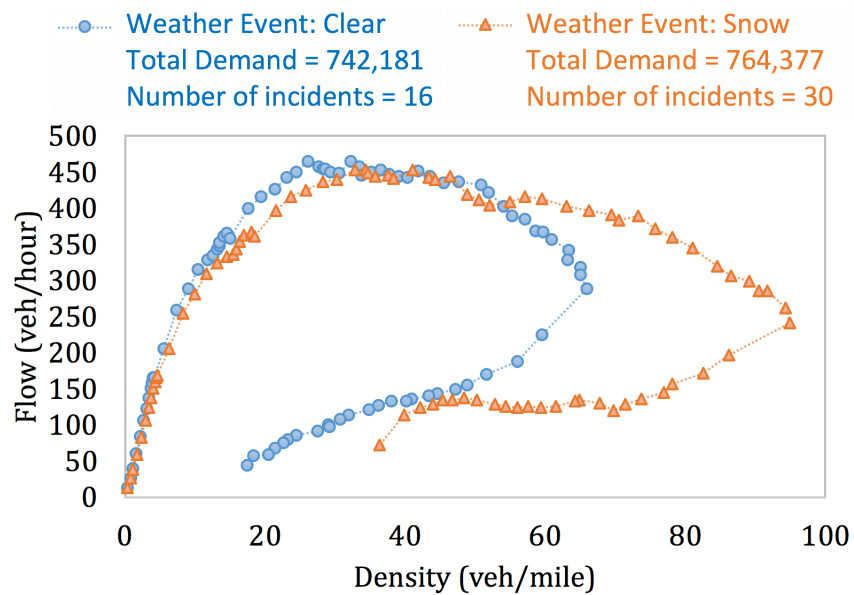


Figure 4-1- Estimated NFDs of the AM-peak period for Chicago downtown network on two days with different observed operational conditions

To capture the effects of stochasticity due to network demand and supply variation in estimation of the NFD, the model proposed in the previous chapter is modified in this study. To this end, the mathematical optimization framework for NFD estimation is updated to capture the resource limitation, traffic heterogeneity, and stochasticity due to day-to-day network demand and supply variations. To estimate the NFD, information from fixed measurement points and probe vehicle trajectories are incorporated and applied to a large-scale real-world network. The main objective, therefore, is to peruse the NFD estimation by solving a resource allocation problem where the network demand and supply vary across multiple days.

The difference between a measured ground-truth NFD and an estimated NFD (based on the selected Lagrangian and Eulerian observations in the simulation model) is calculated for each scenario based on the network demand and supply settings. The sum of these values over all scenarios is minimized by the proposed mathematical model that finds the optimal sub-set of fixed measurement points and probe trajectories while subject to a budget constraint restriction. In the proposed model, the flow information is obtained from the detectors installed on the optimally selected links. However, to use the flow information from a detector, there should be at least one probe trajectory passing through the link to acquire the link's space mean speed information. The pre-known ground-truth NFDs of different scenarios are used as inputs to the proposed framework. Since the ground-truth NFD might not be available, especially under different network demand and supply settings, a surrogate ground-truth NFD is required to be extracted by simulation or an analytical method. The sensitivity of the proposed model to demand variation is discussed in the previous chapter. Note that this study also estimates the network traffic state, which is not obtainable as a historical ground-truth NFD, to be monitored in real-time to incorporate proper control strategies.

The formulated mixed integer problem (MIP) in this study contains non-linear constraints and is an NP-hard problem. MIP refers to the optimization problems that contain both continuous and discrete variables. MIP is utilized to model complex planning and control problems. The main objective is to capture non-convexity by MIP. Although the concept of MIP is not new, the advent of new generation computers proliferated its application. The problem presented in this study is even more complicated due to the non-linear constraints, which provide many locally optimal solutions for the proposed model. Therefore, there is no analytical method to obtain the optimal solution. To solve the problem, a heuristic solution technique based on the Simulated Annealing (SA) concept is employed. This is the same solution algorithm implemented in the previous chapter, which is adjusted here to capture the stochasticity.

A randomly selected initial solution triggers the algorithm and is set as the current solution. Then, a neighbor solution is iteratively and randomly selected, and its objective value is compared with the objective value of the current solution. If the objective value decreases, the neighbor solution will replace the current solution. Also, to avoid being trapped in the local optimal solutions when the objective value is not reduced, the neighbor solution is probabilistically accepted. This probability should be decreased in each iteration to certify the convergence of the algorithm. The final links selected to be equipped with loop detectors and the sample trajectories account for the stochasticity due to day-to-day network demand and supply perturbations. It is shown that how this stochasticity may affect the estimated NFD. To this end, the deterministic and stochastic solutions are compared for different scenarios and show the superiority of the stochastic solution in reflecting the estimated NFDs.

## 4-2- Model Formulation

In this section, building upon the previous chapter, the stochastic NFD estimation is formulated as a resource allocation problem to find the optimal solution given a fixed data provision budget. This solution provides the optimal set of links that should be equipped with loop detectors and the optimal set of OD-pairs whose vehicle trajectories should be collected. Information provided by loop detectors is utilized to estimate the average flow, and data from probe samples are employed to estimate the space-mean speed. Then, the next step is to calculate the density using the fundamental identity equation for each budget scenario. Finally, the objective function will be calculated using Equation 4-1, which is the weighted sum of squared deviations between the ground-truth and estimated average values of density and flow at different time steps for different network demand and supply settings (traffic scenarios).

Model constraints limit the number of links selected to be equipped with loop detectors and the number of probe trajectories based on the available budget. The optimal solution for the proposed model contains the fixed measurement points and OD pairs that give estimated NFDs with minimum deviation from ground-truth NFDs over all given traffic scenarios for different network demand and supply settings. The proposed problem formulation in this chapter is developed based on updating the model presented in the previous chapter to capture stochasticity. The main updates include the definition of the key variables to reflect the scenarios, and modification of the objective function to sum the deviations in the flow and density estimation over all traffic scenarios. However, the structure of the constraints remains the same. The model formulation is as follows.

$$\text{Min } \sum_{s=1}^S \sum_{t=1}^T \left[ \zeta (Q_{st} - \hat{Q}_{st})^2 + \eta (K_{st} - \hat{K}_{st})^2 \right] \quad (4-1)$$

Subject to

$$Q_{st} = \frac{\sum_{i=1}^I (q_i^{st} l_i)}{\sum_{i=1}^I l_i} \quad \forall t = 1, \dots, T, \forall s = 1, \dots, N \quad (4-2)$$

$$K_{st} = \left[ \sum_{i=1}^I (l_i q_i^{st} / v_i^{st}) \right] / \sum_{i=1}^I l_i \quad \forall t = 1, \dots, T, \forall s = 1, \dots, N \quad (4-3)$$

$$\hat{t}t_i^{st} = \frac{\left[ \sum_{j=1}^J \sum_{k=1}^{K(j,s)} (p_{ijk}^{st} \tilde{t}t_{ijk}^{st} y_j) \right]}{\left[ \sum_{j=1}^J \sum_{k=1}^{K(j,s)} (p_{ijk}^{st} y_j) \right]} \quad \forall t = 1, \dots, T, \forall i = 1, \dots, I, \forall s = 1, \dots, N \quad (4-4)$$

$$\hat{v}_i^{st} = l_i / \hat{t}t_i^{st} \quad \forall t = 1, \dots, T, \forall i = 1, \dots, I, \forall s = 1, \dots, N \quad (4-5)$$

$$\sum_{j=1}^J \sum_{k=1}^{K(j,s)} (p_{ijk}^{st} y_j) \leq z_i^{st} M \quad \forall t = 1, \dots, T, \forall i = 1, \dots, I, \forall s = 1, \dots, N \quad (4-6)$$

$$z_i^{st} \leq \sum_{j=1}^J \sum_{k=1}^{K(j,s)} (p_{ijk}^{st} y_j) \quad \forall t = 1, \dots, T, \forall i = 1, \dots, I, \forall s = 1, \dots, N \quad (4-7)$$

$$z_i^{st} + x_i - 1 \leq w_i^{st} \quad \forall t = 1, \dots, T, \forall i = 1, \dots, I, \forall s = 1, \dots, N \quad (4-8)$$

$$w_i^{st} \leq z_i^{st} \quad \forall t = 1, \dots, T, \forall i = 1, \dots, I, \forall s = 1, \dots, N \quad (4-9)$$

$$w_i^{st} \leq x_i \quad \forall t = 1, \dots, T, \forall i = 1, \dots, I, \forall s = 1, \dots, N \quad (4-10)$$

$$\hat{Q}_{st} = \left[ \sum_{i=1}^I (l_i q_i^{st} w_i^{st}) \right] / \left[ \sum_{i=1}^I l_i w_i^{st} \right] \quad \forall t = 1, \dots, T, \forall s = 1, \dots, N \quad (4-11)$$

$$\hat{K}_{st} = \left[ \sum_{i=1}^I \left( \frac{q_i^{st}}{\hat{v}_i^{st}} l_i w_i^{st} \right) \right] / \left[ \sum_{i=1}^I (l_i w_i^{st}) \right] \quad \forall t = 1, \dots, T, \forall s = 1, \dots, N \quad (4-12)$$

$$\sum_{i=1}^I c_i x_i + \sum_{j=1}^J f_j y_j \leq B \quad \forall s = 1, \dots, N \quad (4-13)$$

$$x_i = 0 \text{ or } 1 \quad \forall i = 1, \dots, I, \forall s = 1, \dots, N \quad (4-14)$$

$$y_j = 0 \text{ or } 1 \quad \forall j = 1, \dots, J, \forall s = 1, \dots, N \quad (4-15)$$

$$z_i^{st} = 0 \text{ or } 1 \quad \forall i = 1, \dots, I, \forall s = 1, \dots, N \quad (4-16)$$

$$w_i^{st} = 0 \text{ or } 1 \quad \forall i = 1, \dots, J, \forall s = 1, \dots, N \quad (4-17)$$

In the formulation, use of binary decision variables  $x$  and  $y$  specify if a link or OD pair is selected, respectively. If a link  $i$  is equipped with a detector, then  $x_i = 1$ , and if an OD pair  $j$  is considered to obtain data trajectory, then  $y_j = 1$ . Furthermore,  $z$  and  $w$  are the main binary state variables whose definitions are updated relative to the last chapter. Variable  $z$ , based on the decision variable  $y$  over OD pairs, indicates that if any trajectory crosses the link  $i$  at time  $t$  for scenario  $s$ . Variable  $w$  indicates whether the link should be included in the calculation of average values for the flow and density at the network level or not, based on the detector availability (specified by  $x$ ) and trajectory data crossing the link (specified by  $z$ ). For link  $i$ , time interval  $t$ , and scenario  $s$ ,  $w_i^{st} = 1$  when  $x$  and  $z$  are equal to one for ordered triple of  $(i, t, s)$ .

In Equation 4-1,  $s$  is the scenario index for different days,  $S$  is the total number of scenarios,  $t$  is the time interval index,  $T$  is the total number of time intervals,  $Q_{st}$  and  $\hat{Q}_{st}$  are ground-truth and estimated network-wide average flow at time interval  $t$  for scenario  $s$ ,  $K_{st}$  and  $\hat{K}_{st}$  are ground-truth and estimated network-wide average density at time interval  $t$  for scenario  $s$ , and  $\zeta$  and  $\eta$  are

the weight factors for minimizing the deviations between the estimated and ground-truth network-wide average flow and density, respectively. Equation 4-1 presents the objective function that includes a weighted sum of two main terms over different time intervals and traffic scenarios. The first term presents the difference between the estimated and ground-truth network-wide average flow. The second term calculates the difference between the estimated and ground-truth network-wide average density. Equation 4-1 minimizes the total objective function value over all the time intervals and scenarios. The objective function value for each time interval and scenario is defined as the deviation between the estimated network-wide average values, which are calculated using only the optimal links and trajectories, and ground-truth values, which are calculated using all links and trajectories.

Equations 4-2 and 4-3 calculate the ground-truth NFD for each time interval and scenario assuming all links and trajectories are available. In this equation,  $i$  is the link number index,  $I$  is the total number of links in the network,  $l_i$  is the lane-length of link  $i$ , and  $q_i^{st}$  and  $v_i^{st}$  are the flow and space-mean-speed of link  $i$  at time interval  $t$  for scenario  $s$ . Equation 4-2 uses network-wide link flows and finds the weighted average flow in the network based on link lengths. Equation 4-3 finds the average network-wide density for each scenario and each time interval similar to Equation 4-2. It incorporates the ratio of the link flow to the link space-mean speed to estimate density for each link.

Equation 4-4 presents the average travel time for each link, time interval, and scenario. In this equation,  $k$  is the trajectory index for origin-destination pairs,  $j$  is the index of the origin-destination pair,  $J$  is the number of origin-destination pairs in the network,  $K(j, s)$  is the number of available trajectories for origin-destination pair  $j$  in scenario  $s$ ,  $p_{ijk}^{st}$  is a binary parameter determining if the  $k^{th}$  trajectory of origin-destination pair  $j$  includes link  $i$  at time interval  $t$  for

scenario  $s$ ,  $\tilde{t}_{ijk}^{st}$  is the observed travel time at link  $i$  and time interval  $t$  for the  $k^{th}$  trajectory of origin-destination pair  $j$  for scenario  $s$ , and  $\hat{t}_i^{st}$  is the observed average travel time at link  $i$  and time interval  $t$  for the available trajectory of selected origin-destination pairs for scenario  $s$ . Travel times experienced by probe vehicles at the scenario and time interval of interest are utilized to calculate the average travel time of each link. Simply, in order to calculate the average travel time for the ordered triple  $(i,t,s)$ , this equation considers all the trajectories in the solution. If they have crossed the link  $i$ , it sums up the experienced travel time for link  $i$  along the trajectory with departure time  $t$  with the total travel time for that link, time interval, and scenario. Then it makes an average value by dividing the total experienced travel times for each link in each time interval and scenario by the total number of trajectories associated with it.

Equation 4-5 finds the estimated space-mean speed of each link, time interval, and scenario based on the length of the link and its average travel time. In this equation,  $\hat{v}_i^{st}$  is the calculated space-mean speed from probe trajectories for scenario  $s$ , at link  $i$  and time interval  $t$ . Equations 4-6 and 4-7 are feasibility constrained. In Equation 4-6,  $M$  is a large number. Equation 4-6 ensures that for each time interval and scenario, if there is no trajectory crossing link  $i$  for OD pairs in the optimal solution (which means  $z_i = 0$ ), then there is no probe vehicle for the OD pairs crossing link  $i$  for that specific time interval and scenario. In other words, if there is at least one trajectory that crosses link  $i$  for a specific OD at a given time interval and scenario,  $z$  must be equal to 1 for Equation 4-6 to hold. In this case, Equation 4-7 is not binding. But when such trajectory is not available, based on Equation 4-7,  $z$  for that link at the given time interval and scenario is enforced as zero. Therefore, Equation 4-6 would not be binding. For the sake of simplicity, it is assumed that when an OD pair is chosen, all of its trajectories are available for the NFD estimation. To account for other assumptions, another binary variable should be added to the formulation.

Equations 4-8 to 4-10 show the relationship among the binary variables. They specify if a link and time interval in a certain scenario should be included in the network-wide average calculations considering the availability of both fixed measurement locations and probe vehicles crossing that link (specifying  $w$  based on  $x$  and  $z$ ).

Equations 4-11 and 4-12 respectively calculate the estimated network-wide average flow and the network-wide average density for each time interval and scenario for the cases meeting the  $w_i^{st} = 1$  condition. Equation 4-13 is the budget constraint. In this equation,  $c_i$  and  $f_j$  are respectively the data collection cost associated with installing a loop detector in link  $i$  and the cost of adding a probe trajectory data to the available probes from origin-destination pair  $j$ , and  $B$  is the given budget. Finally, constraints 4-14 to 4-17 are feasibility constraints for different variables.

It is noteworthy that although the model modifications relative to the previous chapter seem to be trivial, the computational complexity is not comparable in the two studies due to the additional dimension in the data structure (scenarios). Computational complexity does not vary linearly by the number of scenarios, resulting in a much more complex problem. Thus, special remedies (e.g. setting number of main and inner iterations) were needed to improve the computational efficiency of the solution algorithm. Moreover, the new proposed model has significant practical implications, especially when a low data collection budget is available.

### **4-3- Solution Algorithm**

The presented MIP minimizes the total difference between the estimated and ground-truth NFDs over all scenarios. The NFD estimation is based on known percentages of links and trajectories, which are constrained by the limited data collection budget. The ground-truth NFD is known through simulation or other methods using all network links and trajectories. The proposed model is NP-hard and requires a metaheuristic algorithm to be solved in a reasonable time. The

algorithm used in this study to solve the proposed mathematical model is based on the Simulated Annealing (SA) approach. SA has been widely used to solve NP-hard problems. The discussed problem contains non-linear constraints, which may result in numerous local optima. This obstacle can be overcome by using proper metaheuristic algorithms. SA is one such algorithm that can find the optimal solution without getting stuck in locally optimal solutions.

Therefore, this study follows the Metropolis algorithm (Hejazi, 1999; Metropolis et al., 1953) and the framework presented in Zockaie et al. (2016) and Ghamami et al. (2016) to implement the SA method. The metaheuristic solution method proposed in this study begins with a feasible initial solution that is set as the current solution. After calculating the objective function based on the current solution,  $C(\cdot)$ , it moves to a neighbor solution through a local search. Then, it evaluates the new objective function for the neighbor solution. The new objective function value is compared to the objective function value of the current solution. If the new solution improves the objective function, then the neighbor solution becomes the new current solution. Even for the cases where the objective function does not improve, the algorithm may move to the neighbor solution probabilistically based on the difference in the objective function values and a control parameter. The probability of accepting a worse solution decreases as the algorithm advances by changing the control parameter to ensure the convergence of the algorithm. This mechanism helps the SA algorithm to not get trapped in local optimum solutions. The above process continues until it reaches the equilibrium point where the objective function value cannot be further improved. Figure 4-2 illustrates the proposed solution framework based on the SA algorithm.

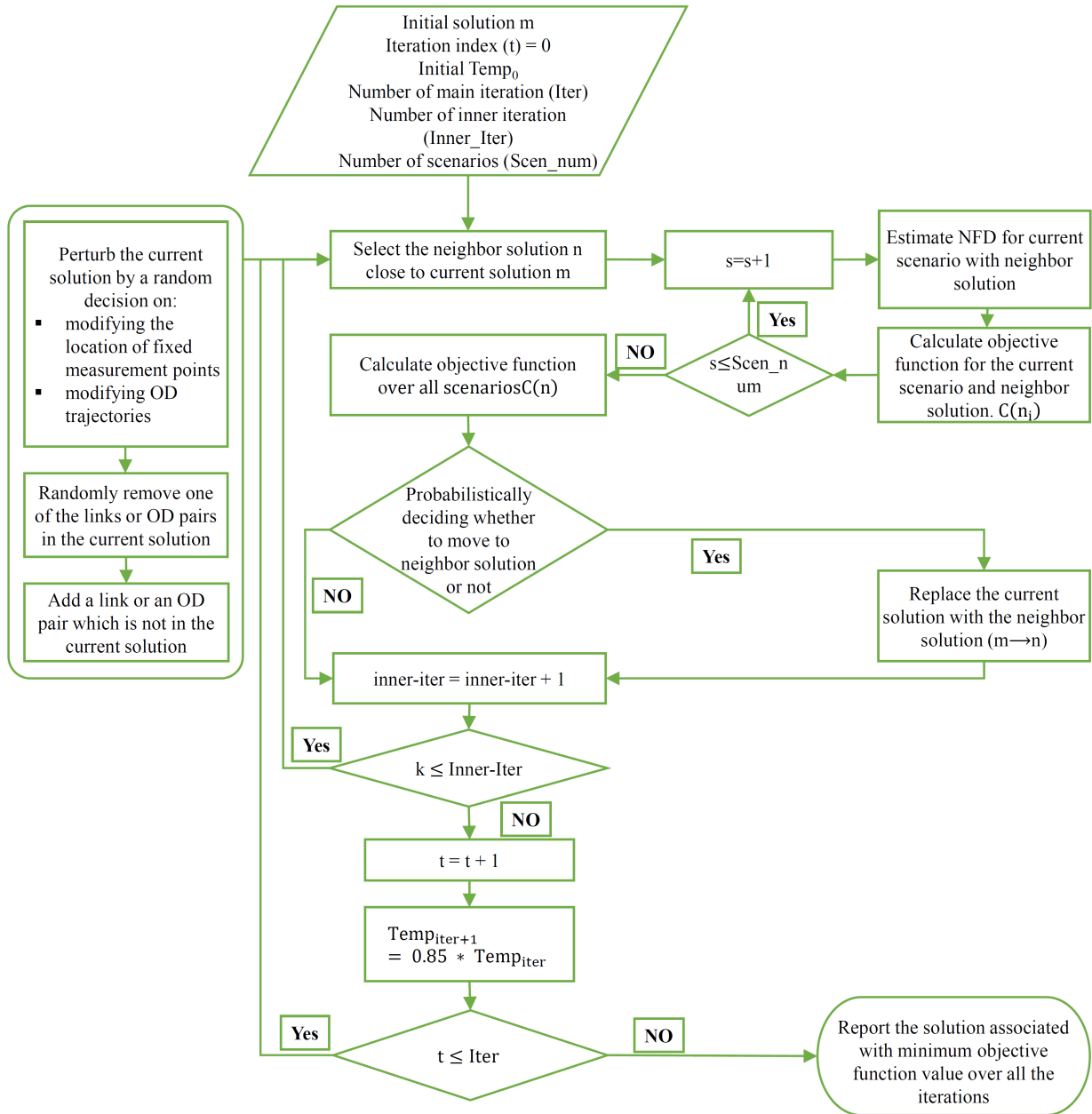


Figure 4-2- The proposed solution framework based on the SA algorithm

### Algorithm

**Input:** Maximum number of main iteration  $Iter$ , maximum number of inner iterations  $Inner\_Iter$ , number of scenarios  $Scen\_num$ , budget.

**Output:**  $x^*$  and  $y^*$

**Initialize:**

An initial random solution (based on the budget constraint, assign 0 or 1 to variables  $x$  and  $y$  for different sets of  $i$  and  $j$ )  $x'^t$  and  $y'^t$

Set the current temperature stage  $t = 0$ , choose initial temperature  $Temp_t$

Set main iteration index  $iter = 0$

Calculate the objective function based on the current solution  $C'(t)$

**While  $t < Iter$ , do**

Set inner iteration index  $k = 0$ . Set  $x^k = x'^t$ ,  $y^k = y'^t$  and  $C(k) = C'(t)$

**While  $k < Inner\_Iter$ . do**

Set  $k = k + 1$

Find a neighbor solution  $x^k$  and  $y^k$  close to the current solution by perturbing either the  $x$  or  $y$  value for a specific  $i$  or  $j$  by taking the budget into account

Set  $s=0$  and  $C(k) = 0$

**While  $s < Scen\_num$** 

Set  $s = s + 1$

Estimate NFD for the current scenario with the neighbor solution

Calculate the objective function for the scenario  $C(k_s)$

$$C(k) = C(k) + C(k_s)$$

**End while**

Draw a random number  $\varepsilon = u[0,1]$ .

**If  $C(k) < C^*$  then**

$$C^* = C(k), x^* = x^k \text{ and } y^* = y^k$$

**End if**

**If**  $C(k) < C(k - 1)$  **then**

$$C'(t) = C(k), x'^t = x^k \text{ and } y'^t = y^k$$

**Elseif**  $\exp\left(\frac{C(k)-C(k-1)}{Temp_t}\right) > \varepsilon$  **then**

$$C'(t) = C(k), x'^t = x^k \text{ and } y'^t = y^k$$

**Else**

Discard the neighbor solution

**End if**

**End while**

Set  $t=t+1$ ,  $C'(t) = C(k)$ ,  $x'^t = x^k$  and  $y'^t = y^k$ ,  $Temp_t = \theta Temp_{t-1}$ , where  $\theta = 0.85$ .

**End while**

Report the optimal solution  $C^*$ ,  $x^*$  and  $y^*$

---

Several remarks are helpful to implement the algorithm efficiently. First, the initial temperature and the reduction rate in each iteration affect the required number of iterations for convergence. Following the previous chapter, the initial temperature is considered to be  $Temp_0 = 0.05$  and is decreased by 0.85 factor for each outer iteration. Second, generating the random neighbor solution is based on the assumption of a uniform cost between all links and all OD pairs for installing loop detectors or being equipped with probe vehicles, respectively. Therefore, considering the available proportional budget for loop detector installment or probe vehicle trajectories data collection, the number of links and ODs are limited based on the given budget. Third, it is assumed that  $\zeta = \eta = 1$ , which implies that the deviation of the estimated flows and densities from their ground-truth values are weighted equally in the objective function. While this

assumption doesn't violate the generality of the modeling framework, estimating the best values for different designs is beyond the scope of this study.

To further clarify the process of finding the neighbor solution, it is important to know that proportion rates  $c$  and  $f$  used in the budget constraint as inputs to the model are the deciding factors for the number of selected links and OD pairs. These parameters are different from the penetration rates of probe vehicles as is mentioned in Chapter 2. They represent the proportion of the estimated budget for providing all the possible loop detectors or probe vehicles. As a uniform cost is assumed for links and OD pairs,  $c$  and  $f$  provide the percentage of links and OD pairs relative to the total number. A group of links and OD pairs are selected randomly to generate the initial solution and are then labeled as the current solution. For the neighbor solution, the algorithm modifies the set of links or the set of OD pairs based on a random variable. According to this modification, a randomly selected link or OD pair is removed from the current solution and is replaced by another link or OD pair, which does not belong to the current solution. With this approach, the budget constraint is always met.

#### **4-4- Numerical Results**

This section presents the case study used for the application of the proposed model. Here, the description of the study network is followed by the numerical results to assess the performance of the proposed algorithm. Downtown Chicago is selected as the large-scale study network. The proposed formulation uses the ground-truth values of flow and density as inputs; these values may not be available or may only be available under limited conditions. Therefore, a surrogate of the ground-truth NFD is used in this study. For small networks, surrogate NFDs can be extracted using analytical and experimental methods. However, for large-scale networks, mesoscopic traffic simulation models can be employed. In this study, the surrogate of the ground-truth NFD is

measured by a calibrated simulation-based dynamic traffic assignment (DTA) model implemented on the Chicago downtown network. The real-world observations from 86 weekdays in winter 2010 are utilized to estimate the ground-truth NFDs as accurate as possible. Different levels of demand, weather conditions, incidents, and routing policies are considered to generate travel time variations in each scenario. For each scenario, a demand factor, which represents the different levels of demand among scenarios, is calculated using the observations of loop detectors (associated with each day/scenario) installed on freeways. Visibility, and rain and snow precipitation intensities are the three measures describing the weather conditions for each scenario. Weather data are extracted from the Automated Surface Observing System (ASOS) station at the Chicago Midway International Airport for each day/scenario. Incident data for each scenario, include the location and time of the occurred incident on each day, and their severity in terms of the capacity drop. These data are obtained from the Illinois Department of Transportation. The actual data of different weather conditions, number of incidents, and OD tables are provided to the simulation tool to extract NFDs. Based on the ground-truth NFDs, an optimal set of links and OD pairs is found for any given budget. The robustness of the scenarios is the main advantage of this method over the deterministic NFD estimation method.

Note that the major contribution of this chapter relative to the previous chapter is capturing the stochasticity. One cannot fully capture stochasticity by counting all possible scenarios due to an endless number of scenarios that may occur at the network level in the real world. Thus, 86 scenarios generated based on data collected over 86 real days are utilized to capture stochasticity. These scenarios, while can be handled reasonably in terms of the computational complexity, provide an acceptable level of stochasticity at the network level while considering different weather conditions, crashes, and demand levels based on actual data sets.

#### 4-4-1- Study Network

In order to implement the proposed framework and to measure the ground-truth NFD, DYNASMART-P (Mahmassani, 1994) is employed as the traffic simulation tool. It generates the trajectory of all vehicles during the simulation time. The large-scale network used in this study, downtown Chicago, is bound from West and East by O'Hare airport and Lake Michigan, respectively. This network includes 4,805 links, 1,578 nodes, and 218 zones. The simulation horizon used in this study is the morning peak period (5:00 AM to 10:00 AM). Chicago Metropolitan Agency for Planning (CMAP) has provided the information of daily demand for the Chicago Regional network. Using the technique presented in Zockaie et al. (2014a), the deterministic demand is converted into a time-dependent OD demand matrix for the extracted sub-network (Chicago downtown network), which provides almost 550,000 vehicles traveling in the sub-network during the AM peak period. The case study considered here for the NFD estimation is the area located in the middle of Chicago downtown sub-network (Figure 4-3), which includes 921 links and 9,406 OD pairs with positive demand.

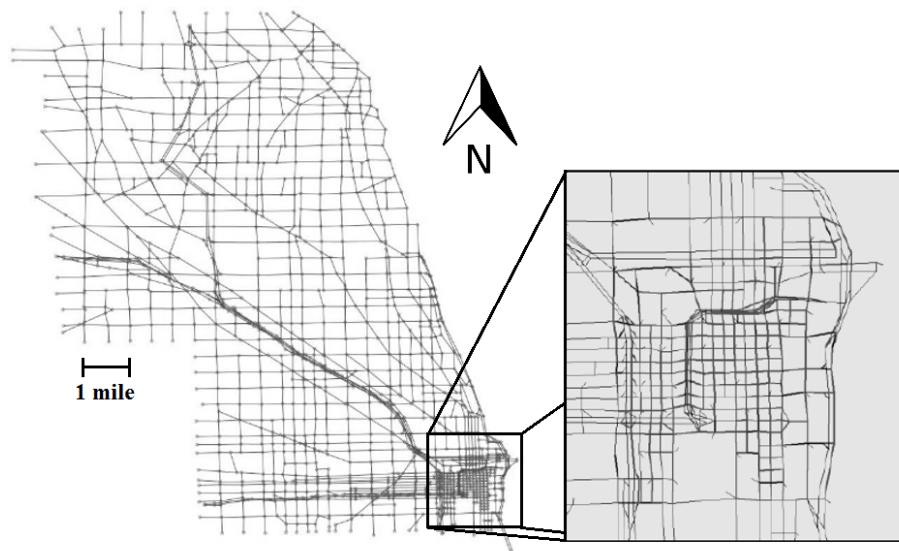


Figure 4-3- Chicago network and its CBD area considered for the NFD estimation

For each demand scenario, the number of OD pairs depends on the travel pattern on that day. This sub-network, Chicago CBD, is the most congested district of the greater Chicago area network. Also, the traffic distribution is more homogeneous there compared to the entire network. Moreover, the NFD is more sensitive to the demand in this area because in less congested areas there are many links with flows below their capacity. As the NFD values are calculated using the total average over the selected area, these links alleviate the effect of peak hour demand in the network. Therefore, the NFD for the whole Chicago network for the AM peak period remains almost the same while for the downtown area changes drastically.

#### *4-4-2- Results*

It is first examined that how considering the stochasticity affects the optimal objective value, which indicates the deviation of the estimated NFDs from the ground-truth NFDs over different scenarios. To this end, NFDs of two randomly selected scenarios (out of 86 actual days) are estimated applying three different methods: simulation (ground-truth), using the solution of the deterministic approach as proposed in Chapter 2, and using the solution of the stochastic approach presented in this chapter. Figure 4-4 indicates the results for the two selected scenarios. The ground-truth NFDs for both scenarios are simulated using DYNASMART-P and follow a smooth trend. Objective functions (Equation 4-1) of the NFDs estimated by the stochastic solution hold values less than 750 for both scenarios A and B. Considering the nature of the objective function, which represents the sum of squared values, the obtained objective values by the stochastic method (746 and 682) show that the estimated NFDs imitate the ground-truth NFDs with an acceptable accuracy. The third NFD for both scenarios A and B are estimated using the deterministic solution of scenario A. It is quite clear that using the deterministic solution of scenario A to estimate the NFD of the same scenario leads to minimal deviation (=64) from the ground-truth NFD (this was

shown in Chapter 2). However, using the deterministic solution of scenario A to estimate the NFD of scenario B results in a higher objective value (2,392), which is significantly greater than the objective value estimated by the stochastic method (=682). In Figure 4-4(b), although the stochastic and deterministic NFDs follow the same shape, there is about 10% error in the estimation of the maximum network-wide average density once the deterministic approach is used (based on scenario A). This is a significant amount at the network level. This shows the importance of considering stochasticity in NFD estimation. Figure 4-5 depicts the convergence pattern for 4 budget configurations  $\{(a=0.2, b=0.2), (a=0.4, b=0.4), (a=0.6, b=0.6), (a=0.8, b=0.8)\}$ .

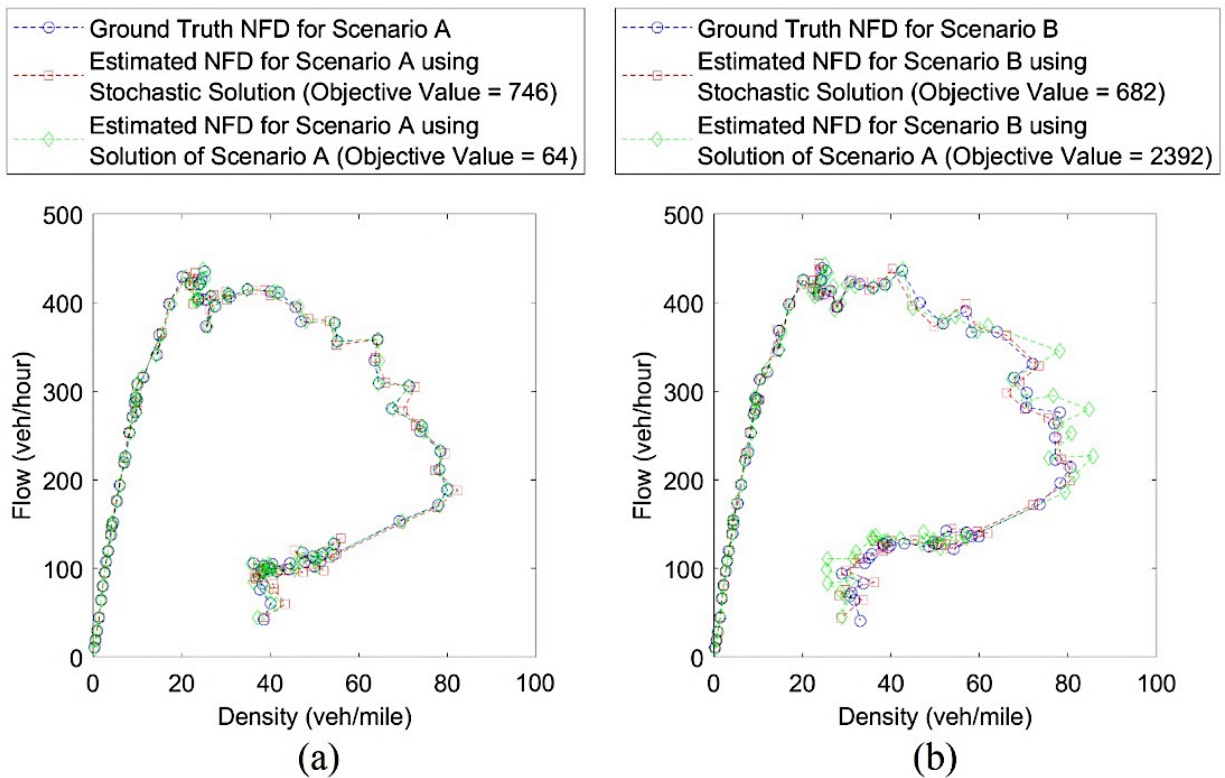


Figure 4-4- Estimated NFDs for two randomly selected scenarios A and B using three methods: simulation (ground-truth), the stochastic solution, and the deterministic solution based on scenario A

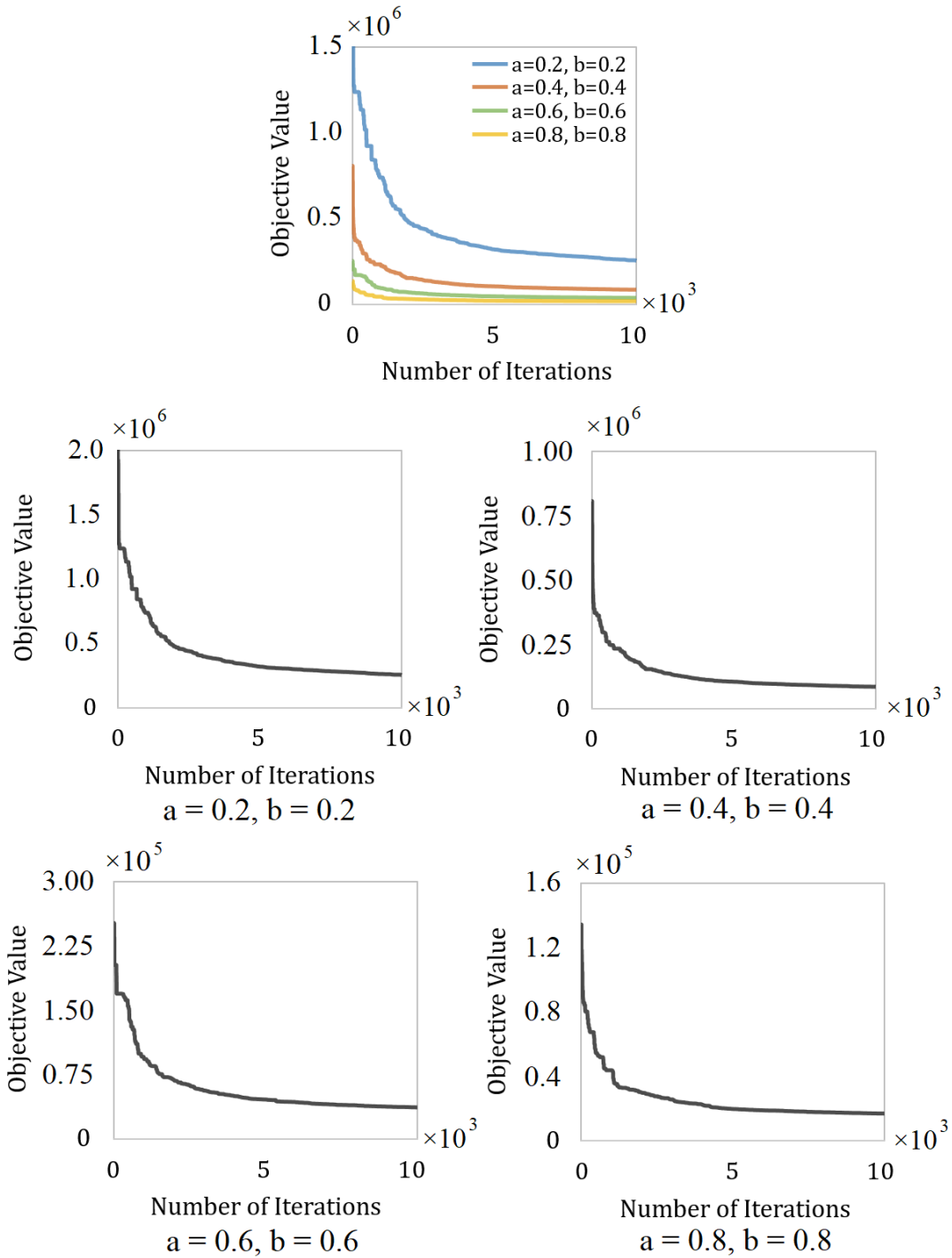


Figure 4-5- Convergence pattern for different budget scenarios

Note that here  $a=0.2$  means the budget is available to equip 20% of all links with loop detectors and  $b=0.2$  represents an available budget to obtain trajectories of 20% of all OD-pairs.

Figure 4-5(a) compares the convergence pattern for all budget configuration in one graph. Unscaled graphs are presented in Figures 4-5(b) to 4-5(e) for each budget configuration. Results show that for a large number of iterations, the objective function values decrease at a very slow rate. Therefore, the optimization is stopped at the iteration of  $100 \times 100$  to make the results comparable with the findings of the previous chapter. As expected, the optimal objective function decreases when the budget level is increased. Figure 4-6 depicts the optimally selected links in the downtown Chicago network for different budget configurations. As the available budget increases, more links are selected to be equipped with loop detectors and more OD pairs are selected to have probe vehicles.

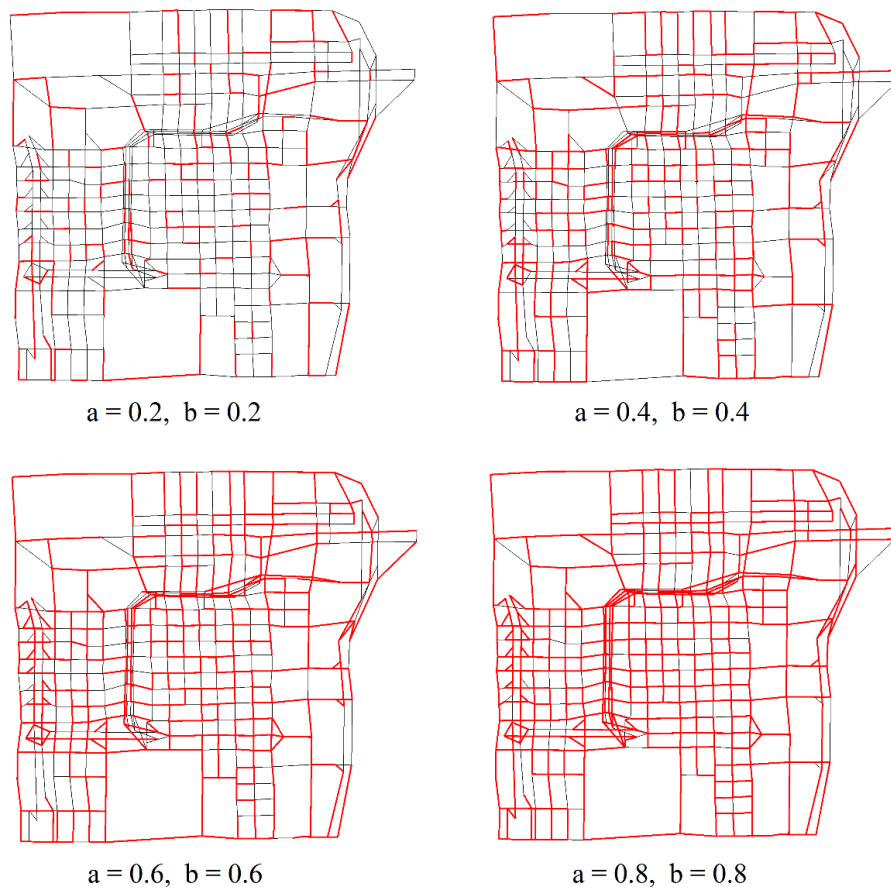


Figure 4-6- Location of the links selected to be equipped with loop detectors for different budget configurations

To further investigate the impact of stochasticity on NFD estimation, a comparison between the deterministic approach proposed in the previous chapter and the stochastic approach presented in this chapter is conducted. The objective value of the stochastic method (Equation 4-1) reflects the cumulative deviation of the estimated NFDs for different traffic scenarios from the corresponding ground-truth NFDs for each scenario. Therefore, to make the objective values comparable between the two methods, the deterministic solution is found for every single day. Then the deterministic solution of each scenario is implemented to estimate NFDs for all scenarios including the same day. Finally, the objective values are summed up and designated as cumulative deterministic objective values associated with each deterministic solution. The same procedure is performed for all demand scenarios (different days), and the results are compared with the objective value evaluated by the stochastic approach.

Figure 4-7 shows the sorted cumulative deterministic objective values for the 86 demand scenarios alongside the objective value evaluated by the stochastic approach for all 4 budget combinations. In all cases, the stochastic method has provided a better solution compared to the deterministic approach. By increasing the budget, not only the objective values for both stochastic and deterministic approaches decrease, but also their difference reduces as well. The reason is that by providing more links and OD pairs for data collection, the discrepancy between the solution of stochastic and deterministic approach decreases, which makes the solutions more similar. For the fourth case ( $a=b=0.8$ ), almost all of the links and OD pairs are selected; therefore, the discrepancy is at minimum, which makes the stochastic method less effective. The extreme case would use all of the samples, including all links and OD pairs ( $a=b=1$ ), which would lead to equal solutions for both stochastic and deterministic approaches.

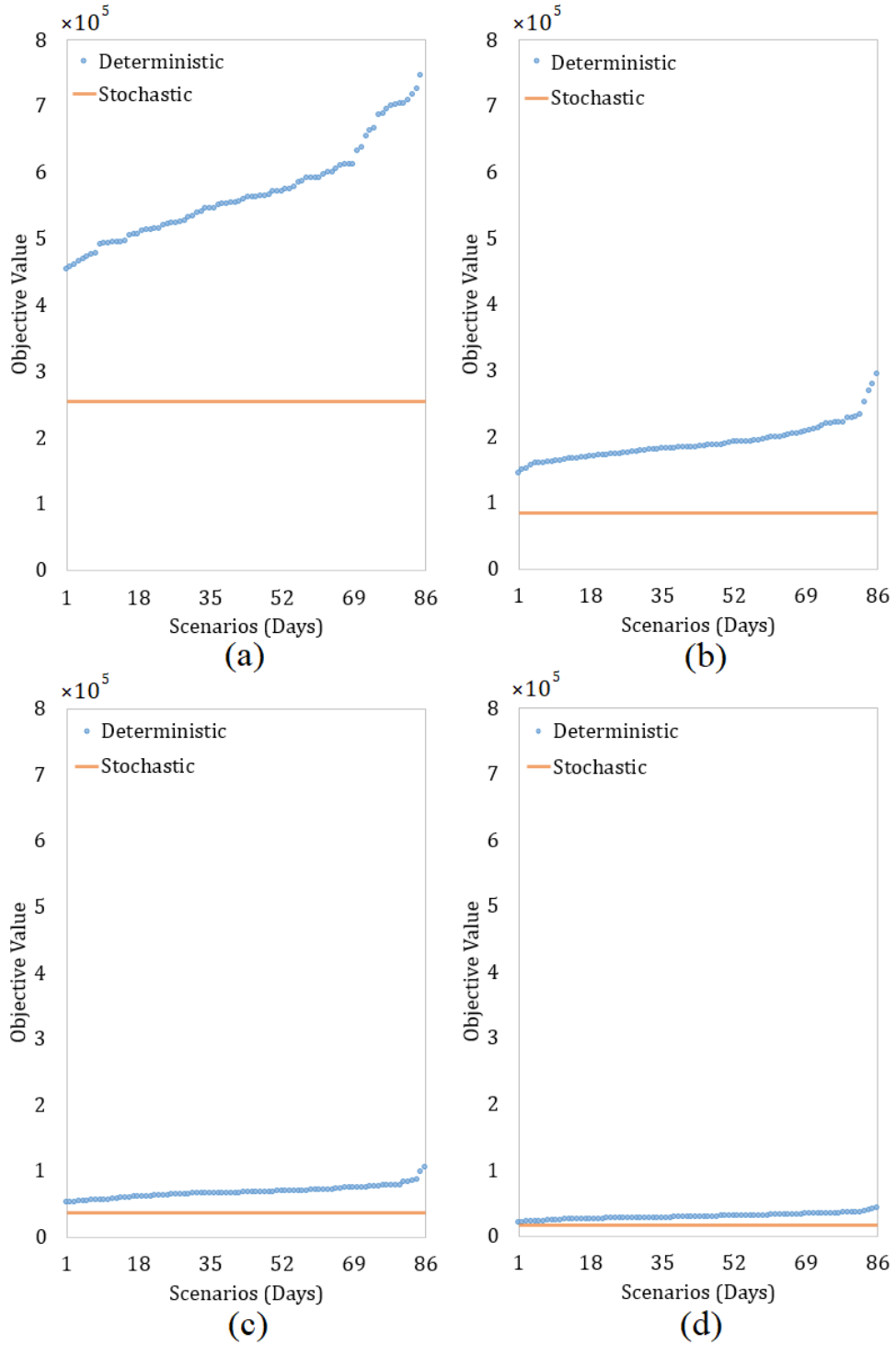


Figure 4-7- Comparison of stochastic objective values with cumulative deterministic objective values for different traffic scenarios (sorted) and different budget configurations

Figure 4-8 illustrates the ratio of the maximum, average, and minimum objective function values for the deterministic approach relative to the stochastic method. For the first budget case ( $a=b=0.2$ ), the maximum objective function value of the deterministic method is more than three times that of the stochastic objective function value. For the same budget, the minimum value for the deterministic objective function is almost 1.7 times that of the stochastic value. This ratio is decreased to 1.3 for the budget with  $a=b=0.8$ , but it is still more than 1, which shows that the stochastic method always provides a better estimation.

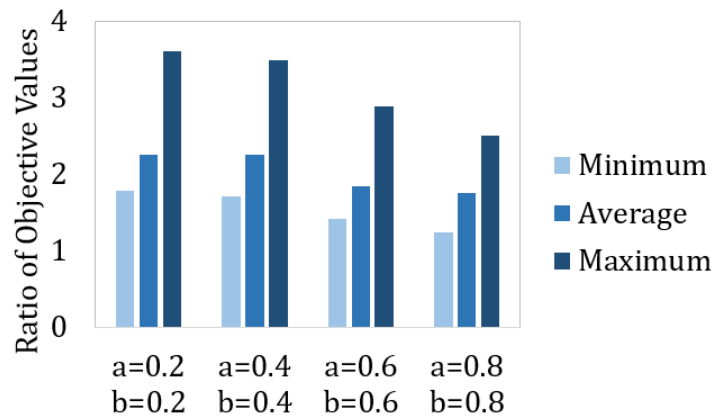


Figure 4-8- Ratio of the maximum, average, and minimum objective function values for the deterministic approach relative to the stochastic method

#### 4-5- Summary

This study presents a modified version of the mathematical model proposed in Chapter 3. It is formulated as a resource allocation problem to find the optimal set of links for loop detector installment and the optimal sample of OD pairs to be equipped with probe vehicles to estimate the NFD in a large-scale network with stochastic day-to-day demand and network supply. The objective function minimizes the discrepancy between the estimated flow and density and their ground-truth values to find the optimal set of links and OD pairs. The robustness of the model including different scenarios with different demands, weather conditions, and other influential

factors in the NFD estimation is the main advantage of this approach compared to the method presented in Chapter 3. The major findings of the chapter are summarized below:

- The numerical experiments confirm successful implementation of the methodology for a large-scale network.
- Exploring the convergence pattern of the algorithm shows that the optimal objective function is achieved and is sensitive to the budget level, which limits the estimation accuracy.
- Mainly, the comparison of the stochastic approach proposed in this chapter with the deterministic approach in Chapter 3 shows that the stochastic approach is superior.
- Once the budget level is at 20%, the deterministic approach leads to a 70-250% error relative to the stochastic approach.
- Increasing the budget decreases the relative error, but even at the 80% budget level, a minimum 30% relative error is observed over various scenarios.

## **CHAPTER 5 – Network-wide Travel Time Reliability Analysis**

### **5-1- Overview**

This chapter incorporates different network partitioning and travel time reliability estimation approaches in a large-scale network of Chicago using a 24-hour dynamic traffic simulation model. It shows that partitioning a large-scale heterogeneous network into multiple homogeneous sub-networks improves the travel time reliability estimation. Indeed, the proposed method captures travel time variations in high resolution (among different sub-networks), while still using the benefits of an aggregate model. It also indicates that the network travel time reliability relation depends on the coefficient of variation of density calculated over the simulation horizon and across the links in each cluster. This coefficient itself relates to the network partitioning based on the density variations. The study also demonstrates an application of partitioning on an actual large-scale network, exploring the impacts of different congestion patterns in the morning and afternoon peak periods. Two partitioning approaches (directional vs. non-directional), and two methodologies for the network travel time reliability estimation, called trajectory and sub-trajectory approaches, are compared. It is shown that the sub-trajectory approach is a more robust method capturing the travel time variations properly.

### **5-2- Methodology**

The study investigates how the spatial distribution of congestion affects the shape and scatter of NFD and derives a robust relationship for travel time reliability analysis.

### 5-2-1- NFD estimation

To estimate NFD (Daganzo, 2007; Gonzales et al., 2011; Mahmassani and Peeta, 1993; Saberi and Mahmassani, 2012; Williams et al., 1995; Williams et al., 1987), network-wide average flow and density are calculated as follows (Mahmassani et al., 1984; Saberi et al., 2014a):

$$Q = \frac{\sum_i^M l_i q_i}{\sum_i^M l_i} \quad (5 - 1)$$

$$K = \frac{\sum_i^M l_i k_i}{\sum_i^M l_i} \quad (5 - 2)$$

where

$Q$ : distance-weighted average of flow;

$K$ : distance-weighted average of density;

$q_i$ : individual link average flow;

$k_i$ : individual link average density;

$l_i$ : lane-length  $i$ ,  $i = 1. \dots M$ ; and

$M$ : total number of links.

There also exists a growing number of studies on NFD estimation in real networks (for example see (Du et al., 2016; Leclercq and Geroliminis, 2013; Ortigosa et al., 2014). In recent studies, Zockaie et al. (2018) and Kaviani-pour et al. (2019) formulated resource allocation problems to estimate NFD accounting for the limited resources of data collection, network traffic heterogeneity, and asymmetry in OD demand in a real-world network.

### 5-2-2- Network partitioning

The general formulation of a contiguity-constrained partitioning problem for a pre-specified number of clusters ( $N_c$ ) is presented here. Each cluster should contain a connected set of links with similar level of congestion, where connectivity is explicitly imposed by a set of constraints as introduced in Saeedmanesh and Geroliminis (2017). Connectivity is defined using the concept of directed acyclic graph. Here, a modified objective function is introduced which needs a smaller number of variables and is tractable for networks with larger sizes. The new objective function calculates the summation of weighted variances, named total variance (TV), of all the clusters which is defined as follows:

$$\begin{aligned} \sum_{t=1}^T \sum_{i=1}^{N_c} \sum_{j \in C_i} \left( k_j(t) - \bar{\omega}_i(t) \right)^2 &= \min \sum_{i=1}^{N_c} \sum_{t=1}^T \sum_{j=1}^N x_{ij} \times \left( k_j(t) - \frac{\sum_{j=1}^N x_{ij} \times k_j(t)}{\sum_{j=1}^N x_{ij}} \right)^2 \\ &= \sum_{t=1}^T \sum_{i=1}^{N_c} \sum_{j=1}^N x_{ij} \times \left( k_j(t) - \bar{\omega}_i(t) \right)^2 \end{aligned} \quad (5 - 3)$$

where  $k_j(t)$  is the measured data (density) for link  $j$  and  $\bar{\omega}_i$  is the estimated average for cluster  $i$  ( $C_i$ ) at time  $t$ .  $x_{ij}$  is a binary variable indicating if link  $j$  belongs to cluster  $i$  or not.  $T$  is the number of time intervals in the simulation horizon and  $N_c$  is the number of clusters. It is clear that the average value of each cluster depends on the partitioning result and is not known before partitioning is done. Moreover, the term  $\left( \frac{\sum_{j=1}^N x_{ij} \times k_j(t)}{\sum_{j=1}^N x_{ij}} \right)$ , calculating the average density in cluster  $i$  is the main source of non-linearity. Hence, the algorithm starts from a random guess for  $\bar{\omega}_i$  and solves a Mixed Integer Linear Program (MILP) to find the best partitioning for the current set of  $\bar{\omega}_i$  (optimization step). Then, the  $\bar{\omega}_i$  variables are updated by taking the real average values of clusters (updating step). This approach follows a similar concept to the K-means method (heuristic) to find

the best clusters. It can be shown that the objective function (minimum distance of the points to their center) at each of the two steps is decreasing and since there is a lower bound (i.e. minimum summation of distances of different points to their clusters' center), the method will converge. Specifically, there are at most  $N_c^N$  ways to partition  $N$  data points into  $N_c$  clusters. This is a large but finite number. As mentioned before, for each iteration of the algorithm (including the two steps), a new clustering is produced only based on the old clustering (previous step). Note that: (a) if the old clustering is the same as the new one, then the next clustering will again be the same; and (b) if the new clustering is different from the old one then the newer one has a lower cost. Since the algorithm iterates a function whose domain is a finite set, the iteration must eventually enter a cycle. The cycle cannot have length greater than "1" because otherwise by (b) one would have some clustering that has a lower cost than itself, which is impossible. Hence the cycle must have length of exactly 1. Hence k-means converges in a finite number of iterations to a local minimum.

To avoid being trapped in local minima, different sets of initial points are chosen for the algorithm. This is a common approach for frameworks that may be trapped in a local minimum (e.g. steepest (gradient) descent methods). The best clustering is the one with smallest objective function. The proposed Mixed Integer linear programming algorithm follows the same logic as K-means, but with more complicated algorithmic steps that are imposed by the nature of graph clustering problems. Specifically, the connectivity constraint makes the first step (step a) of each iteration a complex MILP problem to assign the set of connected roads to each cluster; whereas in conventional K-means approach the labeling of each point is done based on the nearest center. The detailed mathematical formulation is described in Saeedmanesh and Geroliminis (2017).

In this chapter, the time-independent partitioning of network is considered. It is known that during different times of simulation the configuration of homogeneous clusters might vary and then time-dependent clusters can provide a better representation of homogeneous regions that can also capture congestion propagation (Saeedmanesh and Geroliminis, 2017). Despite these advancements, the integration of dynamic clustering is not straightforward in many applications, due to the nature of the problem. For example, there is a vast literature on MFD/NFD perimeter control with static clusters. It has been shown that these methods perform very well in alleviating congesting compared to standard local traffic control strategies. To account for these temporal variations, the clusters are obtained by minimizing the variance of road densities in all clusters (i.e. obtaining homogeneous clusters) over different time periods. In other words, the obtained clusters are the best (in terms of homogeneity) time-invariant clusters for the entire simulation horizon. Note that, the first summation in Equation 5-3 takes all desired time periods, rather than a single time point, into account, which ensures having homogeneous clusters and improving the reliability parameter estimation. It should be mentioned that having time-invariant clusters is a pre-requisite condition for travel time reliability analysis. Hence, the best homogeneous time-invariant clusters are obtained by considering temporal interactions to the maximum possible extent.

### *5-2-3- Network travel time reliability estimation*

The distance-weighted standard deviation of travel time per unit of distance is often used as a measure of travel time variability. Network travel time reliability can be characterized by a travel time distribution, with corresponding mean and standard deviation. The first component describes the central tendency and the second shows the dispersion. To control for the impacts of trip distance variations on travel time reliability, the travel time ( $t$ ) needs to be normalized by the trip distance ( $d$ ). So, the travel time per unit of distance ( $t'=t/d$ ) is considered as the travel time

measure (Mahmassani et al., 2013). Thus, the distance-weighted mean and standard deviation of the travel time rate can be estimated as follows:

$$\mu = \frac{\sum_{i=1}^M d_i t'_i}{\sum_{i=1}^M d_i} = \frac{\sum_{i=1}^M t_i}{\sum_{i=1}^M d_i} \quad (5 - 4)$$

$$\sigma = \sqrt{\frac{\sum_{i=1}^M d_i (t'_i - \mu)^2}{\sum_{i=1}^M d_i}} \quad (5 - 5)$$

In Equation 5-4,  $\mu$  is the inverse of spatial mean speed (Mahmassani et al., 2013). To construct the relationship between distance-weighted mean and standard deviation of travel time rate, a linear model has been suggested in the literature (Jones, 1989; Richardson and Taylor, 1978):

$$\sigma(t') = p_1 + p_2 \mu(t') \quad (5 - 6)$$

where

$\sigma(t')$ : standard deviation of the trip time rate  $t'$ ,

$\mu(t')$ : mean value of  $t'$ , and

$p_1, p_2$ : coefficients

This study uses simulation-generated vehicle trajectories in a network to explore this relationship for each identified cluster in the network. To obtain the distribution of travel time per unit of distance in the network, two approaches are proposed:

**Trajectory Approach:** This approach consists of the following steps to specify the relationship between  $\mu$  and  $\sigma$ :

1. Extract the travel time and travel distance for each set of consecutive links that are traveled by a certain vehicle. The set is the longest consecutive sub-set of the vehicle trajectory links that belong to the same sub-network. The entry time to the first link of the set determines the time interval that the set belongs to as an observation (Figure 5-1a). The observations from different pieces of vehicle trajectories associated with each sub-network and time interval are used to compute the mean and standard deviation of travel times per unit of distance. Each observation has two components: a travel time, which is the total elapsed time by vehicle  $i$  at set  $j$ , and a travel distance, which is the total length of links belonging to set  $j$ .
2. Calculate the distance-weighted mean and standard deviation of travel times per unit of distance for each time interval in each sub-network (Equations 5-4, and 5-5). Each time interval in each sub-network is a sample point to be used in the next step.
3. Plot the standard deviation of travel time per unit of distance versus its mean value for each sub-network and estimate the coefficients (Equation 5-6).

The same process is followed to specify the travel time distribution measures for the study area network (union of all clusters). However, in this case the entire vehicle trajectory is considered for the time interval associated with the vehicle departure time.

***Sub-trajectory Approach:*** This approach also requires three steps to specify the relationship between  $\mu$  and  $\sigma$ . The second and third steps are exactly the same as steps 2 and 3 of the trajectory approach. However, step 1 is modified as follows:

1. Extract the travel time and travel distance for each segment. A segment is a piece or entire of a trajectory produced by a vehicle traveling in a sub-network during a certain time

interval (Figure 5-1b). Each segment is considered as one observation for the associated sub-network and time interval to be used for mean and standard deviation calculations. In this approach, the entire segment is traveled during the associated time interval and the maximum travel time is equal to the time interval length. This is unlike the trajectory approach, in which each set is assigned to a time interval solely based on the departure time.

The same process is conducted to specify the travel time distribution measures for the study network. However, in this case, as the vehicles do not travel in different clusters, their trajectories over each time interval are not separated into multiple segments.

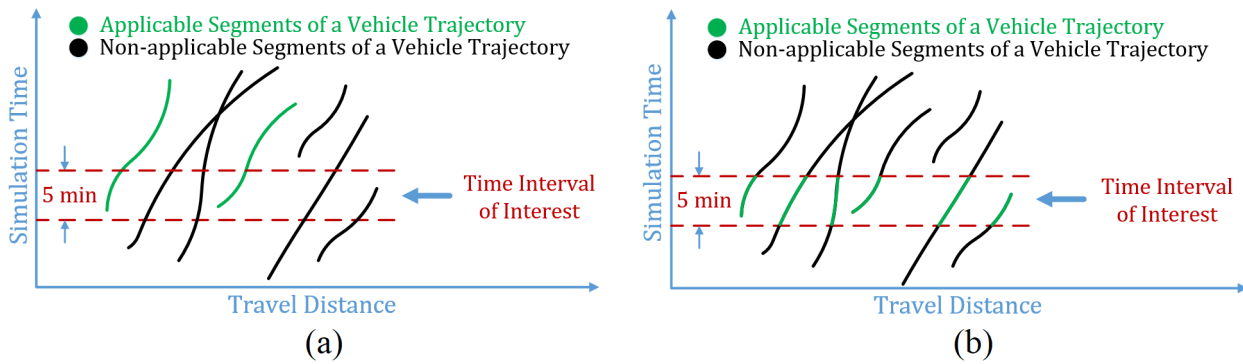


Figure 5-1- Extracted observations from vehicle trajectories for (a) Trajectory and (b) Sub-trajectory approaches to estimate travel time reliability measure

### 5-3- Data Description and Study Area

The Regional Chicago network is considered for the case study (Figure 5-2a). This network contains 40,443 links, 13,093 nodes, and 1,961 traffic analysis zones. Traffic data are simulated using DYNASMART. Figure 5-2b illustrates the hourly network loading profile over the 24-hour simulation horizon. The data for the demand and network is obtained from Chicago Metropolitan Agency for Planning (CMAP). A subset of 9,915 links around the CBD area is selected for

partitioning based on link density variations over time and space. This subset forms the study network depicted in Figure 5-2a. Five-minute time intervals are considered in order to analyze the network characteristics including NFD, reliability measure estimation, and network partitioning. Figure 5-3 illustrates the entire day NFD and travel time reliability measures calculated by both trajectory and sub-trajectory approaches. Network-wide average flow, average density, and weighted average mean/standard deviation of the travel times per unit of distance are calculated for each 5-minute time interval, resulting in 288 sample points on each graph. Morning peak, evening peak, and off-peak periods are separated by different colors to provide a better interpretation of the simulation results.

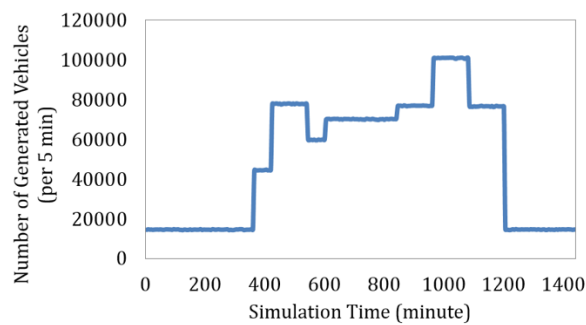
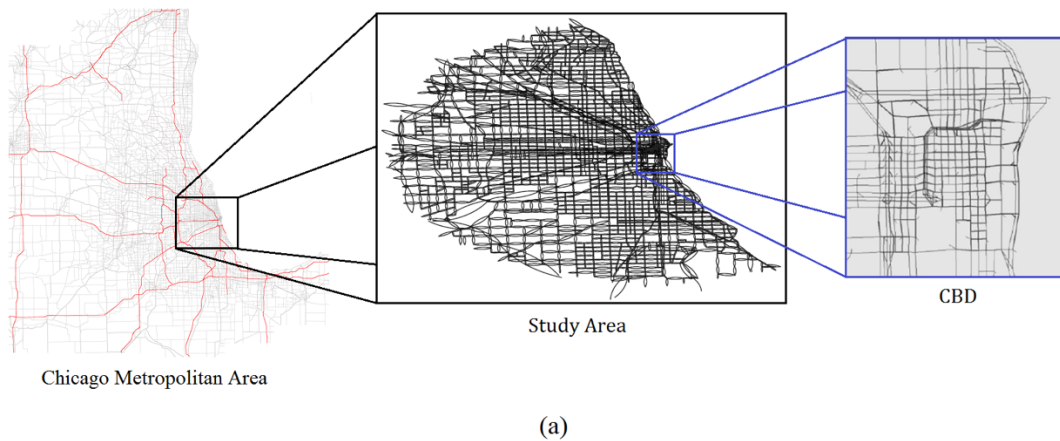


Figure 5-2- (a) Schematic sketch of the Chicago metropolitan network, the study network including 9,915 links, and Chicago CBD; (b) Chicago metropolitan network 24-hour loading profile

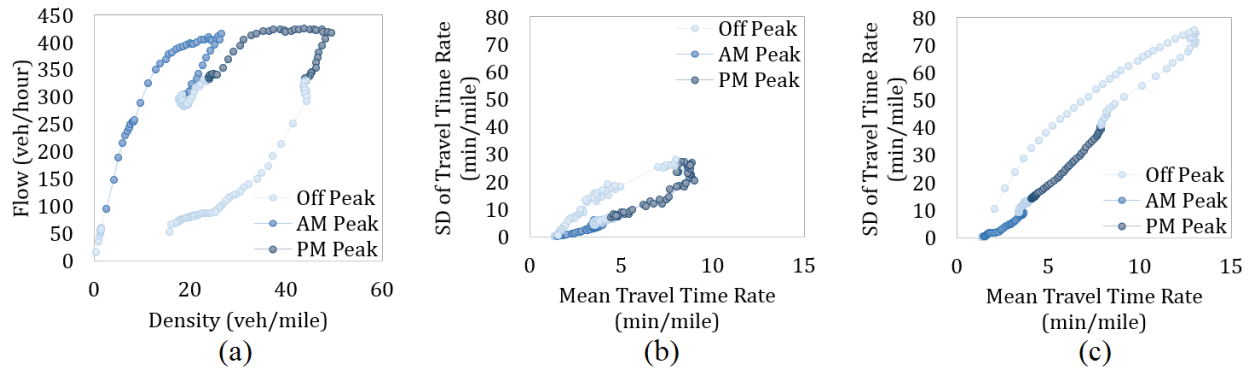


Figure 5-3- (a) NFD, (b) Reliability graph estimated by the trajectory approach, and (c) Reliability graph estimated by the sub-trajectory approach for the study network over the 24-hour simulation horizon

In Figure 5-3, the flow-density NFD is plotted (Figure 5-3a), while the standard deviation versus mean of travel time rates measured through the trajectory and sub-trajectory approaches are shown as well (Figure 5-3b and 5-3c, respectively). Note that the evening peak experiences larger values compared to the morning peak for both average flow and density in the NFD. The NFD follows a smooth trend as it reaches the maximum AM peak flow around 9:00 AM. Afterward, the network is in the unloading phase, and the system begins to recover while there is a decrease in average flow. As the demand level increases at mid-day, the system becomes congested again, and density increases. When the average flow reaches the maximum value sometime during the PM peak (at around 6:00 PM), the network maintains the maximum average flow, while the average density increases, reflecting a growing congestion pattern. The average density keeps increasing up to the point that the network is in the unloading phase again and begins to recover to a stable condition.

The very large number of vehicles loaded onto the network (according to the time-dependent demand table) are not able to complete their trips during the unloading phases of AM

peak and (especially) PM peak periods. The trapped vehicles cause the formation of gridlock, which brings traffic to a complete standstill with zero flow. A higher percentage of adaptive drivers results in more homogenous distribution of the congestion in the network due to avoiding super congested areas by these drivers. This would prevent or recover gridlocks in the network. Formation of the clockwise hysteresis loop in the NFD diagram is due to the gridlock formation in the network and shows the degree to which the system is unstable during the unloading period. In Figure 5-3a an incomplete hysteresis loop is formed during the AM peak period followed by a complete hysteresis loop during the PM peak period.

In the trajectory approach, the reliability measure (slope of the estimated linear relation) is almost the same for AM and PM peak periods, and substantial fluctuations can be observed in both time periods. This is not the case for the sub-trajectory approach. The range of observed values for the mean travel time per unit of distance during the peak periods are exactly the same for the two methods. However, the sub-trajectory approach provides larger estimated values for the standard deviation of travel time per unit of distance compared to the trajectory approach. There are fewer fluctuations in the sub-trajectory approach since each travel time segment occurs in the same time interval. However, in the trajectory approach, different sets of a certain time interval might occur at different simulation time intervals as they only share the same departure time. The trajectory approach has a lower standard deviation as it ignores the variation of travel time over each vehicle trajectory by simply assuming that the travel time is uniformly distributed over the traveled distance (which might occur in multiple time intervals). However, in the sub-trajectory approach, each vehicle trajectory is divided into multiple segments associated with each time interval, and as a result better captures the variation of travel time over the traveled distance. In other words, the trajectory method for any given departure time interval (5-minute time intervals in this study)

considers the portion of trajectories entering to a sub-network (departing their trips or transferring from other sub-networks) until they exit that sub-network. Given that some sub-networks are large, this might take a significant amount of time (maybe multiple 5-minute time intervals). However, in the sub-trajectory approach, the maximum length of each applicable trajectory portion is the length of the departure time interval (5-minute in this study). Therefore, temporal variations of travel time are smoothed in the trajectory approach resulting smaller variances relative to the sub-trajectory approach.

A four-hour AM-Peak (from 6:00 AM to 10:00 AM) and a four-hour PM-Peak (from 3:00 PM to 7:00 PM) are considered in order to perform detailed analyses for different partitioning approaches in the next two sections. Note that each of these periods includes the peak hours and pre- and post- peak hours to demonstrate the network traffic flow dynamics.

#### **5-4- Partitioning the Heterogeneous Network**

This section elaborates on the propagation and distribution of congestion in the study network during the morning and evening peak periods. The density of different links measured every 5 minutes is utilized as an indicator representing the level of congestion. First, a detailed analysis is performed to find a proper configuration to run the partitioning algorithm. As the analysis approach is the same for both the morning and evening peak, here only the evening peak data analysis is explained. Figure 5-4, which is built on the idea presented in Mazlounian et al. (2010), illustrates the specification of the heterogeneous network that is considered for the partitioning and provides insights on the properties of the network and the purpose of partitioning. Figure 5-4a depicts a box-plot representation of density at different time intervals during the evening peak. As seen in Figure 5-4b, the average and standard deviation of density increase over time. Average and median values are depicted using blue and red colors, respectively. To

demonstrate the spatial distribution of congestion, the time interval associated with 6:00 PM is selected, where the average and standard deviation of density are at a very high level. This time represents a condition where the network is heterogeneously congested. The histogram of densities at this time (Figure 5-4c), shows that the density holds a bi-modal distribution (i.e. many links have a small density while some links have a very high density), which is the reason for the existence of many outliers in the box-plot representation.

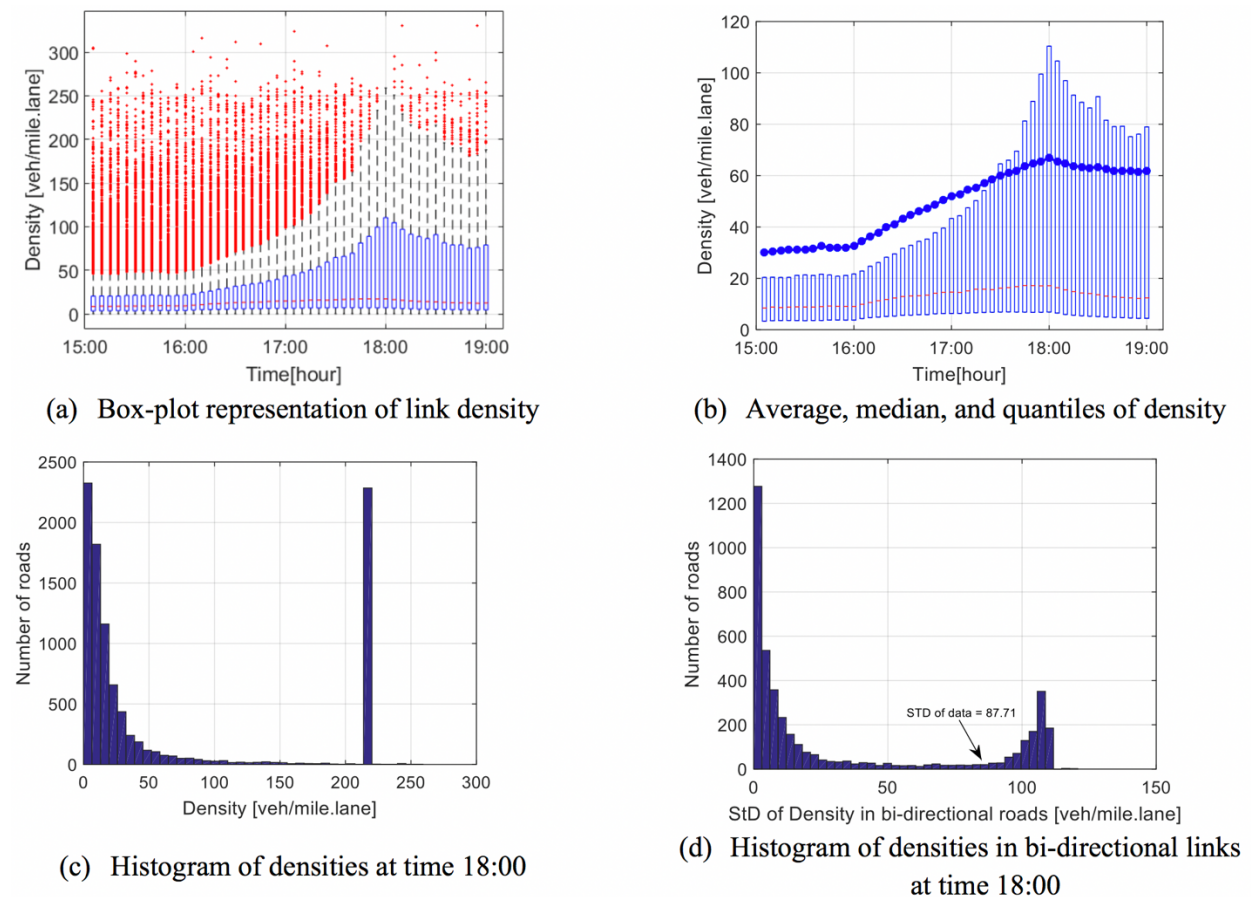


Figure 5-4- Density temporal and spatial distributions for the PM peak period

The study network contains many bi-directional links (4307 pairs). To investigate the effect of directional congestion, the histogram of standard deviation in bi-directional links is plotted in Figure 5-4d. Many bi-directional links have a smaller standard deviation than the average standard

deviation in the network. However, some of the bi-directional links experience different congestion levels during the peak hours. The impacts of the directional versus non-directional partitioning of bi-directional links are investigated in the numerical results section. In the non-directional approach, the bi-directional links are forced to be in the same cluster. In the directional partitioning, two directions of a roadway may assign to different clusters.

The proposed mixed integer linear programming optimization is a precise formulation of the clustering problem, which formulates a common heterogeneity measure (total variance: TV) as the objective function, and explicitly enforces connectivity. However, the optimization problem is efficiently solvable within a reasonable amount of time (i.e. with zero gap which implies optimality) for networks up to a certain number of decision variables (approximately for networks with up to 2,000 links), while the size of study network is very large (about 10,000 links). Hence, it is not practical to apply the exact formulation. To tackle the computational issue, a simplification step is introduced to improve computational efficiency, by finding and grouping nearby links with similar level of congestion throughout the network. This leads to a set of homogeneous and non-overlapping groups, named local “homogeneous components”. Finally, the exact formulation can be applied to the reduced network including obtained components and remaining individual links. In the following, different simplification steps are explained in more detail.

The simplification step of the partitioning methodology finds a set of similar links (i.e. set of links with similar density values over the time) in the network. A similar approach to the “Snake” methodology introduced in Saeedmanesh and Geroliminis (2016) is utilized. The snake method iteratively obtains the most homogeneous neighboring link around the set and adds it to the current set. In this approach, each individual link is considered as one snake at the beginning. Then, snakes start growing and merging until a certain number of components is obtained. At each

iteration, the most similar (i.e. the one with smallest average density differences over the time) links or snakes are merged. Note that, connectivity holds by construction in this method. This homogeneous non-overlapping component is utilized as an input for the exact optimization method in the next step. At this stage, groups of homogeneous links and single non-assigned links can be partitioned using the exact formulation introduced in Saeedmanesh and Geroliminis (2017) with feasible computational efficiency.

The performance of the proposed methodology is examined for the study network using directional and non-directional approaches for different numbers of clusters (2, 3, and 4 clusters). As an example, the results of partitioning into two clusters with the non-directional approach for the morning peak period are depicted in Figure 5-5a.

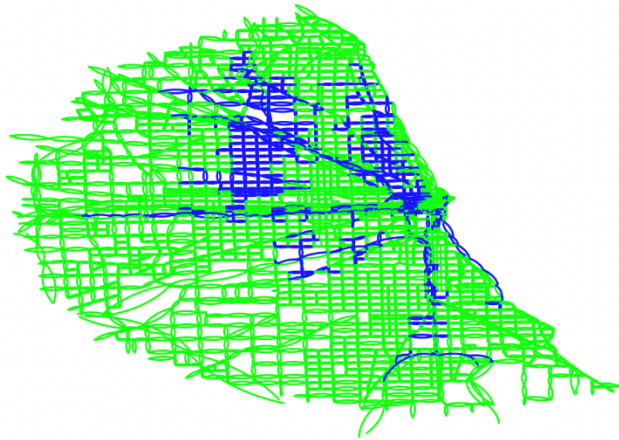
Determining the optimal number of clusters in a data set or network is a fundamental challenge in almost all partitioning (clustering) methods including k-means clustering, which requires the user to specify the number of clusters to be generated. Unfortunately, there is no definitive answer to this question. The optimal number of clusters is somehow subjective and depends on the method used for measuring similarities and the parameters used for partitioning. There are couple of methods (which can be categorized into direct and statistical methods) designed for obtaining optimal number of clusters. A common direct method, called “Elbow” method has been utilized, which looks at the objective function (total weighted sum of squared errors) as a function of the number of clusters (see Bholowalia and Kumar, 2014). The number of clusters should be chosen so that adding another cluster does not significantly improve the objective function. In the objective function vs. number of clusters curve, the location of a bend (knee) is generally considered as an indicator of the appropriate number of clusters. For the number of clusters, note that in addition to 2 and 3 clusters, the 4-cluster case is also considered.

The results show no significant improvement in terms of both reliability parameter estimation and  $TV_n$  values. This is the reason that the 3-cluster case is selected as the final configuration for further analysis. In other words, the analysis is begun with 2 clusters and this number is increased until no significant improvement is attained.

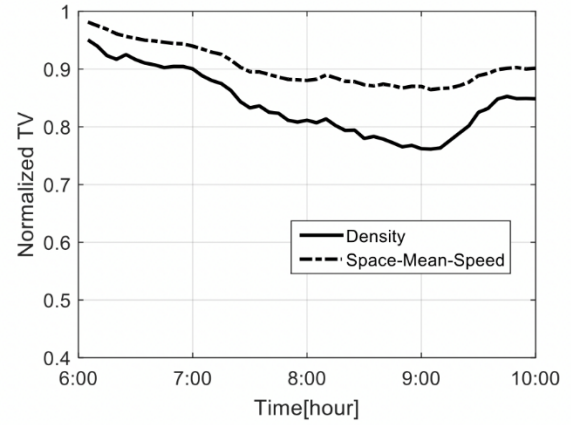
Normalized total variance  $TV_N$  is a well-established metric utilized to evaluate the efficiency of the partitioning algorithm for a single time period (i.e. the objective function of the partitioning algorithm is TV). The average value of  $TV_N$  over the entire time period (4 hours or 48 time intervals for each peak period) is considered to account for the performance of each partitioning approach. This metric is defined as the ratio between the weighted variance of density in the partitioned case to the un-partitioned case:

$$TV_N(t) = \frac{\sum_{i=1}^{N_c} N_i \times \{\text{var}(C_i)|t\}}{N \times \{\text{var}(C)|t\}} \quad (5 - 7)$$

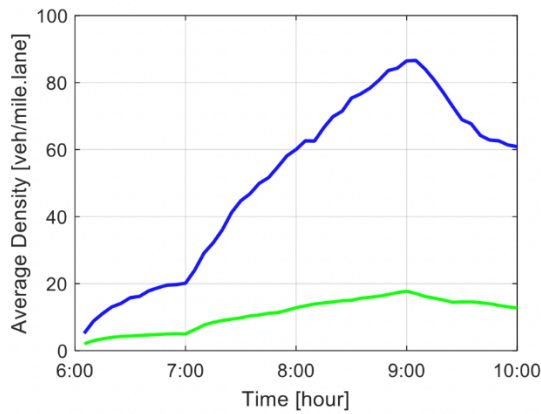
where  $N_i$  denotes the number of links in cluster  $i$  and  $C = \cup_{i=1}^{N_c} C_i$ . Note that  $\{\text{var}(C_i)|t\}$  is the variance of densities at time interval  $t$  for the links belonging to cluster  $i$ . It should be noted that there is no overlap between different clusters (i.e.  $\cap_{i \neq j} (C_j, C_i) = \emptyset$ ). The value of  $TV_N$  is demonstrated at different time intervals in Figure 5-5b. The dashed-line curve represents the efficiency of obtained clusters for the speed data and the solid-line curve represents the density-based measure.  $TV_N$  takes lower values in more congested time intervals, when the need for partitioning is more crucial. A similar pattern is observed for both speed and density data; however, the solid-line curve has a lower  $TV_N$  value, since the density data is utilized as an input for the partitioning algorithm. Figures 5-5c and 5-5d depict the average density and speed for the obtained clusters during the AM peak. Figures 5-6a to 5-6d present the same results for directional partitioning with three clusters during the evening peak period from 3:00 PM to 7:00 PM.



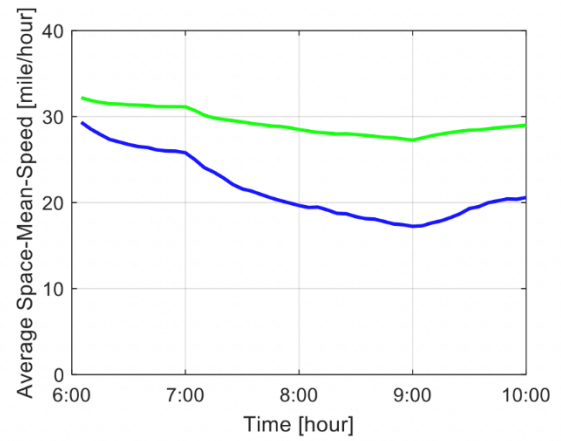
(a)



(b)

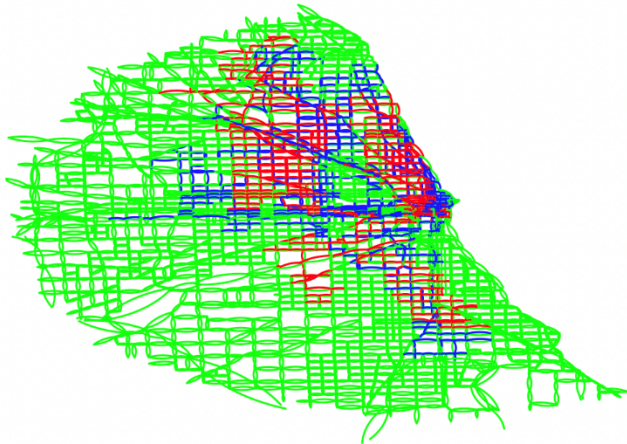


(c)

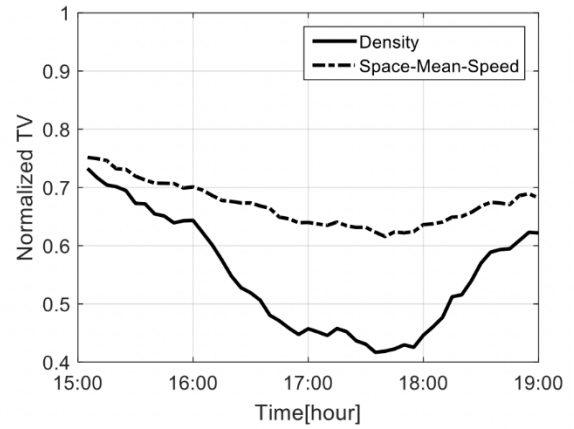


(d)

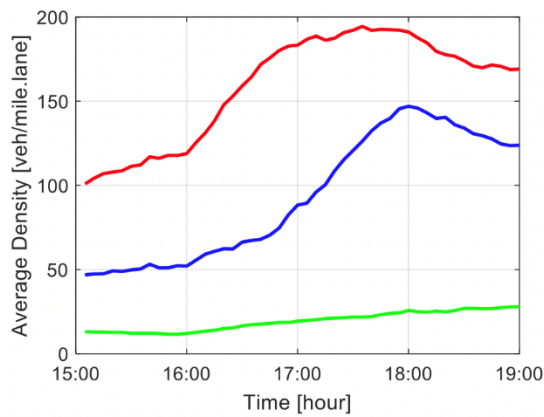
Figure 5-5- Partitioning results: (a) Two clusters for AM peak and non-directional approach, (b) Speed and density descriptor of partitioning quality during the AM peak, (c) Average density for the AM peak, and (d) Average space-mean-speed for the AM peak



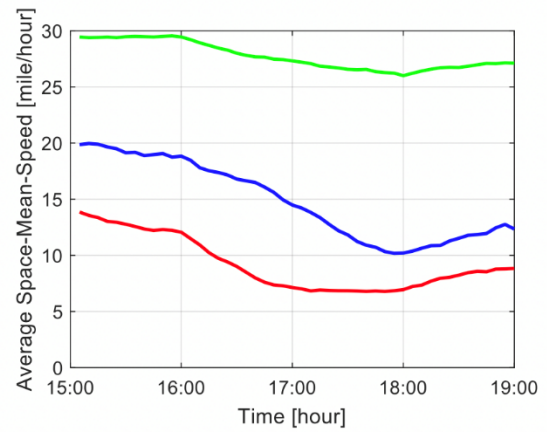
(a)



(b)



(c)

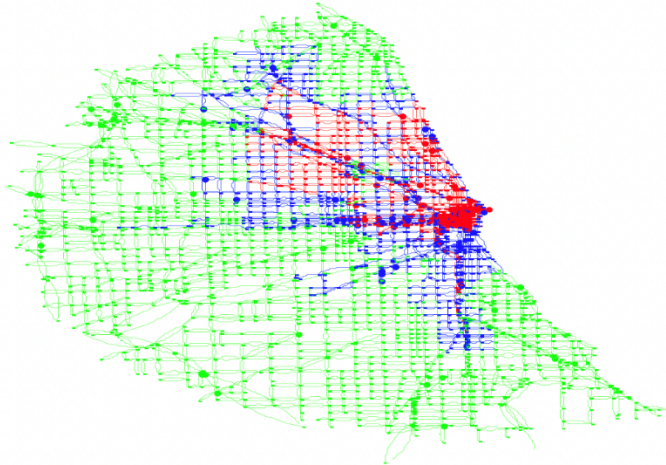


(d)

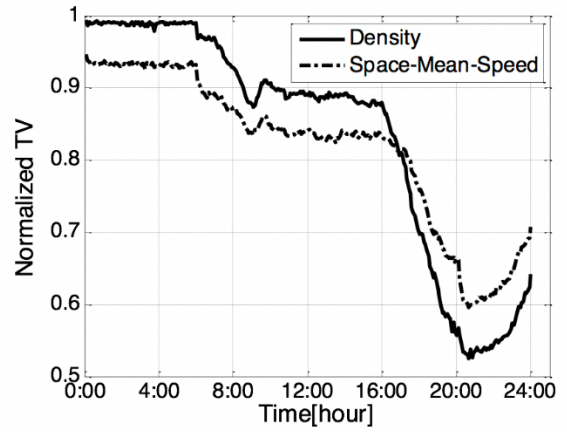
Figure 5-6- Partitioning results: (a) Three clusters for PM peak using directional approach, (b) Speed and density descriptor of partitioning quality during the PM peak, (c) Average density for the PM peak, and (d) Average space-mean-speed for the PM peak

Figures 5-7a to 5-7d present the same results for the non-directional partitioning with three clusters defined over the entire simulation time (24 hours). By minimizing average  $TV_N$  for the entire day, the algorithm tends to find homogeneous clusters over the entire day. The solution has lower  $TV_N$  values in the PM peak period compared to the AM peak. This is due to the fact that the congestion level is higher during the PM peak period and therefore a more accurate partitioning is needed there.

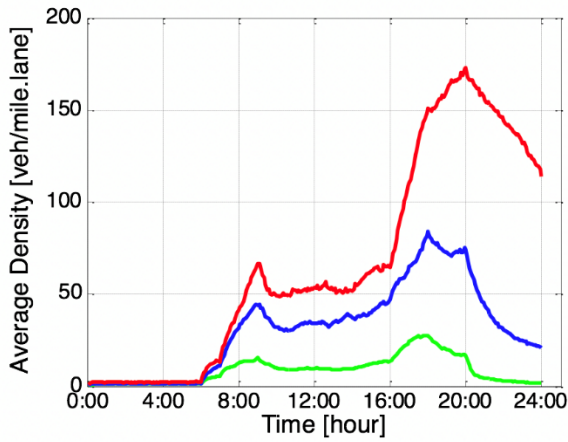
A detailed comparison of the minimum and average values of  $TV_N$  over the AM peak period, PM peak period, and the entire day for different partitioning approaches is illustrated in Figure 5-8. Results confirm superiority of the directional partitioning. In addition, partitioning into three clusters instead of two clusters improves the quality of the partitioning in AM peak, PM peak, and the entire day results. However, partitioning into four clusters does not significantly improve the partitioning quality as compared to the 3-cluster case. Furthermore, partitioning is more important for the PM peak period, where heterogeneity of the congestion pattern over the simulation horizon is more significant. Therefore, directional partitioning into three clusters for the PM peak period is considered for detailed analyses of NFD and travel time reliability measures, as described in the next sections.



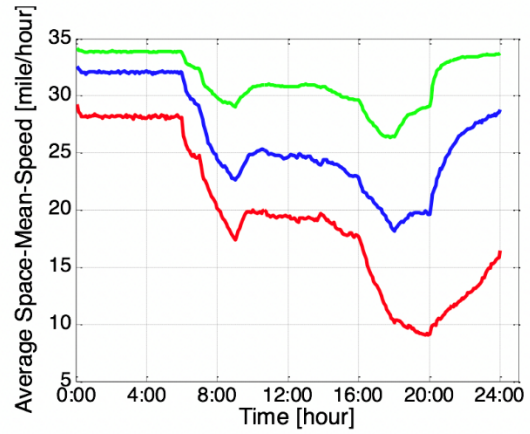
(a)



(b)



(c)



(d)

Figure 5-7- Partitioning results: (a) 3 clusters for the Entire day using non-directional approach, (b) Speed and density descriptor of partitioning quality during the entire day, (c) Average density for the entire day, and (d) Average space-mean-speed for the entire day

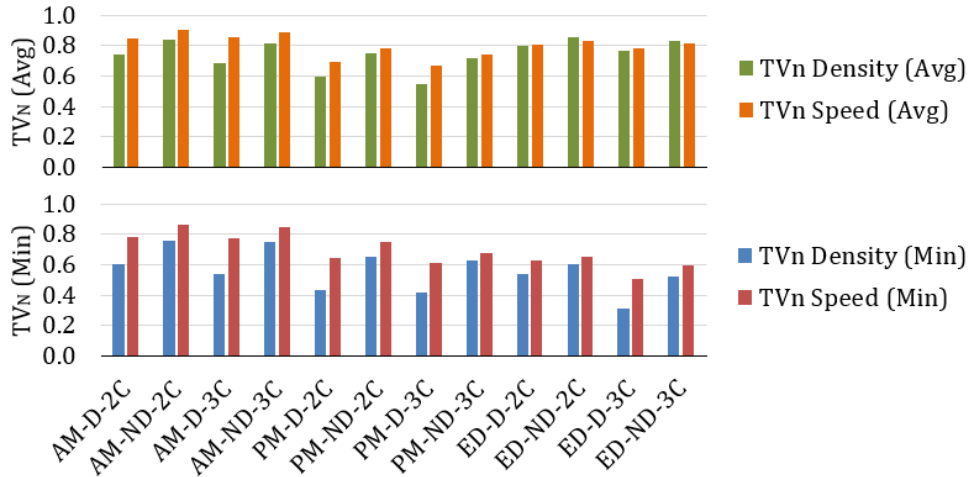


Figure 5-8- Minimum (lower graph) and average (upper graph) values of TVN over various time intervals (AM peak, PM peak, and entire day) for different partitioning approaches with 2 and 3 clusters [in each X-Y-Z scenario in horizontal axis, X represents AM or PM peak period or the entire day (ED), Y represents directional (D) or non-directional (ND) partitioning, and Z represents the number of clusters (2C or 3C)]

### 5-5- NFD and Travel Time Reliability Estimation

In this section, the AM and PM peak periods are considered to establish a relation between travel time reliability relation estimation and the network partitioning. First, average flow and density at each 5-minute interval during the AM and PM peak periods are calculated based on the simulated vehicle trajectories for different partitioning approaches. The trajectories are divided into segments based on the link assignment to each cluster. The relationship between the average flow and density over different 5-minute time intervals is considered as the NFD for each cluster. Then, the trajectory and sub-trajectory approaches are applied with the 5-minute interval and for each cluster to estimate the reliability measures.

Figure 5-9 shows NFDs and mean versus standard deviation of travel times per unit of distance, by both the trajectory and sub-trajectory approaches, for the study network and its three

clusters. The directional partitioning method is used for the evening peak period. The average density in the network is 36.9 veh/mile. The ordered pair of size (number of links) and average density (veh/mile) for these three clusters are (7038, 19.1), (1563, 84.3), and (1314, 151.5), respectively.

Figures 5-9a to 5-9d show that clusters reflect different NFDs in terms of the shape, maximum and average density and flow, and the area of the hysteresis loop. This emphasizes one of the main contributions of the partitioning approach, which states that a single NFD for the entire network cannot properly describe the network performance because in most cases, congestion is heterogeneously distributed throughout the network. In the least congested cluster, the average flow and density grow at the same time until a maximum flow rate and density are observed in the first phase. In the second phase, the unloading process begins and a reduction in both average flow and density can be observed. In the medium congested cluster, the maximum average flow is maintained, while the density grows in the first phase. In the second phase, similar to the previous case the unloading process begins. In the most congested cluster, a maximum average flow with growing average density is maintained for a while. Then, at a certain point the average network flow drops while the average density still increases. Finally, at a certain point both average flow and density begin to decrease as the unloading phase starts. Depending on the congestion level, the NFD shape varies and the hysteresis loop size might be different.

In Figures 5-9e to 5-9h, upper and lower diagrams are estimated by the trajectory and sub-trajectory approaches, respectively. The ranges of the mean and standard deviation of travel time per unit of distance are almost identical in both approaches for all sub-networks and the overall study network. The slope of the diagrams, which captures the rate at which variability increases with the mean trip time per unit distance, varies from one cluster to another, while the trend is

consistent for both estimation approaches: trajectory, and sub-trajectory. However, there are more fluctuations in the trajectory approach diagram relative to the sub-trajectory approach, due to assigning trajectories to time intervals solely based on their departure times.

Detailed descriptors of the reliability diagrams besides the calibration results for the linear model are given in Table 5-1. This table presents the point estimates of the model coefficients, t-statistics, associated p-values, and adjusted R-squared values with 95% confidence bounds. The results illustrate that all coefficients are statistically significant for the linear model in both approaches. The adjusted R-squared values are generally high, which indicates an acceptable fit. The overall R-squared values estimated by the sub-trajectory approach are higher. The loading and unloading phases follow different paths in the reliability diagrams, although in many cases, the relation between the mean and variability of travel time is still linear. Figure 5-9 illustrates only the loading phase in the reliability diagrams.

The proposed linear travel time reliability relation provides more robust estimation, when it is applied on time of day periods with certain spatial and temporal demand distribution (AM peak or PM peak versus the entire day). In a heterogeneously congested large-scale network both NFD and travel time reliability diagrams experience hysteresis loop and different phases of these diagrams experience distinct trends. Therefore, a single robust travel time reliability relationship might not exist for the entire day time period. Disaggregating the entire day to AM and PM Peak periods improves the accuracy and precision of the proposed model for travel time reliability relation and captures the network dynamics as well. However, the resolution of the selected time span cannot be stretched beyond a specific point. By increasing the resolution (selecting smaller periods) the concept of the network-wide relationship is violated as the network dynamic is disregarded. The same concept is true for partitioning a large-scale network. However, in case of

rapid and sudden changes in the demand level, the rate of demand variations would not be smooth. In this case, one might not be able to easily identify a proper time period with a robust linear reliability relation.

It should be noted that partitioning a large-scale heterogeneous network into multiple homogeneous clusters provides a less aggregate travel time reliability measure at sub-network level compared to network level. Indeed, the proposed method captures travel time variations in high resolution (among different sub-networks), while still using the benefits of an aggregate model. This is considered an improvement in travel time reliability estimation. Table 5-1 suggests that the estimated travel time reliability relations for all sub-networks and the entire network have almost the same attributes. However, a large-scale heterogeneous network is divided into some small size homogeneous sub-networks. Therefore, more information about the variability of travel time is provided by the sub-network level relation without loss of accuracy in this estimation.

The two results produced by the two methods of travel time reliability estimation follow the same pattern from one cluster to another in terms of changes in the reliability measure, however, they estimate slightly different parameter values. The sub-trajectory approach, which produces somewhat larger reliability coefficient estimates than the other (trajectory) approach; it is also the preferred approach. First, in this method, considering the travel information during each time step (5 minutes) reflects a more detailed description of travel time reliability than only focusing on the departure time interval. Second, results of the sub-trajectory approach reflect a smooth change of mean and standard deviation of travel time rate during the simulation time, whereas considerable fluctuations are observed in the results of the trajectory approach. This is due to combining travel time information of trajectories that share the same departure times but might take place over different time intervals. In other words, the trajectory method considers the

trajectories until they exit a region. Given that some regions are large, this might take a significant time interval (maybe multiples of 5-min). Accordingly, temporal variation of travel time is smoothed resulting in much smaller variances in the trajectory approach. All in all, the sub-trajectory approach is selected to explore the connection between the network partitioning and the variability of travel time. The slope of the linear relationship between the mean and standard deviation of travel time per unit of distance indicates the degree to which the system reliability degrades with increasing congestion.

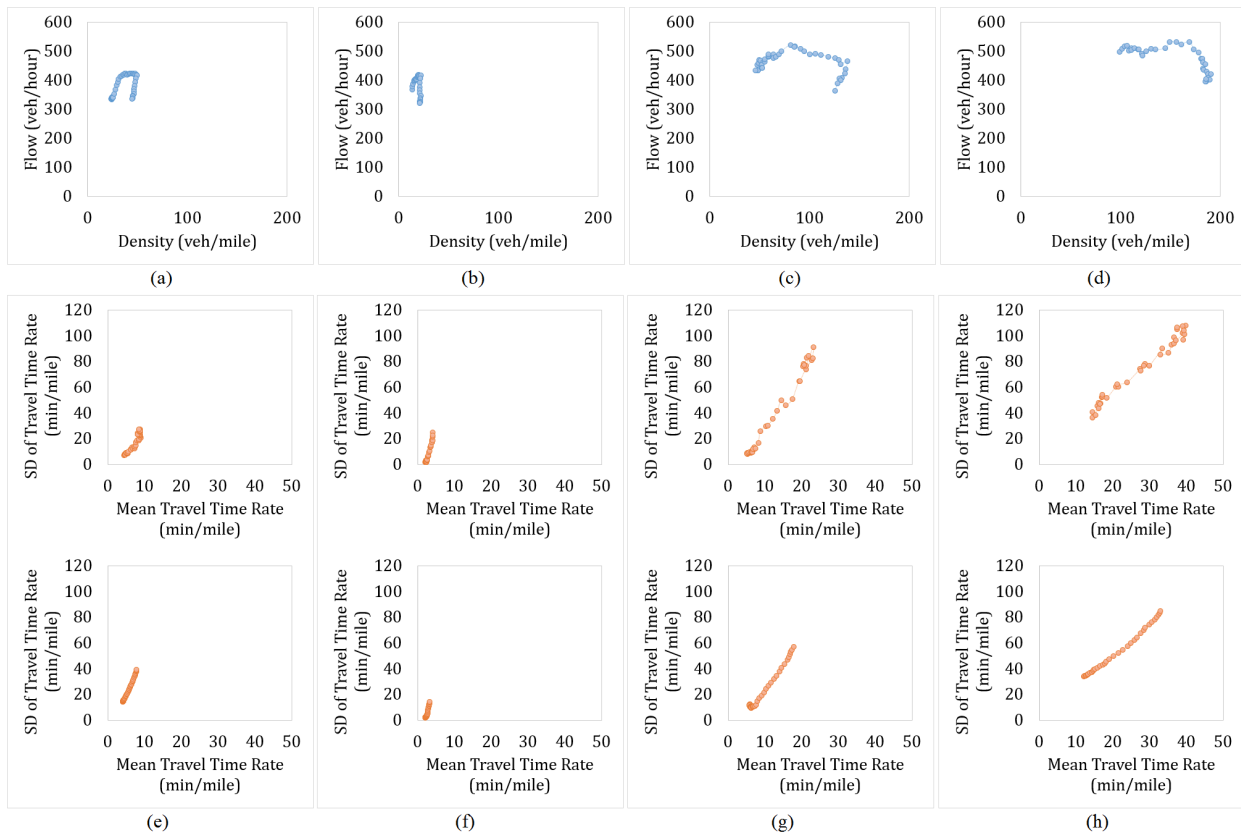


Figure 5-9- NFDs over the PM peak period for the directional partitioning approach for (a) study network; (b) cluster 1 with 19.1 veh/mile average density; (c) cluster 2 with 84.3 veh/mile average density; (d) cluster 3 with 151.5 veh/mile average density; and associated travel time reliability diagrams for trajectory (upper diagrams) and sub-trajectory (lower diagrams) approaches in (e) study network; (f) cluster 1; (g) cluster 2; and (h) cluster 3

Table 5-1- Estimation of the Reliability Coefficient for PM-Peak Directional Partitioning

<b>Reliability: Trajectory Approach</b>						
<b>Network / Sub-network</b>	<b>Size (Links)</b>	<b>Linear Model Constant (<math>p_1</math>)</b>	<b>Linear Model Coefficient</b>			<b>Adjusted R<sup>2</sup></b>
			$p_2$	t-stat	p-val.	
<b>Study Area</b>	9915	-12.58	4.08	17.56	<10 <sup>-10</sup>	0.87
<b>Sub-network 1</b>	7038	-22.89	10.58	30.33	<10 <sup>-10</sup>	0.97
<b>Sub-network 2</b>	1563	-18.05	4.48	59.67	<10 <sup>-10</sup>	0.99
<b>Sub-network 3</b>	1314	6.07	2.49	39.57	<10 <sup>-10</sup>	0.98

<b>Reliability: Sub-trajectory Approach</b>						
<b>Study Area</b>	9915	-12.55	6.41	90.1	<10 <sup>-10</sup>	0.99
<b>Sub-network 1</b>	7038	-21.56	10.47	16.8	<10 <sup>-10</sup>	0.90
<b>Sub-network 2</b>	1563	-14.05	3.81	51.4	<10 <sup>-10</sup>	0.99
<b>Sub-network 3</b>	1314	3.48	2.36	64.4	<10 <sup>-10</sup>	0.99

Here, the impact of the network partitioning on the reliability coefficient is explored. Figure 5-10 illustrates the relation between the coefficient of reliability with different congestion measures (average density, standard deviation of density, and density coefficient of variation) for the morning (Figure 5-10a) and evening (Figure 5-10b) peak periods. The horizontal axis shows different cases of partitioning for both directional (blue bars) and non-directional (orange bars) approaches with different sizes versus the estimated value for the entire study network (the green bar). Clusters are sorted based on the increasing order of the sub-networks average density. Results indicate that the coefficient of reliability relation (the slope of the linear fit) significantly changes over the clusters in each partitioning approach for both AM peak and PM peak periods (the reliability measure for clusters is in the range of 0.5 to 1.7 times of the measure for the overall study network). This demonstrates the effectiveness of network partitioning in characterizing the reliability performance in different parts of a large regional network.

The average and standard deviation of density are inversely correlated with the coefficient of reliability relation for different partitioning cases. The density coefficient of variation, which is the ratio of the standard deviation to the mean density, seems to play a key role in describing the relationship between the congestion measures and reliability of travel time. The third chart from the top indicates that this variable is directly correlated with the reliability coefficient for both peak periods. The association of these two indicators, which relates a network congestion measure to a reliability indicator, is rather intuitive. It is therefore not surprising that if the network is partitioned based on the congestion distribution, it can affect the reliability measure estimation depending on the level of congestion.

Figure 5-11 reveals the direct correlation between the magnitude of the clockwise hysteresis loop in the entire-day NFD and the anti-clockwise hysteresis loop in the entire-day reliability of travel time graph. This figure represents the results for the study area and sub-networks partitioned based on the entire-day density data. Clusters are sorted based on their average density. Characteristics of the hysteresis loop can be utilized to describe the performance of the network.

By increasing the average density of the clusters, the system becomes more unstable during the recovery phase. As the congestion level of a network intensifies, more vehicles are trapped in the gridlock. Almost immobilized vehicles need a very long time to get out of the gridlock during the recovery phase which implies inefficient recovery of the network (Mahmassani et al., 2013). Consequently, a large hysteresis loop is formed in the NFD, and a larger range of densities become multivalued. Multivaluedness in the NFD implies traffic instability in the network (Saber et al., 2014c; Zockaie et al., 2014b), which leads to multivaluedness in the reliability diagram. As a conclusion, when the size of the hysteresis loop gets larger, and consequently the system becomes

less capable to recover itself efficiently, the average mean travel time rate increases throughout the network, which results in a large hysteresis loop in the reliability of travel time diagram.

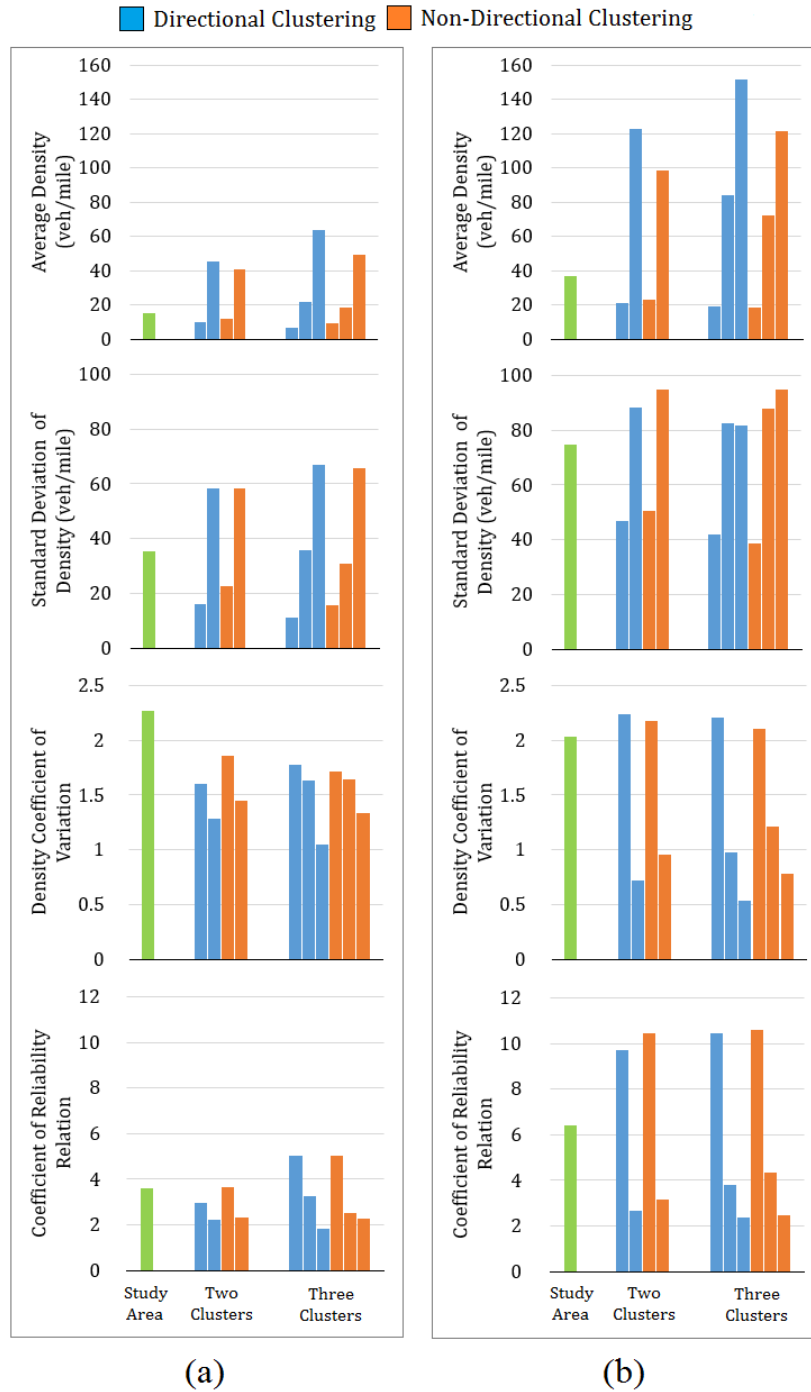


Figure 5-10- Correlation of the coefficient of reliability relation with different congestion measures and the number of clusters during (a) AM Peak Period, and (b) PM peak period

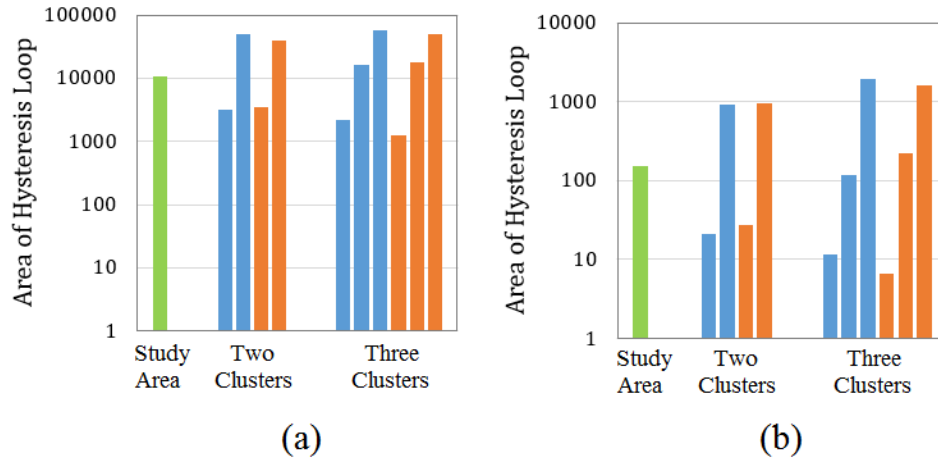


Figure 5-11- Correlation between the area of hysteresis loops in (a) NFD and (b) Reliability of travel time graph (values are presented in logarithmic scale)

## 5-6- Summary

This chapter explores the impact of partitioning a heterogeneous network on the estimated travel time reliability measure, as the main contribution. For this purpose, the reliability measure is estimated for the entire heterogeneous network and different clusters generated by employing directional and non-directional partitioning approaches. The impact of these approaches, as well as the number of clusters on the travel time reliability relation are assessed in this chapter. Two different approaches are also used to allocate vehicle trajectories to different time intervals in the reliability measure estimation, with different implications for the extent of variability that is captured. Applying and comparing two methodologies for partitioning and two approaches for the reliability measure estimation under different actual demand patterns (AM peak versus PM peak) in an actual large-scale network are other contributions of this study. The key findings from the numerical results are as follows:

- Partitioning a large-scale heterogeneous network into optimal number of homogeneous sub-networks improves the travel time reliability estimation. In this study, three-cluster partitioning

is considered as the preferred case. It should be noted that partitioning into four subnetworks improves the partitioning quality, compared to the 3-cluster case, however, it does not provide a significant improvement. On the other hand, partitioning the network into four clusters is much more challenging than the 3-cluster case. Thus, a trade-off between the computational efficiency and the accuracy of the results needs to be made. Thus, the 3-cluster case is adopted for the case study.

- The sub-trajectory approach estimates more robust and higher reliability measures and considers network dynamics in a more coherent manner than the trajectory approach. It also estimates different values for the AM and PM peak periods, unlike the trajectory approach.
- The directional partitioning to three clusters has the best performance relative to the non-directional approach and other cluster sizes based on the defined partitioning quality measure. This highlights the importance of considering regions with homogeneous level of congestion for the aggregated network model.
- In both AM and PM peak periods, there is an inverse relation between the reliability measure, and average and standard deviation of density. A larger density coefficient of variations indicates more uncertainty in the network.
- The density coefficient of variation is another measure to assess the impacts of the network partitioning on the reliability measure which is found to be directly related to the reliability measure.
- The area of hysteresis loops in the entire-day NFD and reliability graphs are directly correlated for all partitioning cases.

## CHAPTER 6 – Estimating Large-Scale Vehicular Emission

### 6-1- Overview

Estimation of vehicular emissions at the network level is a prominent issue in transportation planning and management of urban areas. For large networks, macroscopic emission models are preferred due to their simplicity. However, these models do not consider traffic flow dynamics that significantly affect emission production. This chapter proposes a network-level emission modeling framework based on the network-wide fundamental diagram (NFD), via integrating NFD properties with an existing microscopic emission model. The NFDs and microscopic emission models are estimated using microscopic and mesoscopic traffic simulation tools at different scales for various traffic compositions. The major contribution is to consider heterogeneous vehicle types with different emission generation rates at network-level models. This framework is applied to the large-scale network of Chicago as well as its CBD area. Non-linear and support vector regression models are developed using simulated trajectory data of thirteen simulated scenarios. The results show a satisfactory calibration and successful validation with acceptable deviations from underlying microscopic emission model regardless of the simulation tool that is used to calibrate the network-level emission model. The microscopic traffic simulation is appropriate for smaller networks, while the mesoscopic traffic simulation is a proper means to calibrate models for larger networks. The proposed model is also used to demonstrate the relationship between macroscopic emission and flow characteristics in the form of a network emission diagram. The results of this study provide a tool for planners to analyze vehicular emissions in real-time and implement optimal policies to control the level of produced emission in large cities.

## **6-2- Background and Modeling Tools**

### *6-2-1- Traffic Flow Simulation*

Traffic simulation under the prevalent network and traffic conditions is a common step to model calibration and usage, as well as in the calculation of NFD and microscopic emissions. Dynamic traffic assignment (DTA) is a more suitable choice for this framework, since it effectively incorporates the effects of traffic dynamics on the vehicular mechanical characteristics. DTA involves iteratively finding network user equilibrium based on the best paths in the network that keep changing due to variations in congestion with time while maintaining that no user can unilaterally decrease their travel time by changing the assigned route. This study uses the commercial traffic simulation tool PTV-Vissim for microscopic and DYNASMART-P for mesoscopic traffic simulations.

DTA-based traffic simulation results in detailed vehicular trajectories that include the vehicular properties, such as vehicle class and engine specifications, as well as dynamic properties such as position in the network, speed, and acceleration at each time step. The default simulation time steps of 1 and 6 seconds respectively in PTV-Vissim and DYNASMART-P are used for simulation and generation of vehicle trajectories. Note that the 6-second step size potentially masks the significant speed variations that can occur in this time. Moreover, mesoscopic simulation does not differentiate the values of speed and acceleration of individual vehicles moving on a given link at a given timestep. These drawbacks of mesoscopic modeling are generally acceptable in case of large networks since they are the only viable approach due to the size of the network. Furthermore, these important qualifications of mesoscopic simulators may be rendered insignificant if the resultant emission estimates can be calibrated against and proven similar to the more robust

microscopic emission estimates. Thus, in this study both microscopic and mesoscopic simulation tools are utilized to model emissions for one medium and one large sized network.

In this study, it is assumed that the relevant traffic state of the network at any given time is represented by the network fundamental diagram. In this regard, different sets of conditions hereby called ‘traffic scenarios’ are considered for training the emission estimation model in order to ensure its ability to work over a diverse range of common traffic states. Each traffic scenario leads to an observed network-wide flow-density relation (observed NFD) and is characterized by a number of factors that are known to influence the shape and existence of the NFD. These factors include network size and configuration, traffic demand and capacity, traffic composition, signal timing, dynamic user behavior, incidents as well as local weather conditions (Nesamani et al., 2007). Two key variable factors used as inputs to the traffic simulator are demand level and profile, and prevalence of adaptive drivers, which are shown to have significant impacts on network traffic state (Ji et al., 2010; Mahmassani et al., 2013; Saberi et al., 2014c).

#### *6-2-2- Traffic Composition*

Vehicular emission rates are significantly dependent on the size of vehicle and its engine and fuel characteristics. Based on factors such as the used microscopic emission model, a simplified nested traffic composition scheme with four vehicle types is considered for a two-level modeling process based on size and fuel type. In this classification scheme, vehicles are first categorized as either light (cars, vans, and sports utility vehicles) or heavy vehicles (buses, trucks, and tractor-trailers). The light vehicles are then classified on the basis of fuel type—petrol (gasoline), diesel, and liquefied petroleum gas (LPG) cars. It is assumed that for a given NFD, the proportion of heavy vehicles is fixed and therefore, the fleet composition of the light vehicles can vary freely without affecting NFD. Thus, the variation of both size and fuel type can be effectively

captured without significant increase of computational complexity. The choice of these specific subcategories is based on the availability of calibrated functional coefficients in the micro-emission model.

Since the internal composition of light vehicles is a direct and variable indicator of network-wide emissions, it is to be tested for a wide variety of combinations. For comprehensive and qualitative testing, uniform sampling is a good option. One way of generating these scenarios based on uniform sampling is with the use of linear Diophantine equation  $p_{petrol} + p_{diesel} + p_{LPG} + p_{heavy} = 1$ , where  $p_i$  is the penetration rate of vehicle type  $i$ . Since the proportion of heavy vehicles is fixed and known, sets of the light vehicle composition variables,  $TC = (p_{petrol}, p_{diesel}, p_{LPG}, p_{heavy})$ , hereby called traffic composition sets, can be generated combinatorically at a specific uniform spacing using the number theory concept of the stars and bars problem (Feller, 2008). In this study, for  $p_{heavy} = 0.1$  and a spacing of 10 percent, i.e.,  $p_i \in \{0, 0.1, \dots, 0.9\}$ , a total of  $\binom{10+3-1}{3-1} = 55$  combinations are generated, labeled TC1 through TC55. Once these sets are generated, the trajectories of the light vehicles can be assigned to a fuel type based on a weighted random number using the assumed proportions in each scenario.

### 6-2-3- Micro-Emission Model

The methodology provided in this study does not make any qualifications regarding the choice of a microscopic emission estimation model as long as it takes into account the dynamic behavior of traffic and the distinction between vehicle types. This study, incorporates the polynomial model suggested by Panis et al. (Int Panis et al., 2006) given as:

$$E_n^p(t) = c_1^p + c_2^p v_n(t) + c_3^p v_n^2(t) + c_4^p a_n(t) + c_5^p a_n^2(t) + c_6^p v_n(t) a_n(t) \quad (1)$$

Here,  $E_n^p(t)$  denotes the emission rate of pollutant  $p$  (in grams/second) from a vehicle  $n$  at simulation interval  $t$ ,  $v(t)$  is the vehicle's speed in that time interval (m/s),  $a(t)$  is its acceleration ( $\text{m/s}^2$ ), and  $c_1^p$  through  $c_6^p$  are coefficients of the fitted curve. For more details on the model calibration procedure and coefficients values the readers are referred to Panis et al. (Int Panis et al., 2006). The estimated values of micro-emission at different simulation intervals are aggregated for each 5-minute time interval and values of macro-emission are calculated by summing the values of micro-emission over the simulation period.

Two air pollutants are considered in this study – carbon dioxide ( $\text{CO}_2$ ), and nitrogen oxides ( $\text{NO}_x$ ). These pollutants have significant environmental and health impacts and have been considered by various studies in the literature (Int Panis et al., 2006; Jiang et al., 2015; Niemeier et al., 2006).  $\text{NO}_x$  (which is mostly hydrocarbons derived from fossil fuels) are included in emission standards by many environmental agencies, such as Hong Kong's Environmental Protection Department (Cen et al., 2016).  $\text{CO}_2$  acts as a greenhouse gas that is a major cause of global warming. It should be noted that the transportation sector is one of the largest contributors of  $\text{CO}_2$  emissions worldwide (Liu et al., 2016; López-Martínez et al., 2017). Note that the methodology proposed here provides flexibility to incorporate other pollutants and vehicle types, as long as they fit the general structure of the used micro-emission model.

### **6-3- Modeling Framework**

This study uses a framework that systematically integrates a microscopic emission estimation model with a dynamic traffic assignment simulator to assess the emission characteristics of vehicles at network-level. This model considers the vehicle dynamics at a macroscopic level by generating vehicle trajectories using both microscopic and mesoscopic

simulation tools. This is a variation of the more general format of integration of cross-resolution modeling techniques, whose reliability has been sufficiently validated in the literature (Jamshidnejad et al., 2017; Zhou et al., 2015).

The procedure followed in this study is illustrated in Figure 6-1. The schematic shows the respective steps to be followed for the creation of the model and its validation and application. The modeling process includes feeding network and traffic state inputs to the traffic simulator. The choice of this traffic simulation model largely depends on the size of the network. This study uses two traffic simulation techniques – microscopic and mesoscopic – to distinguish the applicability of these two types of techniques at two scales. Traffic simulation is used to generate two key outputs – aggregate traffic flow indicators and a set of vehicle trajectories. These data are then analyzed to generate NFD and network-wide emission estimates, which can be combined to visualize a network emission diagram (NED).

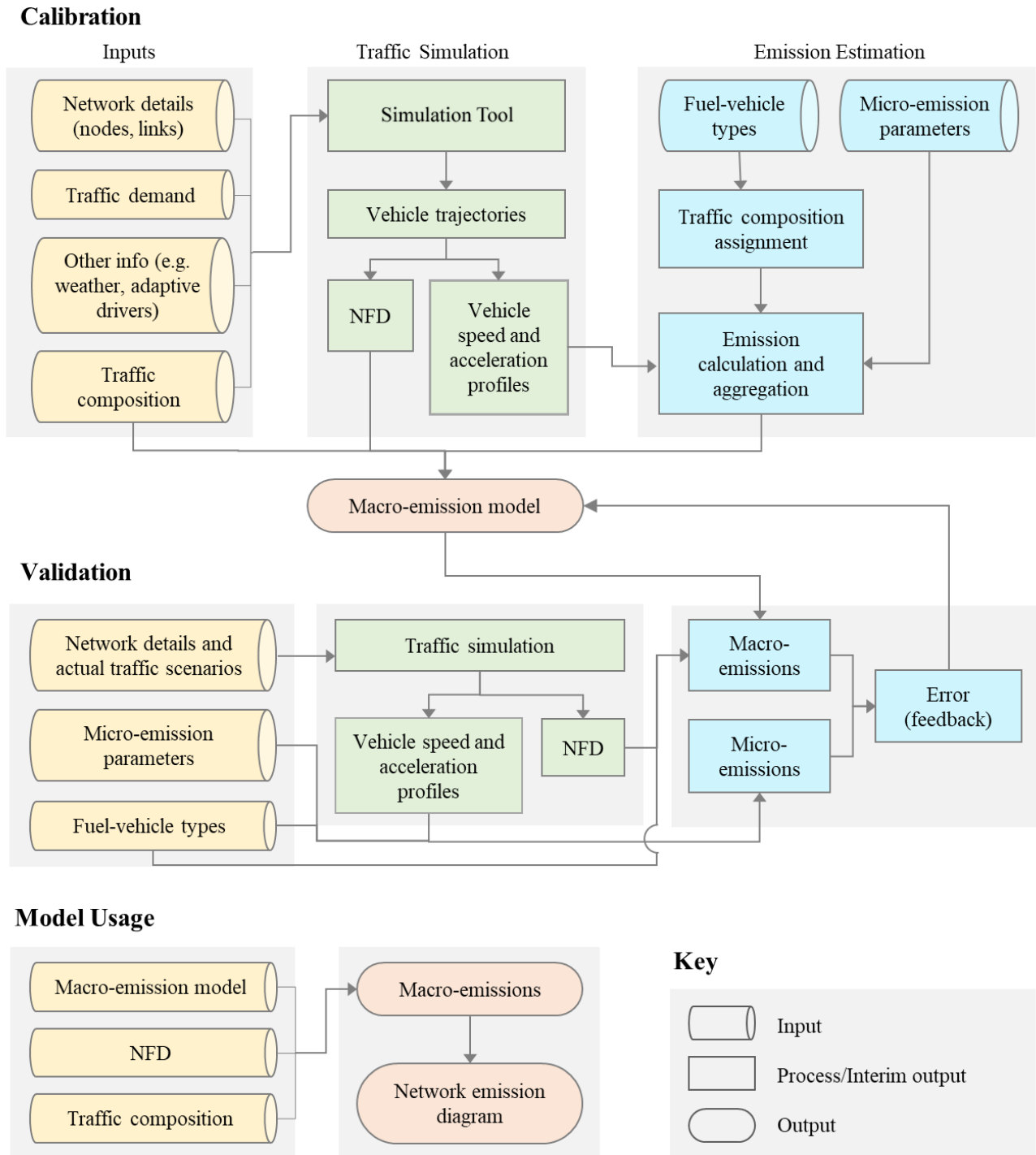


Figure 6-1 Research framework to estimate a macro-emission model

Two members of supervised learning models, non-linear regression and support vector machine (SVM), are utilized to estimate the network-wide emission by incorporating NFD and market penetration rates of different vehicle types in the network. SVM is mainly employed in classification contexts (Suykens and Vandewalle, 1999). It is also a well-recognized regression technique (Smola and Schölkopf, 2004). Support vector regression (SVR) extends sophisticated binary classification via kernel trick to regression. In this study, an SVR model is generated with the input set  $\{K(t), Q(t), p_{petrol}, p_{diesel}, p_{LPG}, p_{heavy}\}$  and the radial basis function kernel as

$$\phi(u, v) = \exp(-\gamma||u - v||^2) \quad (2)$$

Here, the kernel function  $\phi$  measures the degree of similarity between feature vectors (rows of the dataset)  $u$  and  $v$ , and parameter  $\gamma$ , the number of independent variables, is chosen to be 6. In addition to SVR, the following non-linear regression (NLR) model is also formulated as the macro-emission estimator.

$$E_m(t) = \left( \sum_{i=1}^N \alpha_i^m p_i \right) K(t) (\beta_m + V(t)) = \left( \sum_{i=1}^N \alpha_i^m p_i \right) (\beta_m K(t) + Q(t)) \quad (3)$$

Here,  $E_m$  is the rate of emission (in gram/second) of pollutant  $m \in \{\text{CO}_2, \text{NO}_x\}$  at time step  $t$  in the observation period,  $p_i$  is the penetration rate of vehicle type  $i$  in the traffic stream (1: petrol (gasoline) car, 2: diesel car, 3: LPG car, 4: heavy vehicle),  $K(t)$ ,  $V(t)$ , and  $Q(t)$  are respectively network-wide average density, speed, and flow, and  $\alpha_i^m$  and  $\beta_m$  are the model parameters for pollutant  $m$ .  $\beta_m$  represents the offset effect of average density, i.e., the effect of density on emissions at very low speeds. A large value of this parameter implies high emission levels in the highly congested regime (in the limit case, it dictates the effect of traffic jam on emissions).

The proposed macro-emission model integrates the network-wide average density, as a representative of vehicle accumulation in the network, and average speed as the main incorporating

factor in vehicular emission. The macro-emission model follows the structure of the underlying micro-emission model where the speed and its variation are the core factors. Multiplication of the network-wide average density aggregates the individual vehicles emission at network level. The aggregated value then is adjusted by a linear function of different fuel powered vehicles penetration rates. More details will be discussed in the next section.

#### **6-4- Numerical Experiment**

Here, we apply the proposed estimation framework to a large-scale network and a medium size network to estimate the emissions. First, we discuss the study area and traffic scenario specifications followed by the model calibration. To calibrate the model, actual data from ten different days are utilized to generate traffic scenarios. Then, the model is validated employing the actual data from the other three days. To better comprehend the relationship between network dynamics and emissions, we introduce a visualized form of the calibrated model for different pollutants, namely the Network-wide Emission Diagram (NED).

##### *6-4-1- Study Area and Traffic Scenarios*

The proposition of this study requires traffic information for a large urban road network. The city network of Chicago, Illinois is selected as the study area. This network is a part of the Greater Chicago metropolitan area, one of the largest metropolitan areas in the United States. This network is bound by O'Hare airport to the west and Lake Michigan to the east. The schematic of the network and its size parameters are shown in Figures 6-2(a). To include the effects of network loading and unloading during peak and off-peak times, a simulation period of 5:00 AM to 12:00 PM is chosen in this study, which includes the morning peak of traffic rush, as well as the off-peak periods before and after it. For the purpose of calibration of macroscopic emission modeling against the more effective microscopic modeling, a smaller region of this network is also analyzed.

The central business district (CBD) region of this urban network (shown in the right part of Figure 6-2(a)) is simulated using a microscopic traffic simulator.

The network data is provided by the Chicago Metropolitan Agency for Planning. This data includes the network configuration and a base demand matrix. The demand profile of the base calibration scenario and the resultant NFD for both study networks are shown in Figures 6-2(b) and 2c. The daily demand of the base scenario is 742,181 vehicles with a composition of 7 percent heavy and 93 percent light vehicles. For simplicity and clarity of creating traffic composition sets, a base case of 10 percent trucks is assumed for NFD generation and emission estimation.

The real-world data observed over 86 weekdays are used to create 86 variations of the base model. These observations include weather conditions, number of incidents, and total flow observed by 122 loop detectors. To limit the numerical experiments, 13 days with clear weather conditions are randomly selected for analysis and simulation, and an NFD is observed for each day. The selected scenarios are chosen from the days with normal weather conditions to avoid considering the weather condition impacts on emissions. Ten of these NFDs are utilized to calibrate the proposed model (labeled C1-C10), while the remaining three are used for validation (V1-V3). The two parameters used to define these traffic scenarios are aggregate daily traffic demand within the network, and the daily average percentage of adaptive drivers in the circulating traffic.

According to Figure 6-2(c), the larger, low-density NFD of the city network contrasts sharply with the highly congested, smaller CBD network. The NFD progresses with time in the clockwise direction, with a steady increase in both flow and density during the loading phase up to the point of maximum flow and receding to the congested phase after that, with an increase in network density despite a drop in the throughput. In the recovery phase (the two-hour period of

zero total demand), the network readily becomes empty, leading to a decrease in both flow and density, but the NFD does not follow the path as of the loading period, resulting in hysteresis. NFDs of other scenarios are also observed to be shaped similarly and exhibit hysteresis during the recovery phase. The variation of these NFDs is partly represented in Figure 6-3 using three network-level measures – maximum of the flow, maximum density, and the area of hysteresis loop. Since the results are the average values reported at network level, significant fluctuations are observed among different scenarios.

#### *6-4-2- Model Calibration*

Generated emission values are calculated based on trajectory data and the macro-emission model for each pollutant and scenario at every 5-minute time interval for the entire simulation period by summing the values of emission rates (grams per second for micro-simulation or per 6 seconds for mesoscopic-simulation) over 5 minutes across all the links. It is observed that the macro-emission rate increases roughly parabolically with increasing density in the loading phase (see Figures 6-4(a) and 6-4(c)). This is due to the fact that emission rate is more heavily dependent on individual vehicle operational characteristics than their behavior as a group. It should also be noted that despite the positive correlation of speed with emission rate in the microscopic model, its effect is overshadowed by the effect of the network flow rate (throughput). This is evident in Figures 6-4(b) and 6-4(d), where the macro-emission rate increases at the network loading phase due to increased network average flow rate, despite of a steady decrease in the average speed. However, beyond the flow breakdown point the emission generation rate decreases because of a reduction in both the average speed and the throughput in the network. This pattern, however, is less prominent in the case of NO<sub>x</sub> (Figure 6-4(d)). Despite of reduced emission rates in the

congested phase, the longer clearance time for the congested traffic due to reduced flow rates, imply higher overall pollutions in this phase.

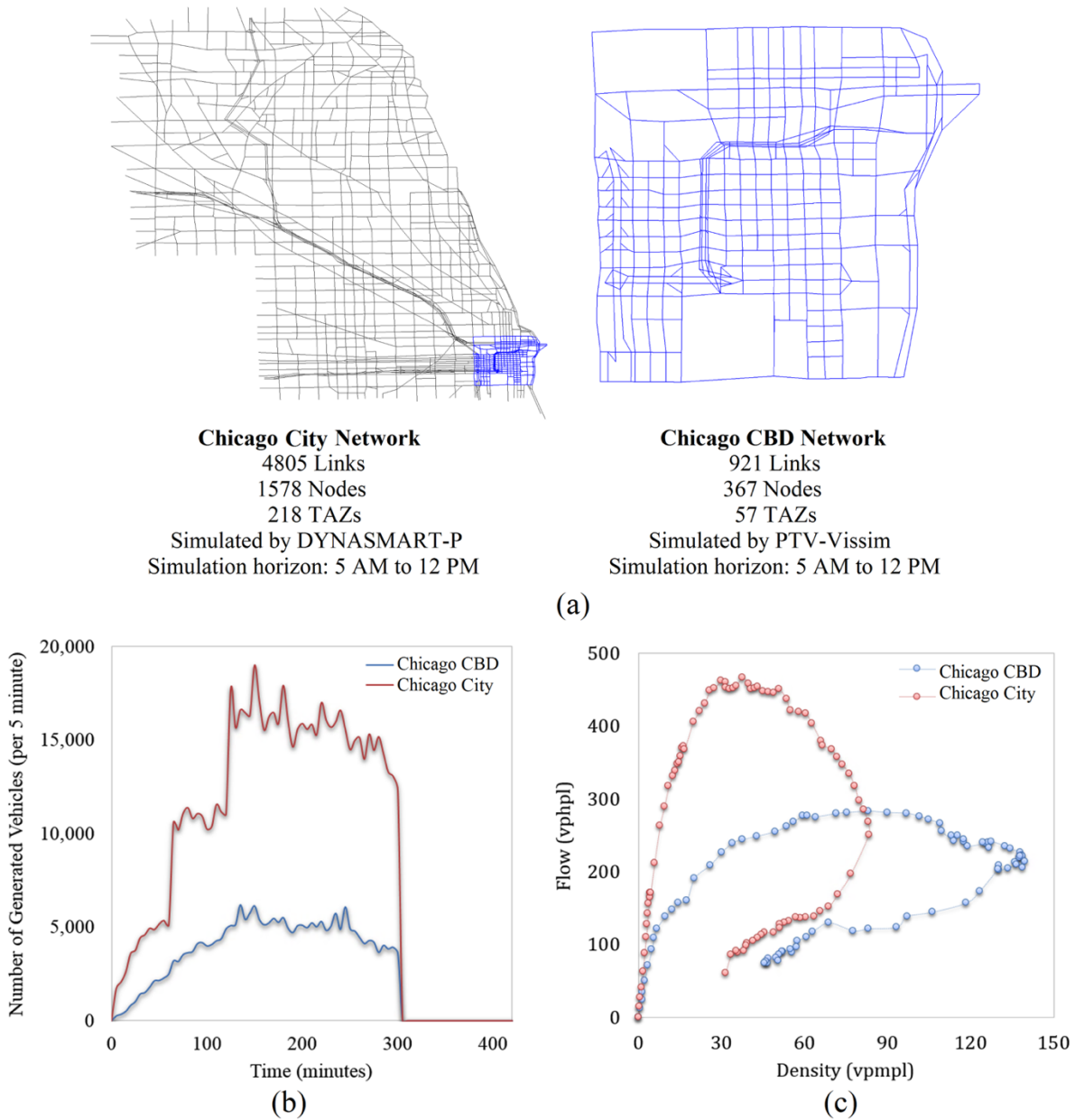


Figure 6-2 (a) Specifications of the study area, (b) simulated demand profiles, and (c) network fundamental diagrams of the Chicago city road network and its CBD (diagrams are for the base calibration scenario C5)

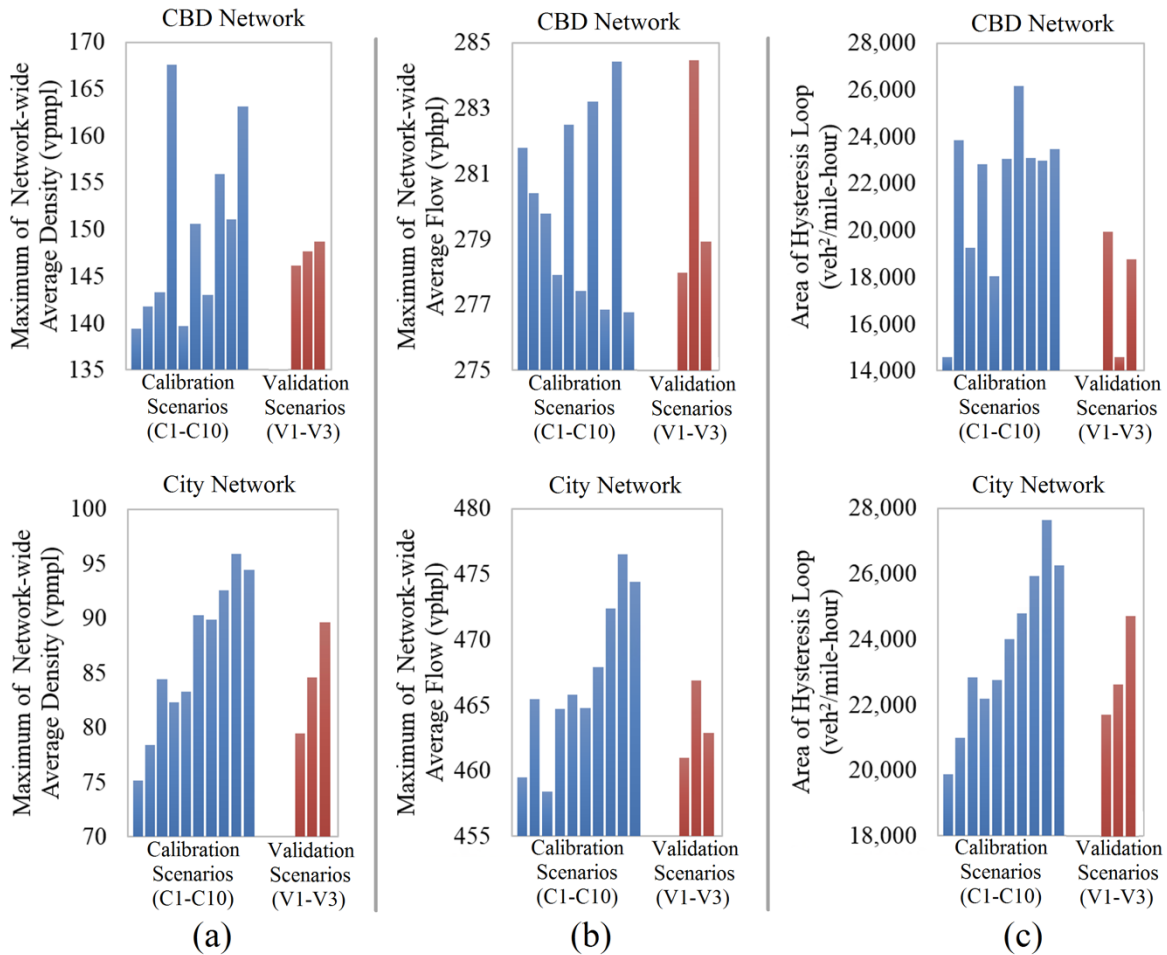


Figure 6-3 Variation of traffic flow characteristics across the different traffic scenarios: (a) Maximum Average Flow, (b) Maximum Average Density, and (c) Area of Hysteresis Loop in NFD Diagram

Figure 6-4 also signifies the independent effect of traffic composition of light vehicles on emission. For demonstration, ten traffic composition sets are uniformly and exhaustively selected and analyzed as seen by the different colored curves in Figure 6-4. They show that for the same value of speed and density, different traffic composition sets only have a scaling effect. Therefore, the model can be simplified by considering a linear combination of the different proportions in the composition set as an independent predictor variable (see Equation 6-3).

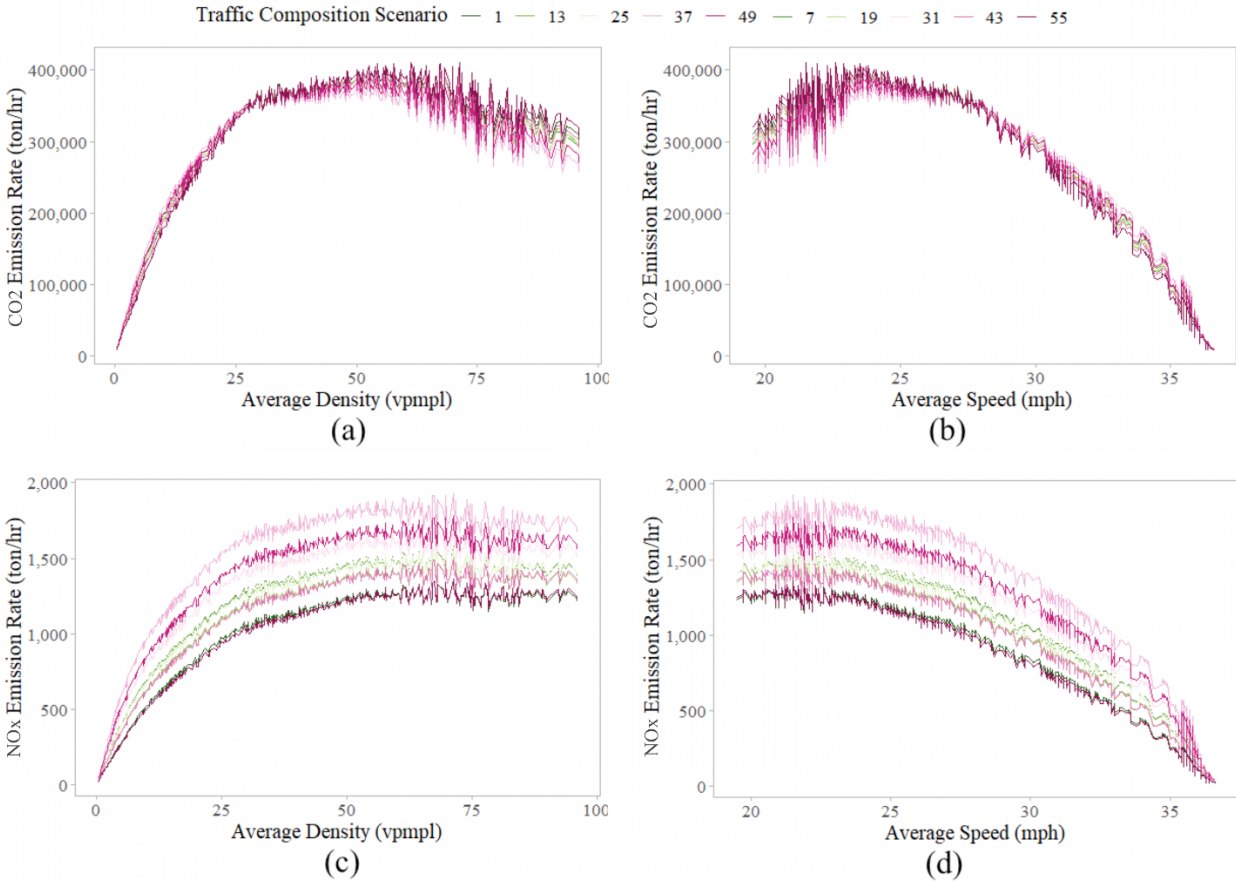


Figure 6-4 Scaling effect of vehicle type percentages on macro emission model in the loading phase of NFD – CBD Network, micro-simulation: (a) emission vs density for CO<sub>2</sub> (b) emission vs speed for CO<sub>2</sub> (c) emission vs density for NO<sub>x</sub> (d) emission vs speed for NO<sub>x</sub> for 10 traffic composition scenarios in the calibration scenario *CI*

The values of the calibrated coefficients of Equation 6-4 for the given study areas are presented in Table 6-1. The p-values associated with all the variables are either exactly or extremely close to zero, and the R-squared values are very close to one, indicating a strong curve fit. Note that the estimated parameters are completely different in two networks, which shows that these parameters need to be calibrate for each network and cannot be transferred. Thus, every application requires a calibration process based on detail analysis of simulation results or available data sets. Using the ten traffic scenarios, an SVR model is also trained to estimate the network-

wide emission. Traffic state at every 5-minute interval and the market penetration rates of different vehicle types are provided to tune the SVR model. The average calibration runtimes of the NLR and SVR models for different pollutants and networks are 0.035 and 3.917 seconds, respectively. These results are obtained using a computer with i7-6700 octa-core CPU with a 3.4 GHz clock and 16 GB memory. It can be seen that SVR training is computationally much more consuming than NLR. In the next sections, it is shown that it also performs slightly better than NLR, leading to the common speed-accuracy tradeoff.

Table 6-1 Parameters of the proposed macro-emission model for the pollutants considered

Network	Pollutant	$\alpha_1$	$\alpha_2$	$\alpha_3$	$\alpha_4$	$\beta$	Adjusted R <sup>2</sup>
CBD (microscopic)	CO <sub>2</sub>	57.52	47.48	59.14	273.6	2.604	0.98
	NO <sub>x</sub>	0.088	0.172	0.089	0.580	6.629	0.99
City (mesoscopic)	CO <sub>2</sub>	483.6	450.6	484.9	2365	2.305	0.99
	NO <sub>x</sub>	1.139	2.210	1.125	7.458	4.686	0.98

### 6-4-3- Model Validation

The calibrated models are validated using the three validation scenarios. The NFDs of the base and validation scenarios are significantly different in terms of congestion pattern (see Figure 6-3). The effectiveness of the validation is quantified using the average of mean absolute relative error (MARE) of the model across each validation scenario. MARE is a widely used error metric that uses range normalization. For a pollutant  $m$ , it is given as:

$$\epsilon_m = \frac{1}{N_C \cdot N_t} \left( \sum_{c=1}^{N_C} \sum_{t=1}^{N_t} \left| \frac{\hat{E}_{c,t}^m - E_{c,t}^m}{E_{c,t}^m} \right| \right) \times 100 \quad (4)$$

Here,  $E_{c,t}^m$  and  $\hat{E}_{c,t}^m$  are the estimates of emission rate of pollutant  $m$  at simulation time step  $t$  for traffic composition set  $c$  made by the reference microscopic emission model and the

calibrated macroscopic model,  $N_c$  is the number of traffic composition sets (in this case, 55), and  $N_t$  is the number of time steps in the simulation period (84 5-minute time intervals for a period of 7 hours). The values of MARE obtained for the validation scenarios are shown in Figure 6-5. It can be seen that all values are reasonably low at the aggregate level, lying below 10 percent. The figures show that the SVR model performs better than the NLR model in all validation scenarios, with an error rate in the range of 2-5 percent. Based on very low error values in the validation scheme, the proposed NLR and SVR models (Equation 6-4 and Table 6-1) are considered valid for application at the study area. Examination of the error distributions across different traffic states did not show any particular pattern, leading us to the conclusion that the errors over different traffic phases are random. Based on this conclusion and very low error values in the validation scheme, the proposed NLR and SVR models (Equation 6-4 and Table 6-1) are considered valid for application at the study area. In summary, the SVR method outperforms NLR, but it must be noted that SVR requires significantly more computation than NLR, and unlike NLR does not provide a closed-form expression for emission rate. The choice of model – either NLR or SVR, thus, is dependent on the practitioner’s preferences. Furthermore, there is no meaningful difference in performance of SVR or NLR for the CBD and city networks that are simulated by microscopic and mesoscopic simulation tools, respectively.

The proposed macro-emission model has some approximations relative to the micro-emission model that is used for its calibration and validation. However, unlike the micro-emission model, once it is calibrated, it does not require detailed trajectory of all traveling vehicles. It only incorporates the network-wide average flow and density given by an available NFD, and the traffic composition, which can be estimated for any given network with various approaches (e.g. see 28, 29, 44). This makes the proposed model a perfect tool for real time control of emissions, unlike

the micro model. Furthermore, it can be used for planning purposes only by changing the traffic composition for the desired scenarios.

The qualitative nature of the inferences made by this model are presented in the next section. Note that in addition to estimating the exact emission rate, the model can capture the variations of the emission rate over the simulation horizon. This is based on a new concept, which is defined as the Network Emission Diagram (NED).

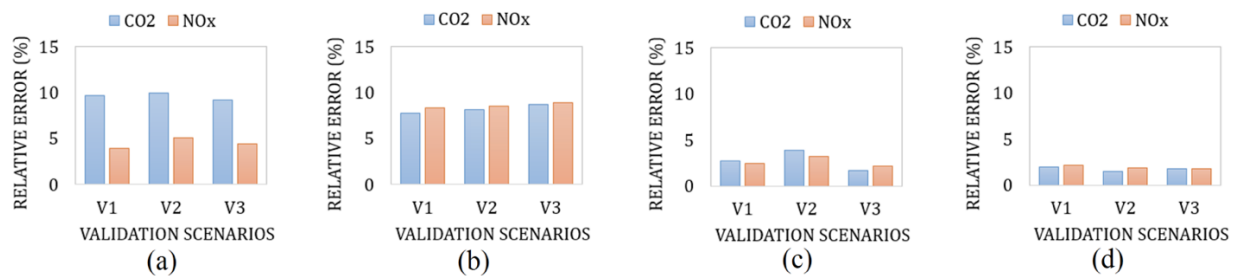


Figure 6-5 Mean absolute relative error in macroscopic emission estimation using the (a) NLR model for CBD, (b) NLR model for city network, (c) SVR model for CBD, and (d) SVR model for city network

### 6-5- Network Emission Diagram

The network emission diagram (NED) is hereby defined as a graphical representation of the relative network-wide emission rates and traffic state variations represented by the network-wide average values of flow and density. It is a three-dimensional graph whose projection on the density-flow plane is simply the network fundamental diagram. In this case, different NEDs are obtained for different pollutants across different traffic scenarios and traffic compositions. Figure 6-6 illustrates an example NED for CO<sub>2</sub> in the traffic scenario V2 and traffic composition set TC25, in which the percentage of each category of light vehicles is equal to 30% and heavy vehicles comprise the other 10%. This figure depicts the three-dimensional NED of CO<sub>2</sub> and its projections

on the two traffic flow variable planes. This figure shows that the model successfully captures variations of the emission generation rate over the simulation horizon with an acceptable precision.

Some important properties of NED can be inferred from Figure 6-6 that are key factors in the analysis of environmental impacts of the network loading mechanism. Macro-emission gets the peak value at the peak flow. This follows from the highly correlated variations of emission with the traffic flow, which is highly intuitive. However, this variation is not strictly linear, and the slopes are different in the two phases. The observations of NEDs of all pollutants show that the flow breakpoint segregates the flow-emission diagram into two phases – stable and unstable. For the same flow in the network, the unstable phase has higher emission rates compared to the stable phase. The unloading phase, characterized by recovering traffic with high density and low speed, is also considered a part of the unstable phase in this case. It can be hypothesized that this occurs because of higher density in the unstable phase, which may have a higher impact than the effect of lower speed in the unstable phase.

Figure 6-6 illustrates that the emission rate increases rapidly with increase in density and reaches a saturation level of maximum at high densities during the loading phase. Then, the flow breakdown occurs and emission rate decreases by density increase until the recovery (unloading phase) begins. The emission rate drops significantly during the unloading phase, reaching its minimum before reloading begins. This is a complementary observation to the varying slopes of the emission function with respect to flow. As mentioned earlier, the unstable phase (loading phase after flow break-down) experiences higher emission rates compared to the stable phase (loading phase before the flow breakdown).

Flow breakdown results in emission rate reduction and it is due to the slowed down vehicles trapped in the gridlock. During the unstable phase (after the flow breakdown), which is stretched

out until the unloading begins, the network-wide average speed and throughput continually decrease and result in less emission rates. It should be noted that it takes a longer time for a more congested network to get recovered from the gridlock. During the unstable phase, vehicles spend more time in the network and produce more emission. Therefore, although the emission rate is decreased for the unstable phase, vehicles stay in the network for a longer time and generate more emissions. So, more congestion results in more cumulative emissions overall. Figure 6-7 illustrates the network fundamental diagrams, emission rates, and cumulative emissions for the city network for two distinct scenarios. This figure demonstrates that a more congested network produces more emission overall, despite the different pattern observed in its NED diagram. Note that the more congested scenario would be recovered much later than the less congested one, increasing the overall generated emission.

Furthermore, the phenomenon of a clockwise and counter-clockwise hysteresis loop can be observed in the emission rate-density and emission rate-flow diagrams, respectively. Existence of the hysteresis loop states that the emission rate is multi-valued for both flow and density. For the same amount of flow, there is a higher emission rate in the unstable phase, owing to the dominant effect of higher density compared to that of lower speed. Also, the maximum emission rate is experienced when the network average flow is near its maximum. A similar phenomenon of multivaluedness is also observed in the emission-density graph. However, unlike the emission-flow diagram, it starts at the beginning of the unloading phase and the emission rate is higher during the loading phase.

Another relevant conclusion that can be drawn from the comparison of NEDs across all scenarios is that the rates of emission vary with the distribution of light vehicles in the network. For example, the increase in the percentage of diesel cars consistently results in an increase in the

emission of nitrogen oxides. A similar case is observed for CO<sub>2</sub> with variations in the percentage of diesel and LPG cars, providing further credibility to the proposed model in this study. These observations collectively provide reasonable evidence to the existence of NED as a general concept. In future studies, the importance and interpretation of this concept will be investigated in detail.

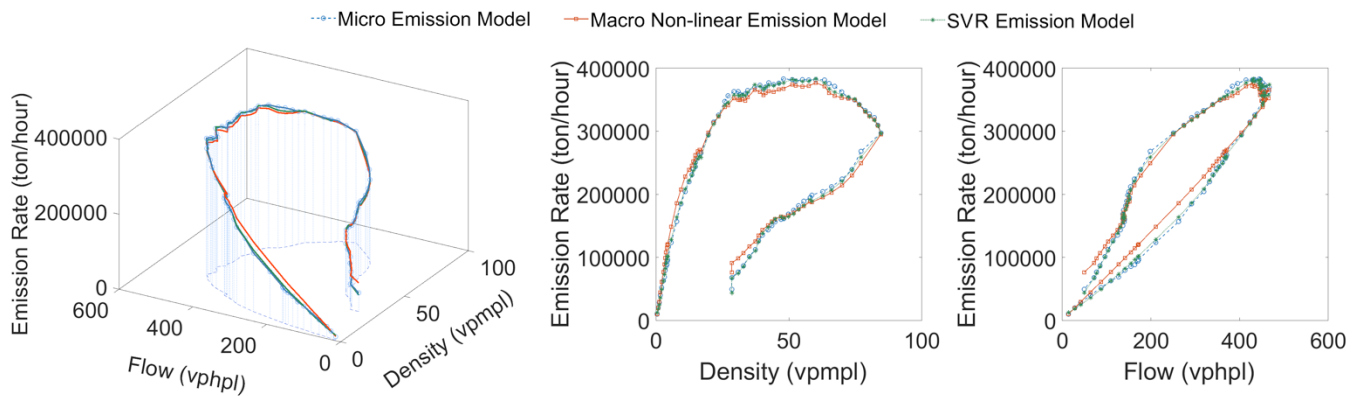


Figure 6-6 The NED of CO<sub>2</sub> for the city network for traffic composition set TC25 in the base validation scenario V2 for the macro-emission models NLR and SVR, along with the base micro-emission model

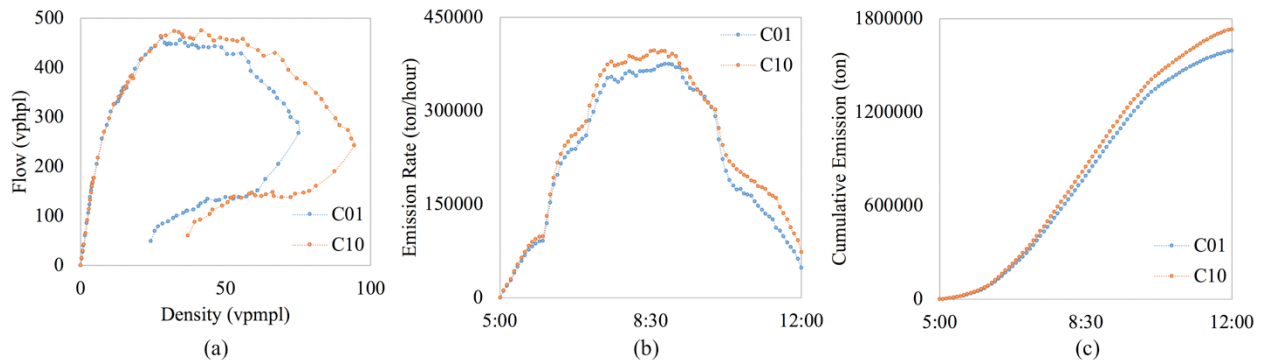


Figure 6-7 (a) network fundamental diagram, (b) emission rates, and (c) cumulative emissions for two scenarios of C01 and C10 for the city network

## 6-6- Summary

This chapter focuses on utilizing the concept of network fundamental diagram (NFD) in conjunction with a microscopic emission estimation model to derive an analytical model of emissions at the urban network level. It involves using network-level traffic demand data to simulate multiple network fundamental diagrams, i.e., sets of macroscopic aggregate flow, density, and speed, and using these diagrams as base feed for a micro-emission model. A macro-emission model is then developed by simulation of different traffic demand and composition scenarios. Once the macro-emission model is calibrated and validated in a specific network, it can be deployed in daily operations for emission estimation addressing typical demand and vehicle composition variations. The major findings of the chapter are summarized below:

- It is demonstrated that while microscopic traffic simulation yields better estimates of macro-emission, it can be replaced with the more resource efficient mesoscopic simulation on larger networks without a substantial loss of accuracy. This is an inevitable replacement for large networks, such as the city network in this study, where the micro simulation is not feasible due to computational complexity.
- A proper regression model (for large-scale emission estimation) needs to be selected depending on the available computational resources. The numerical experiments in this study showed that although SVR outperforms NLR, both models provide acceptable approximations in the validation scenarios.
- The results of the proposed model for the emission estimation strongly support the existence of a relationship between emissions and the traffic state of the network represented by its NFD.

- Based on the network emission diagram (NED), the maximum emission rate occurs at about the maximum network average flow right before the network breakdown due to congestion. However, lower emission rates after the flow breakdown point do not demonstrate total less emission, since the flow breakdown stretches the vehicle presence in the network due to traffic congestion, resulting more emission overall.
- The results of NED analysis suggest that the multivaluedness of emission rates for emission-flow and emission-density diagrams occur at the flow breakdown and unloading points, respectively.

## **CHAPTER 7 – Real-Time Network-Wide Traffic State Prediction Considering Inclement Weather Impact**

### **7-1- Overview**

The problem of real-time traffic state prediction for large-scale urban networks is studied in this chapter. The network traffic state is affected by fluctuations of the network demand and supply. Weather condition is one of the factors that impacts the characteristics of the network-wide traffic flow relationships. The spatiotemporal variations in weather parameters such as visibility, and rain and snow precipitations affect drivers' behavior (Böcker et al., 2013; Saneinejad et al., 2012). This results in distinct characteristics of traffic flow in comparison to a clear weather condition (Hou et al., 2013). The impact of adverse weather conditions has not been considered in the network level traffic estimation problem. So, as one of the applications of network-wide traffic flow relationships, this chapters aims to improve the real-time network-wide traffic state estimation.

First, the impact of various combinations of the weather variables, including visibility, and rain and snow precipitations, on the network-wide traffic flow characteristics is investigated using a stochastic analysis. The two representatives of the traffic flow state at the network level, i.e. network fundamental diagram (NFD) and travel time reliability (TTR), are considered to explore this impact. Then, the adverse weather condition is considered in the real-time traffic state predicting framework for an urban network by modeling the network exit flow as a function of not only the network accumulation, but also the weather variables. To this end, the Support Vector Machine (SVM) algorithm is utilized to model the network exit flow to be able to consider the weather parameters and make the model applicable to general networks (in terms of the congestion level). Then, the network accumulation data is collected using the loop detectors installed on

optimally selected links (unlike the current literature that assumes that the accumulation data from the entire network is available) to facilitate and verify the traffic state prediction process. To this end, the resource allocation problem presented in chapter 3 is reformulated and solved to identify the optimal subset of the links to be equipped by the loop detectors to estimate the network accumulation efficiently.

## **7-2- Data Intuition**

Prior to developing a real-time traffic state prediction framework, the influence of the weather conditions on network-wide traffic flow relationships is investigated. Network fundamental diagram (NFD) and travel time reliability (TTR), as the two representatives of the traffic flow state at the network level, are considered to explore these impacts. These two concepts are introduced and broadly discussed in the previous chapters. The real-world traffic data of 86 weekdays (hereby called scenarios) of the Chicago network is utilized to explore the impacts of weather condition variations on NFD and TTR. For each scenario, a demand factor is calculated using the observations of loop detectors (associated with each day/scenario) installed on the network freeways. This factor represents variations in the base modeled demand among different scenarios, comparing the daily observed counts with the average value over all scenarios. Visibility, and rain and snow precipitation intensities are used to describe the weather conditions for each scenario. Weather data are extracted from the Automated Surface Observing System (ASOS) station at the Chicago Midway International Airport for each scenario. Furthermore, reported crashes for the same set of dates (weekdays over four months) with available loop detector data and weather information are simulated to capture the network supply stochasticity as much as possible.

Out of 86 scenarios, 65 are identified as clear days (no precipitation and no visibility reduction) and 21 are specified as scenarios with adverse weather conditions. Each scenario is attributed by three characteristics of rain and snow precipitation rates, crash records, and the demand factor. Figure 7-1 illustrates the relationship between these two factors and network-wide traffic flow characteristics. The values on the vertical axes are scaled to a number between zero and one (the value one stands for the maximum value among the 21 weather scenarios). Scenarios with different demand factors (in three levels of less than one, equal to one and more than one) are distinguished in this figure and a least square linear regression is fitted to each demand factor category. Figure 7-1(a) indicates that greater values of the demand factor intuitively result in higher values of the maximum density experienced in the network. It also suggests that the network maximum density is positively correlated with the precipitation rate. Figure 7-1(b) illustrates that the maximum throughput (flow rate) of the network is decreased as the precipitation rate increases. The variation of the area of hysteresis loop in NFD (which shows the degree to which the system is unstable during the recovery period) by the precipitation level shows a similar pattern observed in the maximum density of the network versus the precipitation rate. This shows that the higher precipitation rate, the more unstable system would be in the recovery phase (see Figure 7-1 (c)). According to Figure 7-1(d) by intensifying the precipitation rate, network becomes more reliable (the coefficient of the reliability relation is decreased). One possible reason for this observation is the reduced speed variations, which is the case due to lower adopted speeds by travelers under the adverse weather conditions. Therefore, travel time fluctuations are decreased during the high precipitation of snow and rain, and this results in a more reliable system. The same conclusion can be made for the pattern observed for the demand factor in Figure 7-1(d). More congested networks

do not allow travelers to adopt drastically varying speeds, which keeps the travel time fluctuations relatively low.

These results suggest that the macroscopic traffic flow relationships are affected by the descriptive variables of the weather conditions. This calls for incorporating particular weather condition measures in the real-time network-wide traffic state prediction framework, which is explored in this study for large-scale applications in urban areas.

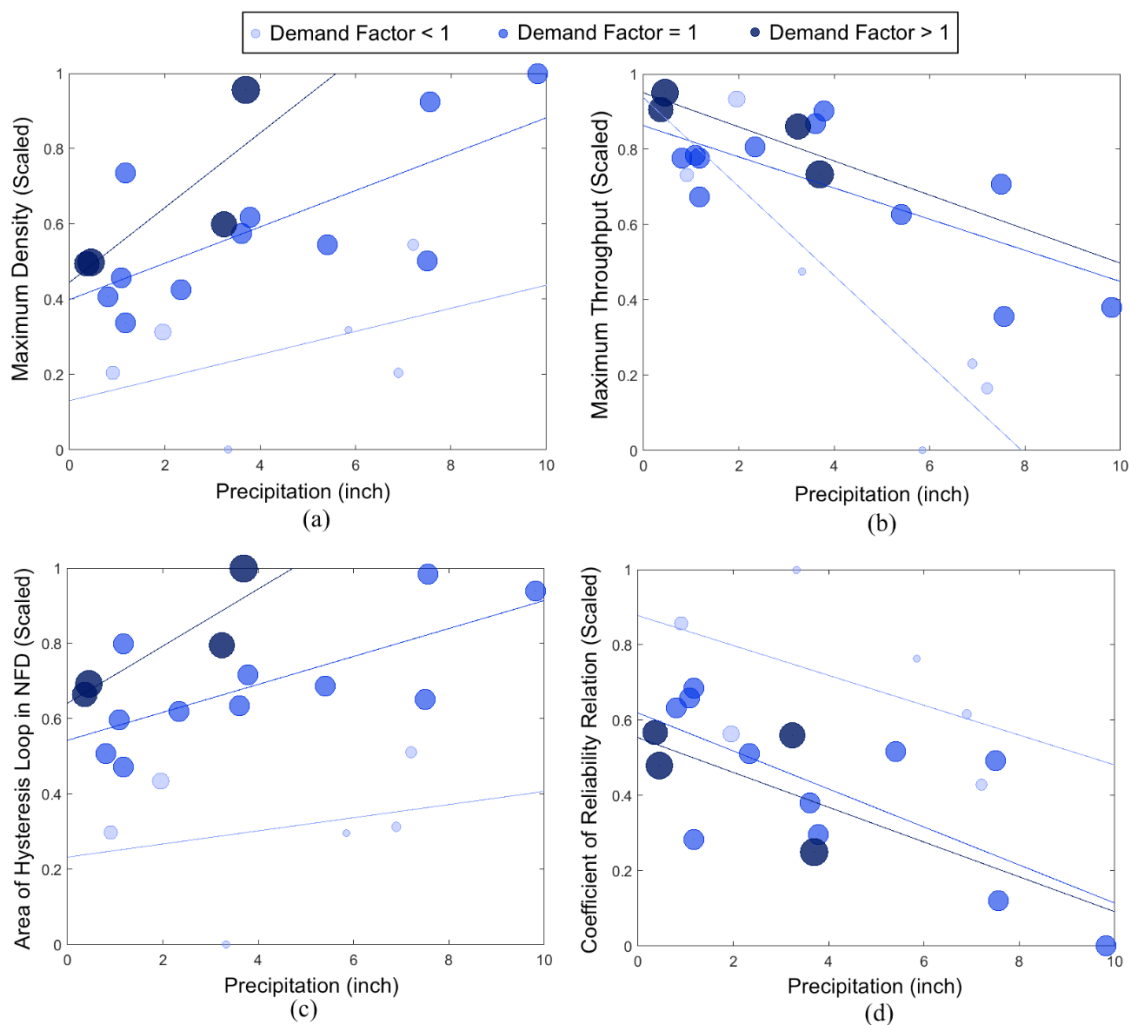


Figure 7-1 Relationship between the precipitation rate and (a) network maximum density, (b) network maximum throughput, (c) area of hysteresis loop in NFD, and (d) coefficient of reliability relation. The vertical axes values are scaled from zero to one, where one stands for the maximum observed value over all weather scenarios

### 7-3- Theory

#### 7-3-1- Network Dynamics

Consider an urban network with a well-defined NFD experiencing weather conditions of  $v(\tau), r(\tau), s(\tau)$ .  $v(\tau)$  is the visibility measure (in mile),  $r(\tau)$  is the rain precipitation rate (in inch/hour), and  $s(\tau)$  is the snow precipitation rate (in inch/hour) at time interval  $\tau$  of the study horizon (i.e. daily or peak periods). The discrete time NFD dynamics of this system can be described by the following first order difference equation (Saeedmanesh et al., 2019):

$$n(\tau) = n(\tau - 1) + T \left( q(\tau - 1) - G(n(\tau - 1)) \right) \quad (7-1)$$

Here,  $n(\tau)$  is the network accumulation at time interval  $\tau$ ,  $q(\tau)$  is the exogenous demand,  $G$  is the network exit flow (arrival rate), which is a function of the network accumulation, and  $T$  is the time interval length (in this study is considered 5 minutes). In this study, we adapt this equation by considering  $G$  as a function of not only the network accumulation, but also the defined weather variables ( $v(\tau), r(\tau), s(\tau)$ ). Equation 7-1 establishes the relationship of the network dynamics between the two consecutive time intervals, which is the basis for the state prediction framework that is discussed as follows.

#### 7-3-2- Extended Kalman Filter (EKF)

Kalman filter is an optimal real-time estimator that is broadly utilized in linear dynamic systems (Kalman, 1960; Kalman and Bucy, 1961). Such systems contain a random noise parameter (generally assumed as a Gaussian noise) and is fed by diffused noisy real-time measurements. Kalman filter was primitively derived for linear systems, however, it is then extended and utilized for nonlinear systems. The extended version of the original Kalman filter is the so-called Extended Kalman Filter (EKF). This extension is facilitated by applying Taylor series in the estimations. EKF transforms the nonlinear function (which is the representative of a nonlinear system) into a

linear function by computing Taylor expansion at every discrete time interval. Simply put, the Taylor series estimate the linear approximation of a nonlinear function. EKF is the fusion of a predefined nonlinear dynamic model (which represents a plant), and real-time noisy measurements (from the plant). Incorporating these two, EKF can provide a real-time prediction of the system state with an acceptable accuracy. In this study, EKF is utilized to predict the traffic state at the network level (i.e. network accumulation). It is also employed to predict an estimation of the network demand as an exogeneous variable, which is difficult to be measured in real-time. Therefore, it is considered as a time-depended model parameter (i.e. random walk). The values of this parameter are predicted in real-time besides the network-side traffic state estimation.

#### **7-4- Methodology**

In this section, a real-time network-wide traffic state prediction framework is designed. First, a plant (here a large-scale traffic network) is attributed by a nonlinear dynamic system. The EKF is utilized then to update the state estimates at each time interval. EKF incorporates a state transition function that is discussed in the Network Dynamics section. This function requires an approximation of traffic exit flow (variable  $G$  in Equation 7-1). The network exit flow is formulated as a function of the network accumulation and weather variables in this study. The traffic simulation of 86 scenarios (discussed earlier) is utilized as a surrogate for the real-world conditions and based on this, an SVM model is calibrated to estimate the network exit flow. The exit flow values are incorporated in the state transition function of the EKF framework to predict the traffic state in real-time. Finally, the methodology developed in chapter 3 and 4 of this dissertation is used to provide an optimal configurations for the real-time measurements in the traffic state estimation and prediction framework. To this end, the resource allocation problem in chapter 3 is reformulated to identify an optimal subset of the links to be equipped by loop detectors

to collect the accumulation data (instead of travel time and traffic flow observations). The predicted values of the traffic state are compared with the ground truth values available from the traffic simulation results.

#### 7-4-1- Nonlinear Dynamic System

Consider a plant with state  $x$ , input  $u$ , output  $p$ , process noise  $\omega$ , measurement noise  $\psi$ , and noisy measurement  $y$ . The plant can be represented as a nonlinear dynamic system (NDS) as follows:

$$\text{NDS: } \begin{cases} x(\tau) = f[x(\tau - 1), u(\tau - 1), \omega(\tau - 1)] \\ y(\tau) = h[x(\tau), u(\tau), \psi(\tau)] \end{cases} \quad (7-2)$$

Exploiting a prediction engine with a known state transition function and available measurements, the traffic state can be predicted in the real time. Figure 7-2 illustrates the framework created for the real-time traffic state prediction for an urban network.

Assume that the traffic state and weather variables are available for a specific time interval, and some noisy measurements of the traffic state (here network accumulation) are accessible. Moreover, assume that the urban traffic network (plant) can be represented by a nonlinear dynamic system. Cyclic exploitation of EKF algorithm facilitates the real-time traffic state prediction, which contains the steps of initialization, prediction, and correction using the available measurements. According to Figure 7-2, the traffic state measurements are collected real-time at each time interval. Incorporating these data and the output of the nonlinear dynamic system into the EKF framework predicts the traffic state updates for the next time interval. This cycle is repeated until the simulation period is completed. Following sections describe the different components of the framework proposed in Figure 7-2.

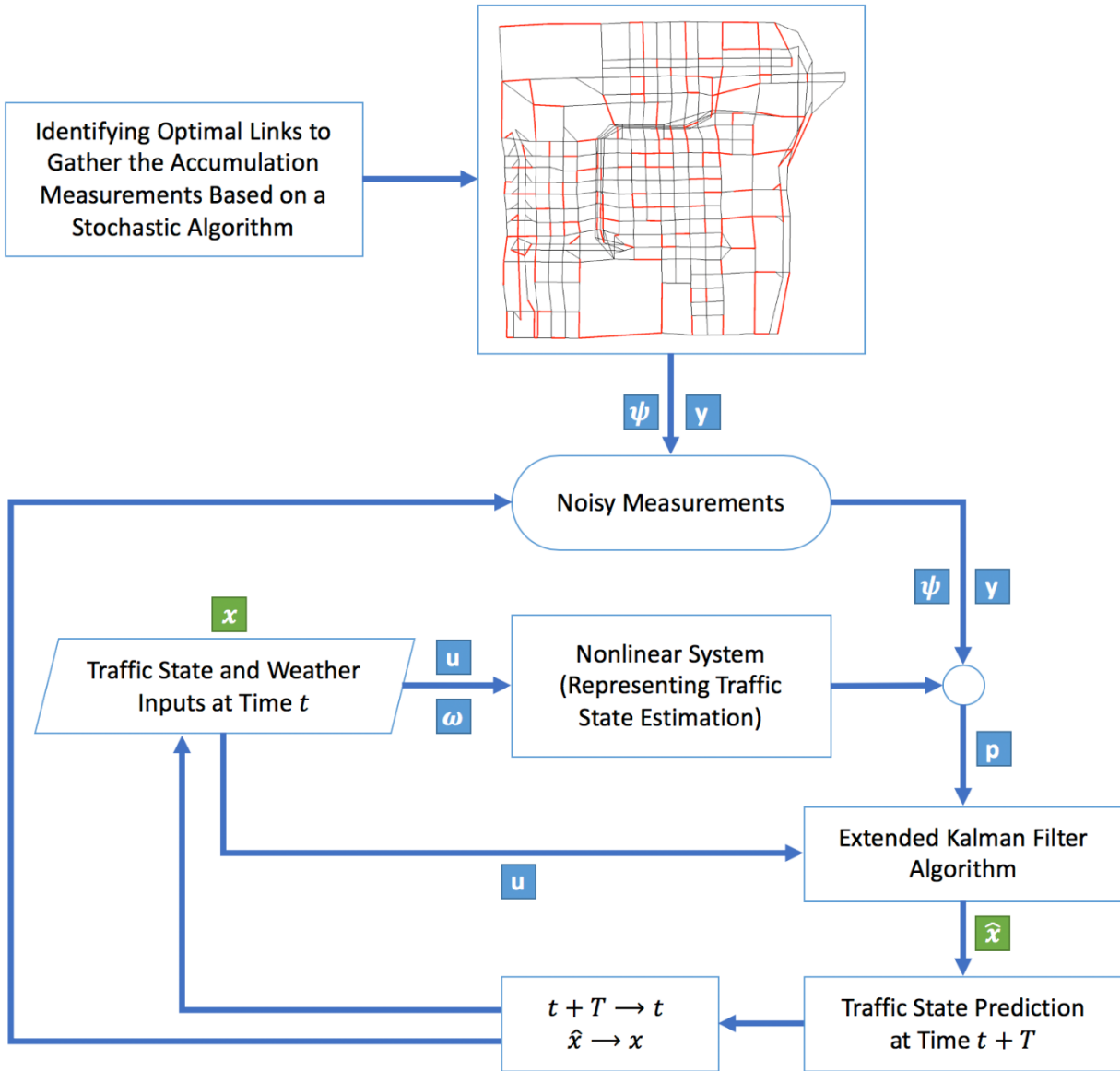


Figure 7-2 Real-time network-wide traffic state estimation with limited observations and incorporating incremental weather impacts

#### 7-4-2- Real-time EKF Traffic State Prediction

The network accumulation and exogeneous demand are the states of interest to be predicted in the real-time. The predicted values then can be incorporated in control strategies. The discrete time NFD dynamics of an urban network, which is represented by the first order difference

equation in Equation 7-1, is utilized as the state transition function for the network accumulation. This function is an input to EKF algorithm and facilitates the real-time prediction. The accumulation measurements are available from the previous time interval. However, it is not feasible to collect the real-time exogeneous demand information at the network level. Therefore, this state is considered as a model parameter (random walk) and is estimated at each run of the framework (see Figure 7-2). Equation 7-3 presents the state transition function for the network accumulation and exogeneous demand.

$$\begin{pmatrix} n(\tau+1) \\ q(\tau+1) \end{pmatrix} = \begin{pmatrix} n(\tau) \\ q(\tau) \end{pmatrix} + \begin{pmatrix} T(q(\tau)-G(n(\tau))) \\ \zeta(\tau) \end{pmatrix} \quad (7-3)$$

Here,  $\zeta(\tau)$  is the noise associated with exogeneous demand and assumed to be a Gaussian noise. Equation 7-4 shows the measurements configuration. It is assumed that the network accumulation measurements are associated with an error (Gaussian noise), which is defined with respect to the latest accumulation value.

$$m(\tau) = n(\tau) + n(\tau)\psi(\tau) \quad (7-4)$$

Here,  $m(\tau)$  denotes the measurement at time interval  $\tau$ , and  $\psi(\tau)$  is the corresponding percentage of the measurement noise in accumulation. Incorporating the state transition function and the measurement configuration, the EKF algorithm estimates the states for the next time interval by minimizing the error between the posterior state estimation ( $\hat{x}(\tau)$ ) and the measured state ( $x(\tau)$ ). Equation 7-5 shows this error term.

$$E = \{[x(\tau) - \hat{x}(\tau)][x(\tau) - \hat{x}(\tau)]^T\} \quad (7-5)$$

### 7-4-3- Exit Flow Function Incorporating Weather Variables

In the literature, the network exit flow function (arrival rate) is approximated by a third-degree polynomial function of the network accumulation (Saeedmanesh et al., 2019) as shown in Equation 7-6:

$$G(n(\tau)) = \alpha_1 n(\tau) + \alpha_2 n^2(\tau) + \alpha_3 n^3(\tau) \quad (7-6)$$

Here,  $\alpha_i$  is the model parameter. There are two certain issues with this model. First, it does not include weather variables and only the accumulation value is incorporated. Second, it does not show a proper fit for any type of network with different congestion levels. The investigative results are presented in the Numerical Results section, showing the improper fit of this model for the considered case study in this dissertation.

In order to overcome these two issues, the network outflow ( $G$ ) is considered as a function of not only the accumulation ( $n(\tau)$ ) but also the weather variables ( $v(\tau)$ ,  $r(\tau)$ , and  $s(\tau)$ ).

$$G(n(\tau)) = f(n(\tau), v(\tau), r(\tau), s(\tau)) \quad (7-7)$$

This function is calibrated utilizing the actual traffic information of 86 days of the Chicago network. Support vector regression is employed to calibrate the exit flow function. Support vector regression (SVR) extends sophisticated binary classification via kernel trick to regression. In this study, an SVR model is generated with the input set of  $\{n(\tau), v(\tau), r(\tau), s(\tau)\}$  and the radial basis function kernel as

$$\phi(p, q) = \exp(-\gamma \|p - q\|^2) \quad (7-8)$$

Here, the kernel function  $\phi$  measures the degree of similarity between feature vectors (rows of the dataset)  $p$  and  $q$ , and parameter  $\gamma$ , the number of independent variables, is chosen to be 4.

#### 7-4-4- Optimal Limited Measurement Configurations

In real world transportation networks, the traffic data (even at the macroscopic level) is not generally available for the entire elements of the network. Even with the help of new emerging technologies, collecting the traffic information requires significant available resources and endures massive complications. To address this issue, it has been previously shown (in Chapters 3 and 4) that the optimal usage of Eulerian observations on a subset of the network links can provide acceptable accuracy of network traffic state information. Based on the proposed approach in Chapters 3 and 4, here, the resource allocation problem is reformulated to identify the optimal subset of the links to be equipped by the loop detectors to gather the accumulation data instead of density and traffic flow. The previously presented stochastic modeling framework (in Chapter 4) is employed to solve the problem. Note that due to considering a scenario-based analysis for the weather factors in this study, using the stochastic resource allocation model is essential. For this specific application, the objective function is considered as follows and the other problem restrictions are still hold as described in Chapter 4 (Equations 4-2 to 4-17).

$$\text{Min } \sum_{s=1}^S \sum_{t=1}^T (n_{st} - \hat{n}_{st})^2 \quad (7-9)$$

Here,  $n_{st}$  is the actual accumulation of the network at time interval  $t$  and scenario  $s$ , and  $\hat{n}_{st}$  is the accumulation of the network at time interval  $t$  and scenario  $s$  based on the accumulation values gathered on the optimally selected links.  $n_{st}$  and  $\hat{n}_{st}$  are calculated using the following equations:

$$n_{st} = \sum_{i=1}^I n_i^{st} \quad (7-10)$$

$$\hat{n}_{st} = \frac{\sum_{i=1}^I \theta_i l_i}{\sum_{j=1}^J \theta_j l_j} \times \sum_{j=1}^J n_j^{st} \quad (7-11)$$

Where,  $\theta_i$  is the number of lanes of link  $i$ ,  $l_i$  is the length of link  $i$ ,  $I$  is the size of the network (number of links),  $J$  is the size of the optimal subset of links and  $n_i^{st}$  is the accumulation data

observed on link  $i$  at time interval  $t$  and traffic scenario  $s$ . Utilizing the solution algorithm presented in Chapter 4 (based on the simulated annealing method) the optimal subset of links for certain predefined amounts of resource availability are identified. The accumulation data from these links are collected at every time intervals and are used as input in the real-time traffic state prediction engine.

### **7-5- Numerical Results**

The proposed mathematical framework is applied to the large-scale network of Chicago and its CBD area. The specification of these two networks are broadly discussed in Chapter 6 (section 6-4-1). Figure 7-3 illustrates the two networks besides their morning demand profile (from 5 AM to 10 AM). The NFDs (here presented by the relationship between the network accumulation and network throughput) of the city and CBD networks of Chicago are presented in Figures 7-3(d) and 7-3(e), respectively. For both NFDs, an SVM regression and a third-degree polynomial curve are fitted. According to Figure 7-3(d), both SVM and polynomial models show a proper fit for NFD, however based on Figure 7-3(e) the polynomial model fails to approximate the NFD for the CBD network. A possible reason can be the different congestion levels of these two networks. The CBD area is reached to its maximum observed flow rate in a shorter time (compared to the city network). The two branches of the NFD (before and after the peak point) in the CBD network have sharper slopes in comparison to the city network. This trend could not be traced by a polynomial model. Even the higher degrees of a polynomial model did not provide a proper fit for the CBD network. However, the SVM model provides an acceptable approximation for both networks.

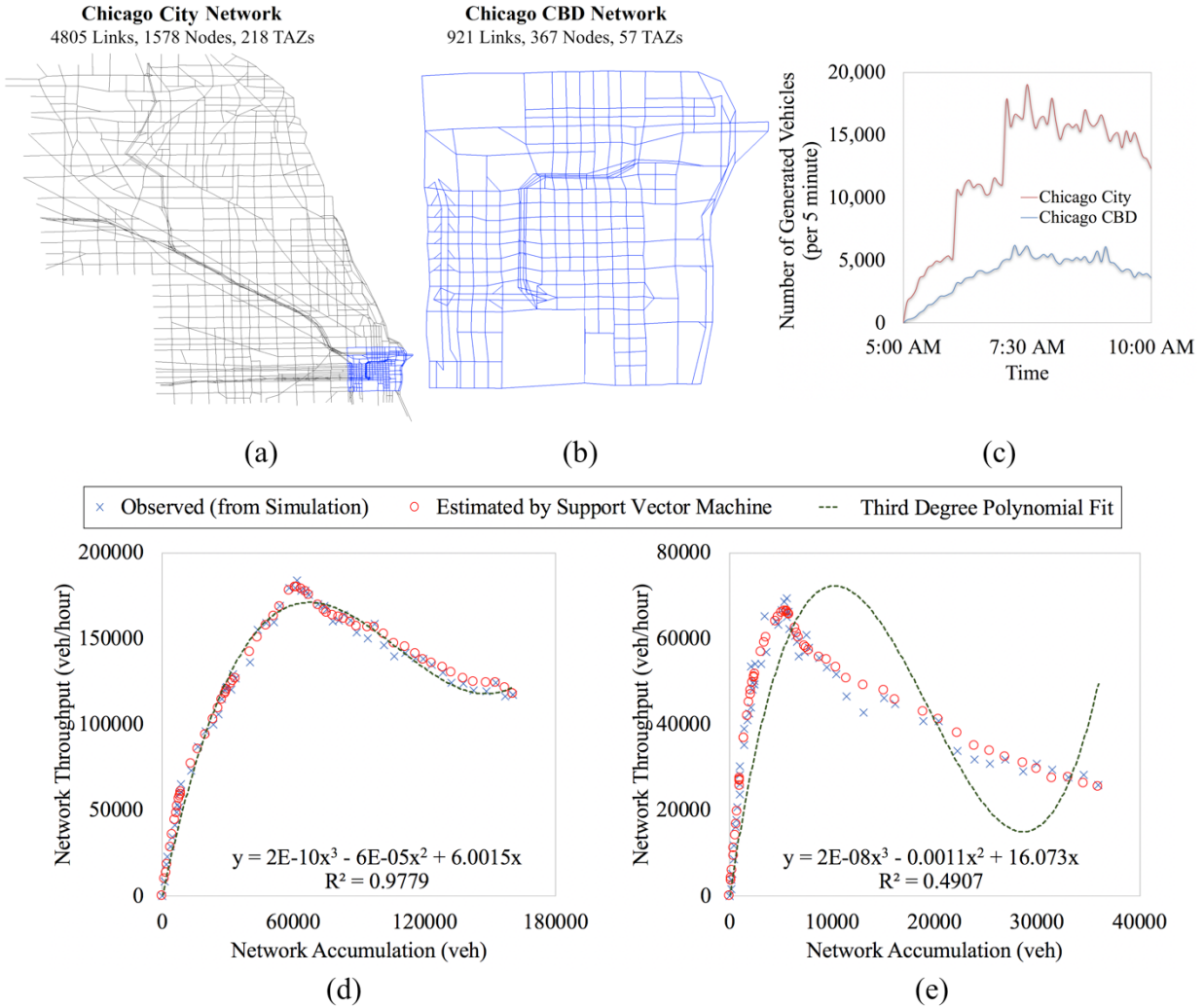


Figure 7-3 (a) Chicago city network, (b) Chicago CBD network, (c) morning demand profiles, (d) Chicago city network NFD, and (e) Chicago CBD network NFD

The capability of the presented framework in predicting traffic state is examined by a calibration and validation process. To this end, 70% of the available scenarios (60 out of 86 days) are exploited to calibrate the presented framework. The calibration process includes tuning the SVM model for the exit flow function and incorporating it in the state transition function. Applying the calibrated SVM model to estimate the network throughput for the validation scenarios (those which were not considered for calibrating the exit function via SVM) is associated with 8.7% relative deviations from the ground-truth values. The prediction framework is only applied for the validation scenarios (26 out of 86 days).

Figure 7-4 shows the real-time traffic prediction results compared with the ground truth values for a randomly selected scenario (out of 26 days). All the three subplots are presented as time series. Figure 7-4(a) indicates a smooth pattern in the real-time prediction made by EKF algorithm for the network accumulation. However, the results in Figure 7-4(b) for the predicted exogenous demand is somehow scattered. The main reason is that no measurement is provided to correct the predicted values for this parameter and the model approximate its value only based on minimizing the error term shown in Equation 7-9, unlike the network accumulation. The exogenous demand is considered as a model parameter (a random walk) and estimated in each run (time interval) of the prediction engine. Figure 7-4(c) illustrates the estimated network throughput incorporating the SVM algorithm. The mean absolute percentage error (MAPE) of the model results is calculated for each validation scenario, and the average value across all the validation scenarios is utilized to quantify the effectiveness of the presented framework. MAPE is a widely used error metric that uses range normalization. For a state  $x$ , it is given as:

$$\epsilon = \frac{1}{N_s \cdot N_t} \left( \sum_{s=1}^{N_s} \sum_{t=1}^{N_t} \left| \frac{\hat{x}_{s,t} - x_{s,t}}{x_{s,t}} \right| \right) \times 100 \quad (7-12)$$

Here,  $\epsilon$  is the average value of MAPE over all scenarios,  $N_s$  is the number of scenarios (which is 26),  $N_t$  is the number of time intervals in the simulation period in each scenarios (here it is 60 5-minute time intervals over 5 hours of traffic simulation from 5:00 AM to 10:00 AM),  $\hat{x}_{s,t}$  is the posterior estimated state at time interval  $t$  in scenario  $s$ , and  $x_{s,t}$  is the actual state value at time interval  $t$  in scenario  $s$ . Overall, 1560 (=60×26) datapoints are incorporated to evaluate the validity of the model. Figure 7-5 illustrates the results of MAPE. Figure 7-5(a) presents the error terms for the network accumulation variable for seven different percentages of resource availability that provides limited observations to correct the predicted values for this variable. Values on the horizontal axis show the proportion of the network links provided with sensors to collect the accumulation data, and the values on the vertical axis illustrate the errors associated with each resource availability level. According to these results, the presented framework shows a successful application for the Chicago CBD network. For the resource availability level as low as only 5%,

the model provides an acceptable accuracy (8.6%) of the real-time network accumulation prediction. Note that the reported error terms should be considered more than acceptable, since they are average values over various scenarios capturing day-to-day variations in the network. This error term is reduced to 1.3% by increasing the resource availability level to 100%. This improvement is expected, since more accurate data are provided to correct the predicted values by the model in the 100% level. Note that in each resource availability level, an optimization problem is solved to identify the optimal set of links to be equipped with sensors to collect link accumulation data.

Figure 7-5(b) presents the error terms for the exogenous demand variable associated with different resource availability levels for the network accumulation observations. Intuitively, the increase in the percentage of the equipped links for collecting accumulation data does not significantly improve the prediction accuracy of the exogenous demand variable (only a slight improvement is observed from 12.4% to 8.8% for resource availability levels of 5% and 100%). Finally, the MAPE for the network throughput is shown in Figure 7-5 (c). These values are the predicted throughputs extracted by placing the predicted accumulation (via framework) values into the calibrated exit flow function (via SVM regression). For this variable, only a slight improvement is observed from 9.9% to 8.2% for resource availability levels of 5% and 100%. Similar to the exogenous demand, no measurement is provided to estimate this variable. Its value is indirectly estimated based on the predicted accumulation and stochastically calibrated exit flow function.

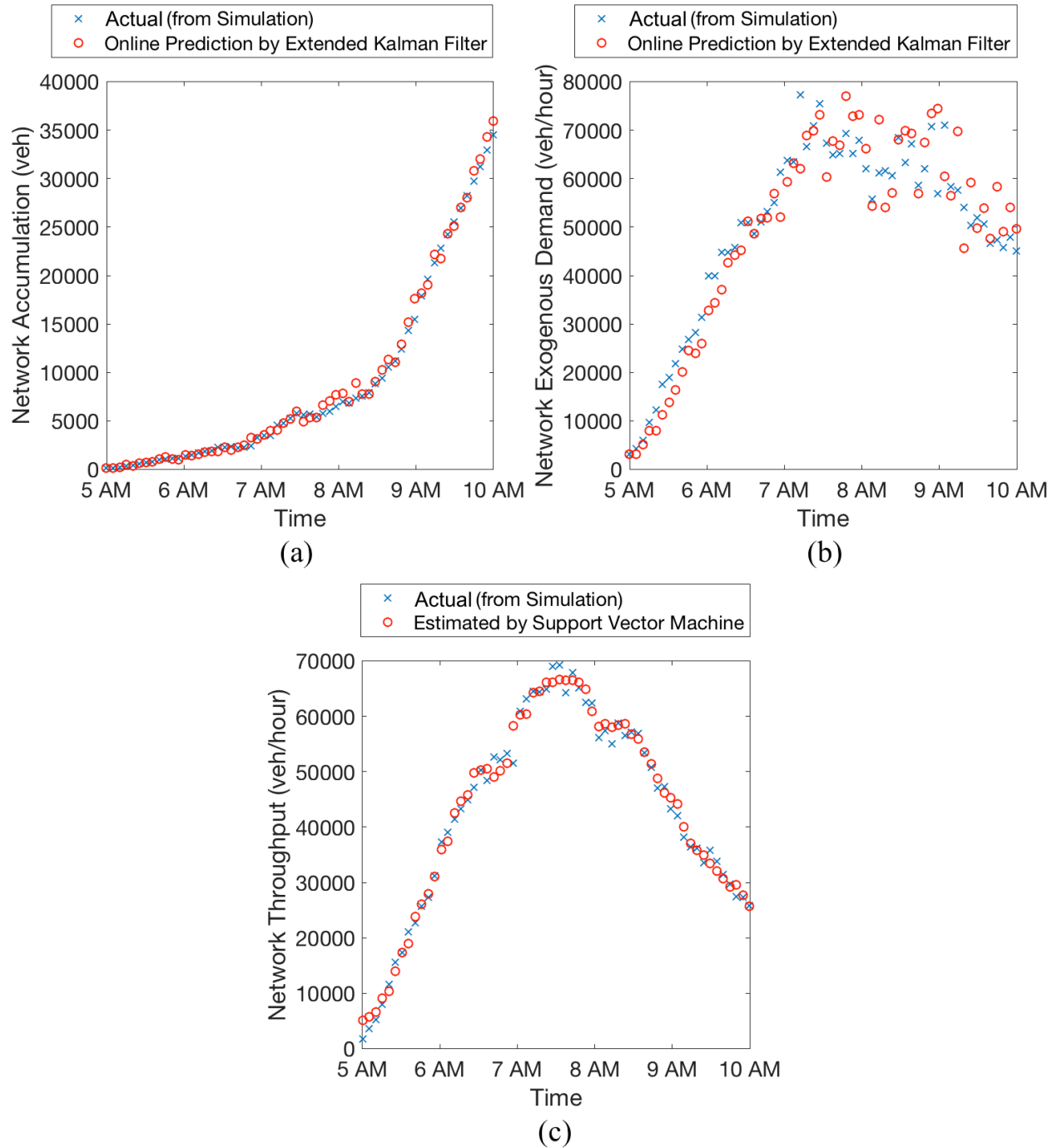


Figure 7-4 Real-time network-wide traffic state prediction results for a randomly selected scenario (a) network accumulation, (b) exogenous demand, and (c) network throughput

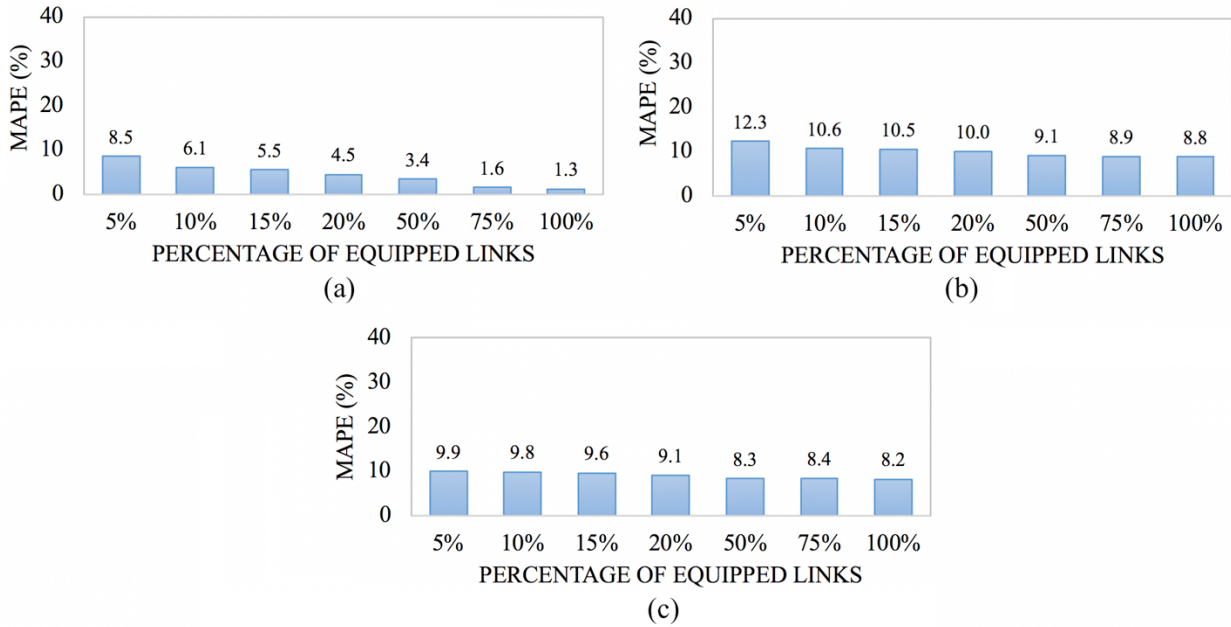


Figure 7-5 MAPE for (a) network accumulation, (b) exogeneous demand, and (c) network throughput considering all validation scenarios (26 days) and prediction time intervals per scenario (60) for different resource availability levels of the network accumulation observations

To assess the effectiveness of using the optimal set of links for observing the network accumulation, instead of a random set of links, the MAPE of the predicted network accumulation values are compared for these two cases. Note that, here, the entire available dataset (all 86 days) are utilized to make this comparison (unlike Figure 7-5 where the results are generated based on a 70% to 30% train and test process). Figure 7-6 illustrates the actual and predicted accumulation values for these two cases (optimal set versus the random set of links equipped with the accumulation sensors) for a randomly selected day (out of 86). The results are provided for four different levels of the resource availability (5% to 20%). As it is shown, collecting the measurements from the randomly selected links does not provide accurate results of the network-wide traffic state variables. The MAPE results over all scenarios are also shown in Figure 7-7 considering all the 86 days (scenario) and 60 time intervals per day. As it can be seen, the MAPE

value is reduced from 18.5% to 7.6 % for 5% to 20% resource availability levels in the case of the random set of selected links for accumulation data measurements. However, incorporating the optimal set of links reduces the MAPE values significantly (from 8.6% to 4.4% for 5% to 20% resource availability levels).

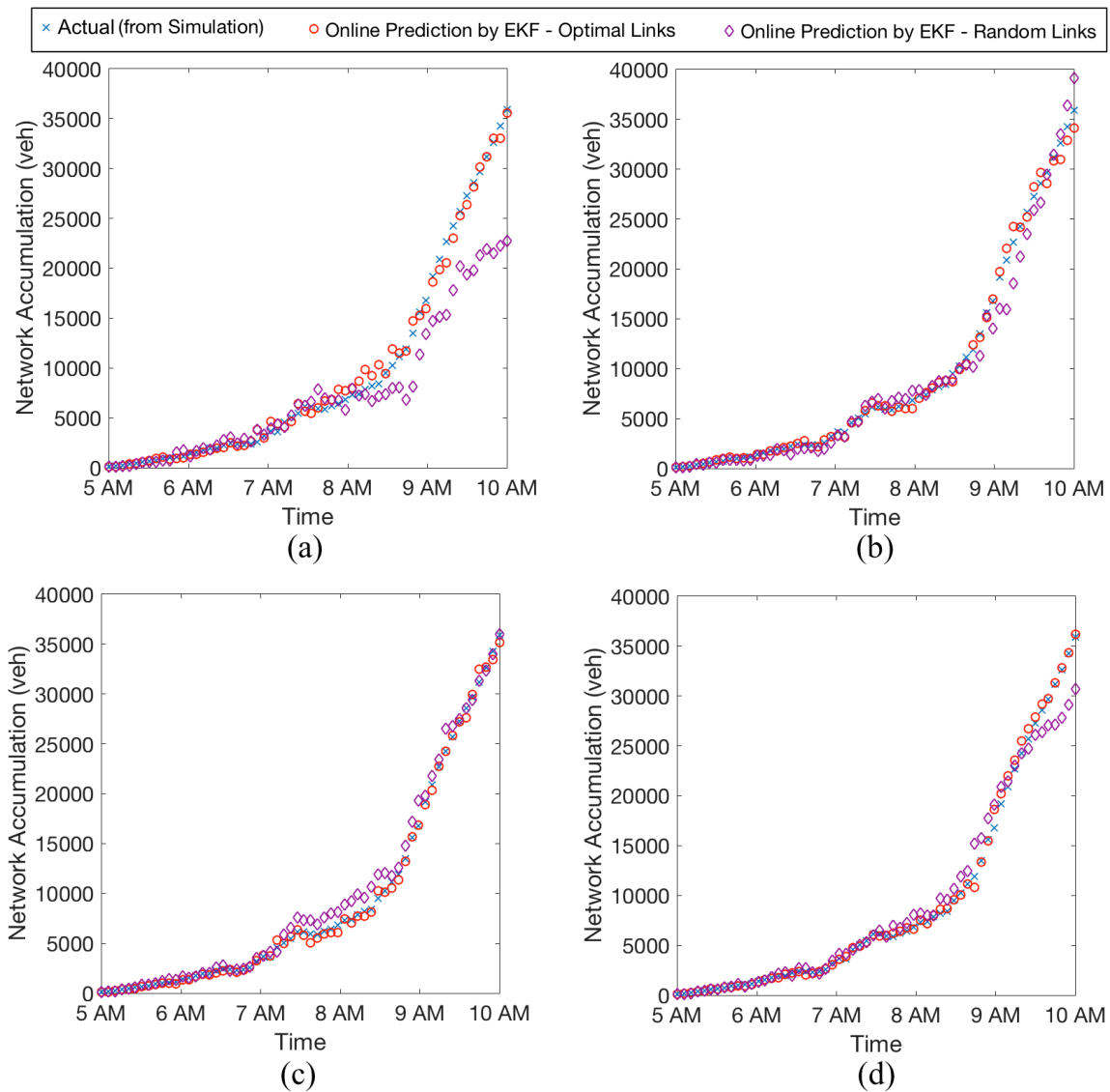


Figure 7-6 Comparing the predicted accumulation values using the optimal set of links for correcting measurements versus a random set of links, in a particular scenario (out of 86 days) with different levels of resource availability for data collection (percentages of the network links equipped with sensors): (a) 5%, (b) 10%, (c) 15%, and (d) 20%

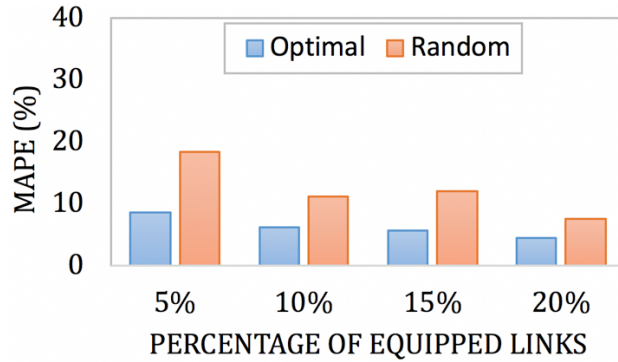


Figure 7-7 MAPE values of the predicted network accumulation over all scenarios (86 days) using the optimal set of links for correcting measurements versus a random set of links, with different levels of resource availability for data collection

The core contribution of this chapter is including the adverse weather impact in the real-time network-wide traffic state prediction model. This is accomplished by incorporating the weather variables in the network exit flow function (see Section 7-4-3). To demonstrate the significance of this contribution, two cases are compared. In the first case, the presented framework is applied utilizing the entire data from all 86 days. However, in the second case, the scenarios with the inclement weather (21 days are in this category) are eliminated from the calibration process of the exit flow function. Figure 7-8 illustrates the throughput estimation results for the two described cases. Figure 7-8(a) shows a randomly selected scenario (day) with clear weather conditions (no precipitation), and Figure 7-8(b) illustrates another randomly selected scenario with snowy weather conditions (with the cumulative precipitation of 4.9 inches). In these figures, the network throughput is estimated by the SVM with and without including the weather variables. As it is shown, for the clear day, the estimated values in both cases (including and excluding weather variables) are very close to the ground truth values (provided by traffic simulation as a surrogate). However, for the snowy day, the estimated values for the case without incorporating the weather

variables does not show a proper fit. To quantify the overall deviations, the average MAPE results over all available scenarios (86 days with various given weather conditions) are presented in Figure 7-9 for the network accumulation, demand, and throughput.

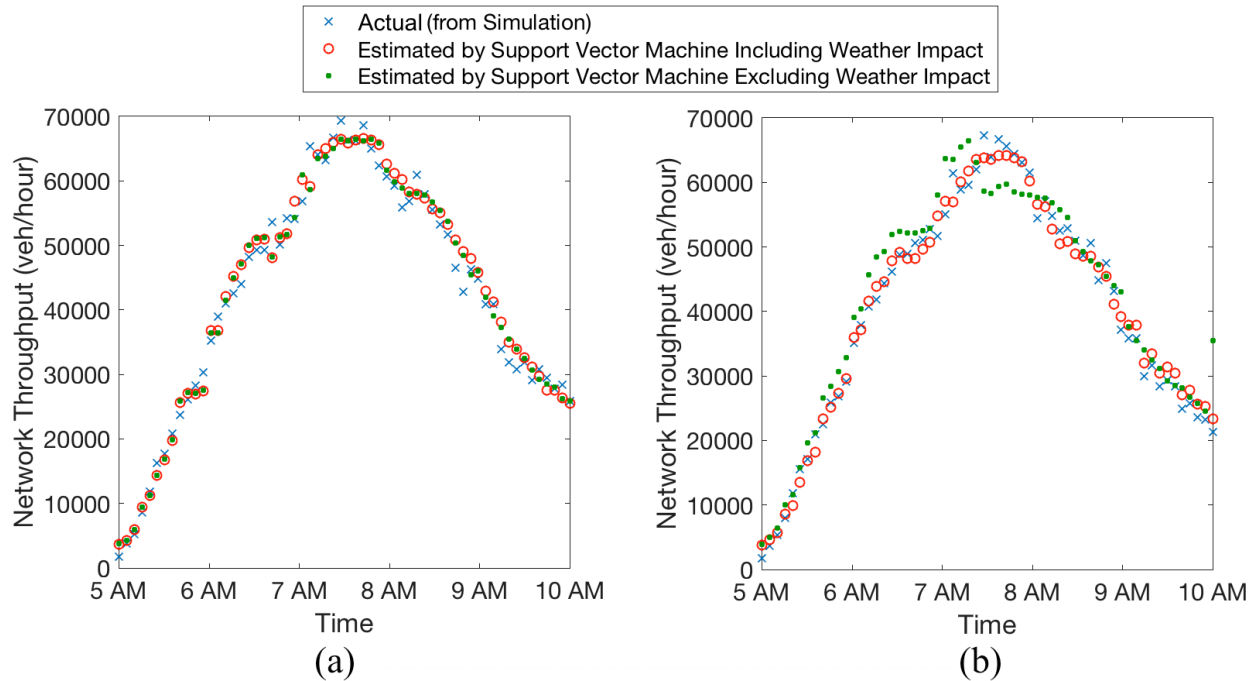


Figure 7-8 Estimated exit flow function (network throughput) using SVM approach including versus excluding weather variables (a) for a clear day scenario and (b) for a snowy day scenario

Figure 7-9(a) shows the results for the network accumulation. Excluding the weather variables in the calibration process of the exit flow function does not drastically impact the real-time prediction of the network accumulation. The main reason is that the predicted values of the network accumulation are corrected by the real-time measurements at every step of the prediction process. In other words, the model parameters are adjusted in a way that the model predicts the accumulation as close as possible to the measured real-time values. However, this impacts the estimation accuracy of the other parameters such as the exogenous demand. As it is shown in Figure 7-9(b) and Figure 7-9 (c), the predicted exogenous demand and network throughput in the case that the weather impact is ignored, endure greater associated errors. Thus, considering the

weather impact in the real-time traffic state prediction is necessary to provide accurate estimations for the real-time traffic state at the network-level.

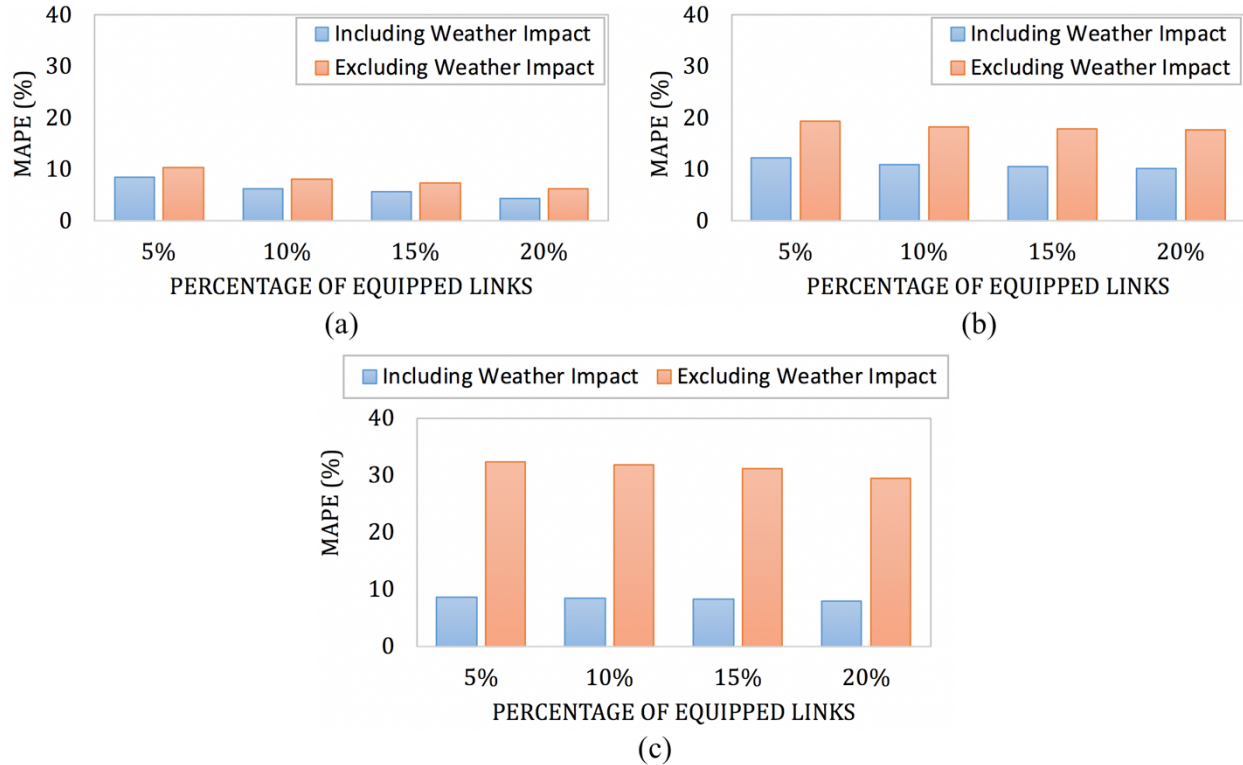


Figure 7-9 Average MAPE values over all scenarios (86 days including various weather conditions) including and excluding weather variables in the exit function: (a) network accumulation, (b) exogenous demand, and (c) network throughput

## 7-6- Summary

The problem of real-time traffic state prediction for large-scale urban networks is studied in this chapter. First, the quantitative difference that the changes in weather variables (visibility and rain and snow precipitations) creates in the network-wide traffic flow characteristics is investigated. Then, a mathematical framework is developed to provide the real-time network-wide traffic state prediction. The proposed framework incorporates different weather variables in the traffic state prediction process using Extended Kalman Filter methodology iteratively. In each

iteration, a calibrated exit function, the predicted values in the previous iterations for the network accumulation, exogeneous demand, and throughput, along with the observed values in the current and previous iterations for the network accumulation are used to predict the network accumulation and exogenous demand in the current iteration. Considering the weather variables in the calibrated exit function is the main contribution of this study. To this end, a Support Vector Machine (SVM) model is trained using 60 traffic simulation scenarios (associated with actual data of 60 weekdays) for the case study. Then, the trained model is evaluated by the remaining 26 traffic simulation scenarios out of 86 scenarios. The major findings of the chapter are summarized as follows:

- The network maximum congestion (maximum observed density) has a direct correlation with the rain and snow precipitation rate.
- The maximum observed throughput of the network is decreased as the rain and snow precipitation rate increases.
- The variation of the area of hysteresis loop in the NFD diagram by the precipitation shows that the higher precipitation causes more instability in the recovery phase of the system.
- Network becomes more reliable (reduced coefficient of the reliability relation), but also more congested, with an increase in the rain and snow precipitation rates.
- Results suggest that the network-wide traffic flow relationships (NFD and TRR) are significantly affected by the changes in the weather variables. This calls for incorporation of the weather variables in the real-time network-wide traffic state prediction problem.
- The proposed SVM model in this study outperforms the third-degree polynomial model (used in the literature) in estimating the network exit flow function. It also provides the opportunity to incorporate different weather variables in the network exit function.

- By optimally selecting a subset of the network links to be equipped with sensors to capture accumulation, instead of using data from the entire network, the cost of the real-world deployment of the prediction model can be significantly reduced. The numerical results provided for the case study demonstrate an acceptable prediction accuracy despite of this cost reduction.
- The successful implementation of the real-time network-wide traffic state prediction problem considering weather variables drastically reduces the error terms for the network exogenous demand and throughput. This reduction is more than 50% of the error when no weather variable is considered in the framework. There is also a slight improvement in the error term for the network accumulation, where the predicted values are corrected by limited observations.

## CHAPTER 8 – Concluding Remarks and Future Research

### 8-1- Concluding Remarks

Network Fundamental Diagram (NFD) represents dynamics of the traffic flow at the network level using main traffic flow elements, namely, flow, density, and speed. It is widely employed to design various network-wide traffic control strategies and explore traffic state analyses to improve mobility and mitigate congestion. This study presents two frameworks (deterministic and stochastic approaches) to estimate NFD and provides three main applications of it in large-scale urban networks: network-wide travel time reliability estimation, network-wide emission estimation, and real-time traffic state prediction for heterogeneous networks experiencing inclement weather conditions. Primarily, a mathematical model and solution algorithm are proposed to find the optimal location of fixed measurement points and sampling of probe trajectories in a resource allocation framework to estimate NFD in a large-scale heterogeneous network with asymmetric demand. The proposed framework, then, is extended to capture the stochasticity due to fluctuations in the network demand and supply.

As the premier application of NFD, the impact of partitioning a heterogeneous network on the estimated travel time reliability measure is investigated. It is shown that the congestion-dependent partitioning of a heterogeneous network can significantly affect the estimated reliability measure for each sub-network. It is also shown that the density coefficient of variation is a key factor that explains the impacts of the partitioning on the reliability measure estimation. As the second application of NFD in this study, a network-level emission modeling framework is developed via integrating NFD properties with an existing microscopic emission model. The NFDs and microscopic emission models are estimated using microscopic and mesoscopic traffic simulation tools at different scales for various traffic compositions. The major contribution is to

consider heterogeneous vehicle types with different emission generation rates at the network-level model. This framework is applied on the large-scale network of Chicago as well as its CBD area. Non-linear and support vector regression models are developed using simulated trajectory data of thirteen simulated scenarios. The results show a satisfactory calibration and successful validation with acceptable deviations from the underlying microscopic emission model regardless of the simulation tool that is used to calibrate the network-level emission model.

Lastly, a real-time network-wide traffic state prediction framework is designed. The core objective is to incorporate the adverse weather conditions in the real-time network-wide traffic state estimation. This is accomplished by incorporating the weather variables in the network exit flow function. Extended Kalman Filter (EKF) algorithm is utilized as the prediction engine. Simulated NFDs of a large-scale network under various weather conditions are used, as surrogate of the ground truth NFDs, to assess the performance of the prediction methodology. A successful application of the presented framework is shown for the Chicago CBD network.

The major findings of this dissertation are summarized below:

- A combination of fixed detectors and probe vehicles provides sufficient data to deterministically estimate NFD with minimal deviation from the ground-truth NFD in a heterogeneous network.
- In deterministic estimation of NFD, the optimal locations of fixed measurement points are not only a function of the proportion rate of fixed measurement points; rather, it also changes when the proportion of probe trajectories varies. Similarly, the optimal set of OD pairs is not only a function of the proportion rates of OD pairs; rather, it also changes when the proportion rates of fixed measurements varies.

- The comparison of the stochastic and deterministic approaches of NFD estimation demonstrates the superiority of the stochastic approach.
- Once the budget level is at 20%, the deterministic approach of NFD estimation leads to a 70-250% error relative to the stochastic approach. Increasing the budget decreases the relative error, but even at the 80% budget level, a minimum 30% relative error is observed over various scenarios.
- Partitioning a large-scale heterogeneous network into optimal number of homogeneous sub-networks improves the travel time reliability estimation.
- For a partitioned network, there is an inverse relation between the reliability measure, and average and standard deviation of density for each subnetwork in both AM and PM peak periods.
- The density coefficient of variation is an important measure to assess the impacts of the network partitioning on the reliability measure, which is found to be directly related to the reliability measure.
- The results of the proposed model for the large-scale emission estimation strongly support the existence of a relationship between emissions and the traffic state of the network represented by its NFD.
- A proper regression model for large-scale emission estimation needs to be selected depending on the available computational resources. The numerical experiments in this study showed that although SVR outperforms NLR, both models provide acceptable approximations in the validation scenarios.

- The results of NED analysis suggest that the multivaluedness of emission rates for emission-flow and emission-density diagrams occur at the flow breakdown and unloading points, respectively.
- The network-wide traffic flow relationships (NFD and TRR) are significantly affected by the changes in the weather variables. This calls for incorporation of the weather variables in the real-time network-wide traffic state prediction problem.
- The proposed SVM model in this study outperforms the third-degree polynomial model (used in the literature) in estimating the network exit flow function. It also provides the opportunity to incorporate different weather variables in the network exit function.
- By optimally selecting a subset of the network links to be equipped with sensors to capture accumulation, instead of using data from the entire network, the cost of the real-world deployment of the prediction model can be significantly reduced. An acceptable prediction accuracy is shown despite of this cost reduction.
- The successful implementation of the real-time network-wide traffic state prediction problem considering weather variables reduces the error terms for the network exogenous demand and throughput by more than 50%. There is also a slight improvement in the error term for the network accumulation, where the predicted values are corrected by limited observations.

## **8-2- Future Research**

Transportation systems have been drastically affected by the advancements in wireless communication during the past three decades. Improvement in mobility, safety, reliability, and sustainability of transportation networks are offered by incorporating the new communication

technologies in traffic management systems. The advent of the new generation of vehicles is a recent wave of technological development in transportation. In particular, more sophisticated autonomous vehicles have been prototyped by exploiting a variety of sensors and intelligent control processors. Vehicle-to-vehicle and vehicle-to-infrastructure communications are provided with pervasive wireless communication technologies in autonomous vehicles with the main aim of efficiency and reliability improvement.

Most of the current principles in traffic management, regulation, and even driving laws will be altered by the massive deployment of autonomous vehicles. The prospective influence of these vehicles on traffic flow properties necessitates implementing a new generation of traffic control strategies. Moreover, there is a need to re-design the traffic infrastructure in a way that both facilitates the smooth movement of driverless vehicles and enhances the overall mobility of transportation networks. This area of study in transportation engineering has only just been inaugurated and generated various future research directions. Incorporating the methodologies presented in this study with the data availability potentials that the new generation of vehicles offer (through the connectivity), establishes a new avenue of research.

## **REFERENCES**

## REFERENCES

- Aboudolas, K., Geroliminis, N., 2013a. Feedback perimeter control for multi-region large-scale congested networks, in: 2013 European Control Conference (ECC). Ieee, pp. 3506–3511.
- Aboudolas, K., Geroliminis, N., 2013b. Perimeter and boundary flow control in multi-reservoir heterogeneous networks. *Transp. Res. Part B Methodol.* 55, 265–281.
- Ahn, K., 1999. Microscopic fuel consumption and emission modeling, in: Proceedings of the 78th Annual Meeting of the Transportation Research Board.
- Ahn, K., Rakha, H., Trani, A., Van Aerde, M., 2002. Estimating vehicle fuel consumption and emissions based on instantaneous speed and acceleration levels. *J. Transp. Eng.* 128, 182–190.
- Ambühl, L., Menendez, M., 2016. Data fusion algorithm for macroscopic fundamental diagram estimation. *Transp. Res. Part C Emerg. Technol.* 71, 184–197.
- Ampountolas, K., Kouvelas, A., 2015. Real-time estimation of critical vehicle accumulation for maximum network throughput, in: 2015 American Control Conference (ACC). IEEE, pp. 2057–2062.
- Andrey, J., Mills, B., Leahy, M., Suggett, J., 2003. Weather as a chronic hazard for road transportation in Canadian cities. *Nat. hazards* 28, 319–343.
- Arman MA, Khademi N, de Lapparent M, Saedi R. Activity-Travel Analysis of Women in a Patriarchal Society with Strong Gender Norms. Transportation Research Board 98th Annual Meeting, Washington, D.C., January 13-17, 2019.
- Arulampalam, M.S., Maskell, S., Gordon, N., Clapp, T., 2002. A tutorial on particle filters for online nonlinear/non-Gaussian Bayesian tracking. *IEEE Trans. signal Process.* 50, 174–188.
- Barceló, J., others, 2010. Fundamentals of traffic simulation. Springer.
- Bholowalia, P., Kumar, A., 2014. EBK-means: A clustering technique based on elbow method and k-means in WSN. *Int. J. Comput. Appl.* 105.
- Böcker, L., Dijst, M., Prillwitz, J., 2013. Impact of everyday weather on individual daily travel behaviours in perspective: a literature review. *Transp. Rev.* 33, 71–91.
- Boulter, P.G., Barlow, T., McCrae, I., Latham, S., Elst, D., BURGWAL, V.A.N.D.E.R., 2006.

Road traffic characteristics, driving patterns and emission factors for congested situations, TNO Automotive, Department Powertrains-Environmental Studies & Testing, Delft, The Netherlands.

- Boyacı, B., Geroliminis, N., 2010. Exploring the effect of variability of urban systems characteristics in the network capacity, in: STRC 2010-10th Swiss Transport Research Conference.
- Briganti, A., Musolino, G., Vitetta, A., 2014. Simulation On A Partitioned Urban Network: An Approach Based On A Network Fundamental Diagram. *WIT Trans. Ecol. Environ.* 191, 957–966.
- Buisson, C., Ladier, C., 2009. Exploring the impact of homogeneity of traffic measurements on the existence of macroscopic fundamental diagrams. *Transp. Res. Rec.* 2124, 127–136.
- CARB, 2007. EMFAC 2007: Calculating emission inventories for vehicles in California.
- Castrillon, F., Laval, J., 2017. Impact of buses on the macroscopic fundamental diagram of homogeneous arterial corridors. *Transp. B* 0, 1–16.  
<https://doi.org/10.1080/21680566.2017.1314203>
- Cen, X., Lo, H.K., Li, L., 2016. A framework for estimating traffic emissions: The development of Passenger Car Emission Unit. *Transp. Res. Part D Transp. Environ.* 44, 78–92.  
<https://doi.org/10.1016/j.trd.2016.02.013>
- Černý, V., 1985. Thermodynamical approach to the traveling salesman problem: An efficient simulation algorithm. *J. Optim. Theory Appl.* 45, 41–51.
- Chen, A., Ji, Z., Recker, W., 2002. Travel time reliability with risk-sensitive travelers. *Transp. Res. Rec.* 1783, 27–33.
- Chen, C., Skabardonis, A., Varaiya, P., 2003. Travel-time reliability as a measure of service. *Transp. Res. Rec.* 1855, 74–79.
- Chiabaut, N., 2015. Evaluation of a multimodal urban arterial: The passenger macroscopic fundamental diagram. *Transp. Res. Part B Methodol.* 81, 410–420.
- Cirianni, F., Panuccio, P., Rindone, C., 2013. A comparison of urban planning systems between the UK and Italy: Commercial development and city logistic plan. *WIT Trans. Built Environ.* 130, 785–797.
- Courbon, T., Leclercq, L., 2011. Cross-comparison of macroscopic fundamental diagram estimation methods. *Procedia-Social Behav. Sci.* 20, 417–426.

- Daganzo, C.F., 2007. Urban gridlock: Macroscopic modeling and mitigation approaches. *Transp. Res. Part B Methodol.* 41, 49–62.
- Daganzo, C.F., Gayah, V. V, Gonzales, E.J., 2011. Macroscopic relations of urban traffic variables: Bifurcations, multivaluedness and instability. *Transp. Res. Part B Methodol.* 45, 278–288.
- Daganzo, C.F., Geroliminis, N., 2008. An analytical approximation for the macroscopic fundamental diagram of urban traffic. *Transp. Res. Part B Methodol.* 42, 771–781.
- Datla, S., Sharma, S., 2008. Impact of cold and snow on temporal and spatial variations of highway traffic volumes. *J. Transp. Geogr.* 16, 358–372.
- Davidovich, L.L., Mikhailovich, L.E., 1980. *Statistical Physics*, 5 (3). Oxford: Pergamon Press.
- Dia, H., Panwai, S., Boongrapue, N., Ton, T., Smith, N., 2006. Comparative Evaluation of Power-Based Environmental Emissions Models 1251–1256.
- Dinopoulou, V., Diakaki, C., Papageorgiou, M., 2006. Applications of the urban traffic control strategy TUC. *Eur. J. Oper. Res.* 175, 1652–1665.
- Dong, J., Mahmassani, H.S., Alfelor, R., 2010. Incorporating adverse weather impacts in dynamic traffic simulation-assignment models: Methodology and application.
- Du, J., Rakha, H., Gayah, V. V, 2016. Deriving macroscopic fundamental diagrams from probe data: Issues and proposed solutions. *Transp. Res. Part C Emerg. Technol.* 66, 136–149.
- Eisenberg, D., Warner, K.E., 2005. Effects of snowfalls on motor vehicle collisions, injuries, and fatalities. *Am. J. Public Health* 95, 120–124.
- El-Shawarby, I., Ahn, K., Rakha, H., 2005. Comparative field evaluation of vehicle cruise speed and acceleration level impacts on hot stabilized emissions. *Transp. Res. Part D Transp. Environ.* 10, 13–30. <https://doi.org/https://doi.org/10.1016/j.trd.2004.09.002>
- Fakhrmoosavi F, Saedi R, Zockaie A, Talebpour A, 2020. Impacts of Connected and Autonomous Vehicles on Traffic Flow with Heterogeneous Drivers Spatially Distributed over Large-Scale Networks. *Transportation Research Record*.
- Fei, X., Eisenman, S., Mahmassani, H., Zhou, X., 2009. Application of DYNASMART-X to the Maryland CHART network for real-time traffic management center decision support, in: *12th World Congress on Intelligent Transport Systems 2005*. pp. 4944–4954.
- Feller, W., 2008. *An introduction to probability theory and its applications*. John Wiley & Sons.

- Gao, X.S., Gayah, V. V, 2017. An analytical framework to model uncertainty in urban network dynamics using Macroscopic Fundamental Diagrams. *Transp. Res. procedia* 23, 497–516.
- Gayah, V. V, Daganzo, C.F., 2011. Clockwise hysteresis loops in the macroscopic fundamental diagram: an effect of network instability. *Transp. Res. Part B Methodol.* 45, 643–655.
- Gayah, V. V, Dixit, V. V, 2013. Using mobile probe data and the macroscopic fundamental diagram to estimate network densities: Tests using microsimulation. *Transp. Res. Rec.* 2390, 76–86.
- Gayah, V. V, Dixit, V. V, Guler, S.I., 2014a. Relationship between mean and day-to-day variation in travel time in urban networks. *EURO J. Transp. Logist.* 3, 227–243.
- Gayah, V. V, Gao, X.S., Nagle, A.S., 2014b. On the impacts of locally adaptive signal control on urban network stability and the macroscopic fundamental diagram. *Transp. Res. Part B Methodol.* 70, 255–268.
- Geroliminis, N., Boyacı, B., 2012. The effect of variability of urban systems characteristics in the network capacity. *Transp. Res. Part B Methodol.* 46, 1607–1623.
- Geroliminis, N., Daganzo, C.F., 2008. Existence of urban-scale macroscopic fundamental diagrams: Some experimental findings. *Transp. Res. Part B Methodol.* 42, 759–770.
- Geroliminis, N., Haddad, J., Ramezani, M., 2012. Optimal perimeter control for two urban regions with macroscopic fundamental diagrams: A model predictive approach. *IEEE Trans. Intell. Transp. Syst.* 14, 348–359.
- Geroliminis, N., Ji, Y., 2011. Spatial and temporal analysis of congestion in urban transportation networks.
- Geroliminis, N., Sun, J., 2011. Properties of a well-defined macroscopic fundamental diagram for urban traffic. *Transp. Res. Part B Methodol.* 45, 605–617.
- Geroliminis, N., Zheng, N., Ampountolas, K., 2014. A three-dimensional macroscopic fundamental diagram for mixed bi-modal urban networks. *Transp. Res. Part C Emerg. Technol.* 42, 168–181.
- Ghamami, M., Zockaie, A., Nie, Y.M., 2016. A general corridor model for designing plug-in electric vehicle charging infrastructure to support intercity travel. *Transp. Res. Part C Emerg. Technol.* 68, 389–402.
- Girault, J.-T., Gayah, V. V, Guler, I., Menendez, M., 2016. Exploratory analysis of signal coordination impacts on macroscopic fundamental diagram. *Transp. Res. Rec. J. Transp.*

Res. Board 36–46.

Godfrey, J.W., 1969. The mechanism of a road network. *Traffic Eng. Control* 8.

Gonzales, E., Chavis, C., Li, Y., Daganzo, C.F., 2011. Multimodal transport in Nairobi, Kenya: Insights and recommendations with a macroscopic evidence-based model.

Gori, S., Spada, S. La, Mannini, L., Nigro, M., 2013. A dynamic mesoscopic emission model for signalized intersections, in: 16th International IEEE Conference on Intelligent Transportation Systems (ITSC 2013). pp. 2212–2217.  
<https://doi.org/10.1109/ITSC.2013.6728556>

Grote, M., Williams, I., Preston, J., Kemp, S., 2016. Including congestion effects in urban road traffic CO<sub>2</sub>emissions modelling: Do Local Government Authorities have the right options? *Transp. Res. Part D Transp. Environ.* 43, 95–106. <https://doi.org/10.1016/j.trd.2015.12.010>

Haddad, J., 2017. Optimal perimeter control synthesis for two urban regions with aggregate boundary queue dynamics. *Transp. Res. Part B Methodol.* 96, 1–25.

Haddad, J., Geroliminis, N., 2012. On the stability of traffic perimeter control in two-region urban cities. *Transp. Res. Part B Methodol.* 46, 1159–1176.

Haddad, J., Mirkin, B., 2017. Coordinated distributed adaptive perimeter control for large-scale urban road networks. *Transp. Res. Part C Emerg. Technol.* 77, 495–515.

Haddad, J., Mirkin, B., 2016. Adaptive perimeter traffic control of urban road networks based on MFD model with time delays. *Int. J. Robust Nonlinear Control* 26, 1267–1285.

Haddad, J., Shraiber, A., 2014. Robust perimeter control design for an urban region. *Transp. Res. Part B Methodol.* 68, 315–332.

Hajiahmadi, M., Haddad, J., De Schutter, B., Geroliminis, N., 2015. Optimal hybrid perimeter and switching plans control for urban traffic networks. *IEEE Trans. Control Syst. Technol.* 23, 464–478.

Hajiahmadi, M., Haddad, J., De Schutter, B., Geroliminis, N., 2013. Optimal hybrid macroscopic traffic control for urban regions: Perimeter and switching signal plans controllers, in: *Control Conference (ECC), 2013 European*. pp. 3500–3505.

Hall, F.L., Barrow, D., 1988. Effect of weather on the relationship between flow and occupancy on freeways. *Transp. Res. Rec.* 1194, 55–63.

Hamilton, A., Waterson, B., Cherrett, T., Robinson, A., Snell, I., 2013. The evolution of urban

- traffic control: changing policy and technology. *Transp. Plan. Technol.* 36, 24–43.
- Han, K., Liu, H., Gayah, V. V., Friesz, T.L., Yao, T., 2016. A robust optimization approach for dynamic traffic signal control with emission considerations. *Transp. Res. Part C Emerg. Technol.* 70, 3–26. <https://doi.org/10.1016/j.trc.2015.04.001>
- Hejazi, B., 1999. Facility location of bus terminals in urban areas using simulated annealing algorithm.
- HEMDAN, S., WAHABALLA, A.M., KURAUCHI, F., 2017. Evaluating travel choices effect on multimodal network performance using vehicle and passenger macroscopic fundamental diagrams. *J. East. Asia Soc. Transp. Stud.* 12, 1710–1727.
- Herman, R., Lam, T., 1974. Trip time characteristics of journeys to and from work. *Transp. traffic theory* 6, 57–86.
- Herring, R., Hofleitner, A., Abbeel, P., Bayen, A., 2010. Estimating arterial traffic conditions using sparse probe data, in: 13th International IEEE Conference on Intelligent Transportation Systems. IEEE, pp. 929–936.
- Hofleitner, A., Herring, R., Abbeel, P., Bayen, A., 2012. Learning the dynamics of arterial traffic from probe data using a dynamic Bayesian network. *IEEE Trans. Intell. Transp. Syst.* 13, 1679–1693.
- Hou, T., Mahmassani, H.S., Alfelor, R.M., Kim, J., Saberi, M., 2013. Calibration of traffic flow models under adverse weather and application in mesoscopic network simulation. *Transp. Res. Rec.* 2391, 92–104.
- Hranac, R., Sterzin, E., Krechmer, D., Rakha, H.A., Farzaneh, M., Arafteh, M., 2006. Empirical studies on traffic flow in inclement weather.
- Huang, Y., Gao, X., 2014. Clustering on heterogeneous networks. *Wiley Interdiscip. Rev. Data Min. Knowl. Discov.* 4, 213–233.
- Hunt, P.B., Robertson, D.I., Bretherton, R.D., Royle, M.C., 1982. The SCOOT on-line traffic signal optimisation technique. *Traffic Eng. Control* 23.
- Ibrahim, A.T., Hall, F.L., 1994. Effect of adverse weather conditions on speed-flow-occupancy relationships.
- Int Panis, L., Broekx, S., Liu, R., 2006. Modelling instantaneous traffic emission and the influence of traffic speed limits. *Sci. Total Environ.* 371, 270–285. <https://doi.org/10.1016/j.scitotenv.2006.08.017>

- Jamshidnejad, A., Papamichail, I., Papageorgiou, M., De Schutter, B., 2017. A mesoscopic integrated urban traffic flow-emission model. *Transp. Res. Part C Emerg. Technol.* 75, 45–83. <https://doi.org/10.1016/j.trc.2016.11.024>
- Ji, Y., Daamen, W., Hoogendoorn, S., Hoogendoorn-Lanser, S., Qian, X., 2010. Investigating the Shape of the Macroscopic Fundamental Diagram Using Simulation Data. *Transp. Res. Rec. J. Transp. Res. Board* 2161, 40–48. <https://doi.org/10.3141/2161-05>
- Jiang, Y.Q., Ma, P.J., Zhou, S.G., 2015. Macroscopic modeling approach to estimate traffic-related emissions in urban areas. *Transp. Res. Part D Transp. Environ.* <https://doi.org/10.1016/j.trd.2015.10.022>
- Jones, E.G., 1989. Travel time variability in a commuting corridor : Implications for electronic route guidance, in: *International Conference on Applications of Advanced Technologies in Transportation*.
- Kalman, R.E., 1960. A new approach to linear filtering and prediction problems.
- Kalman, R.E., Bucy, R.S., 1961. New results in linear filtering and prediction theory.
- Kavianipour, M., Saedi, R., Zockaie, A., Saberi, M., 2019. Traffic State Estimation in Heterogeneous Networks with Stochastic Demand and Supply: Mixed Lagrangian–Eulerian Approach. *Transportation Research Record*. 0361198119850472.
- Keyvan-Ekbatani, M., Gao, X., Gayah, V. V, Knoop, V.L., 2016. Examining Perimeter Gating Control of Urban Traffic Networks with Locally Adaptive Traffic Signals, in: *Traffic and Granular Flow'15*. Springer, pp. 579–586.
- Keyvan-Ekbatani, M., Kouvelas, A., Papamichail, I., Papageorgiou, M., 2012. Exploiting the fundamental diagram of urban networks for feedback-based gating. *Transp. Res. Part B Methodol.* 46, 1393–1403.
- Keyvan-Ekbatani, M., Papageorgiou, M., Papamichail, I., 2014. Perimeter traffic control via remote feedback gating. *Procedia-Social Behav. Sci.* 111, 645–653.
- Keyvan-Ekbatani, M., Yildirimoglu, M., Geroliminis, N., Papageorgiou, M., 2013. Traffic signal perimeter control with multiple boundaries for large urban networks, in: *16th International IEEE Conference on Intelligent Transportation Systems (ITSC 2013)*. IEEE, pp. 1004–1009.
- Khademi N, Saedi R, 2019. Latent Learning and the Formation of a Spatiotemporal Cognitive Map of a Road Network. *Travel Behaviour and Society*. <https://doi.org/10.1016/j.tbs.2018.09.003>

- Khademi N, Behnia K, Saedi R, 2014. Using Analytic Hierarchy/Network Process (AHP/ANP) in Developing Countries: Shortcomings and Suggestions. *The Engineering Economist*. <https://doi.org/10.1080/0013791X.2013.855856>
- Khademi N, Saedi R. Getting Knowledge without Through Experiencing: Exploring the Phenomena of Driver's Latent Learning. Transportation Research Board 98th Annual Meeting, Washington, D.C., January 13-17, 2019.
- Khattak, A.J., Knapp, K.K., Giese, K.L., Smithson, L.D., 2000. Safety implications of snowstorms on interstate highways, in: 79th Annual Meeting of the Transportation Research Board, Washington, DC.
- Kim, J., Mahmassani, H.S., 2015. Compound Gamma representation for modeling travel time variability in a traffic network. *Transp. Res. Part B Methodol.* 80, 40–63.
- Kirkpatrick, S., Gelatt, C.D., Vecchi, M.P., 1983. Optimization by simulated annealing. *Science* (80-. ). 220, 671–680.
- Knoop, V.L., Hoogendoorn, S.P., 2013. Two-variable macroscopic fundamental diagrams for traffic networks, in: *Traffic and Granular Flow'11*. Springer, pp. 351–360.
- Knoop, V.L., van Lint, H., Hoogendoorn, S.P., 2015. Traffic dynamics: Its impact on the macroscopic fundamental diagram. *Phys. A Stat. Mech. its Appl.* 438, 236–250.
- Kouvelas, A., Saeedmanesh, M., Geroliminis, N., 2017. Enhancing model-based feedback perimeter control with data-driven online adaptive optimization. *Transp. Res. Part B Methodol.* 96, 26–45.
- Kouvelas, A., Saeedmanesh, M., Geroliminis, N., 2015. Feedback perimeter control for heterogeneous urban networks using adaptive optimization, in: *Intelligent Transportation Systems (ITSC), 2015 IEEE 18th International Conference On*. pp. 882–887.
- Kumar Pathak, S., Sood, V., Singh, Y., Channiwal, S.A., 2016. Real world vehicle emissions: Their correlation with driving parameters. *Transp. Res. Part D Transp. Environ.* 44, 157–176. <https://doi.org/10.1016/j.trd.2016.02.001>
- Laval, J.A., Castrillón, F., 2015. Stochastic approximations for the macroscopic fundamental diagram of urban networks. *Transp. Res. Procedia* 7, 615–630.
- Laval, J.A., Leclercq, L., Chiabaut, N., 2017. Minimal parameter formulations of the dynamic user equilibrium using macroscopic urban models: Freeway vs city streets revisited. *Transp. Res. procedia* 23, 517–530.

- Leclercq, L., Chiabaut, N., Trinquier, B., 2014. Macroscopic fundamental diagrams: A cross-comparison of estimation methods. *Transp. Res. Part B Methodol.* 62, 1–12.
- Leclercq, L., Geroliminis, N., 2013. Estimating MFDs in simple networks with route choice. *Procedia-Social Behav. Sci.* 80, 99–118.
- Liu, C., Susilo, Y.O., Karlström, A., 2016. Estimating changes in transport CO2 emissions due to changes in weather and climate in Sweden. *Transp. Res. Part D Transp. Environ.* 49, 172–187. <https://doi.org/10.1016/j.trd.2016.09.004>
- Lo, H.K., Chang, E., Chan, Y.C., 2001. Dynamic network traffic control. *Transp. Res. Part A Policy Pract.* 35, 721–744.
- Loder, A., Ambühl, L., Menendez, M., Axhausen, K.W., 2017. Empirics of multi-modal traffic networks—Using the 3D macroscopic fundamental diagram. *Transp. Res. Part C Emerg. Technol.* 82, 88–101.
- López-Martínez, J.M., Jiménez, F., Páez-Ayuso, F.J., Flores-Holgado, M.N., Arenas, A.N., Arenas-Ramirez, B., Aparicio-Izquierdo, F., 2017. Modelling the fuel consumption and pollutant emissions of the urban bus fleet of the city of Madrid. *Transp. Res. Part D Transp. Environ.* 52, 112–127. <https://doi.org/10.1016/j.trd.2017.02.016>
- Lopez, C., Krishnakumari, P., Leclercq, L., Chiabaut, N., Van Lint, H., 2017a. Spatiotemporal Partitioning of Transportation Network Using Travel Time Data. *Transp. Res. Rec. J. Transp. Res. Board* 98–107.
- Lopez, C., Leclercq, L., Krishnakumari, P., Chiabaut, N., Lint, H., 2017b. Revealing the day-to-day regularity of urban congestion patterns with 3D speed maps. *Sci. Rep.* 7, 14029.
- Mahmassani, H., Williams, J.C., Herman, R., 1987. Performance of urban traffic networks, in: *Proceedings of the 10th International Symposium on Transportation and Traffic Theory.* Elsevier Amsterdam, The Netherlands, pp. 1–20.
- Mahmassani, H.S., 1994. Development and testing of dynamic traffic assignment and simulation procedures for ATIS/ATMS applications.
- Mahmassani, H.S., Dong, J., Kim, J., Chen, R.B., Park, B.B., 2009. Incorporating weather impacts in traffic estimation and prediction systems. United States. Joint Program Office for Intelligent Transportation Systems.
- Mahmassani, H.S., Hou, T., Dong, J., 2012a. Characterizing travel time variability in vehicular traffic networks: deriving a robust relation for reliability analysis. *Transp. Res. Rec.* 2315, 141–152.

- Mahmassani, Hani S, Hou, T., Saberi, M., 2013. Connecting networkwide travel time reliability and the network fundamental diagram of traffic flow. *Transp. Res. Rec.* 2391, 80–91.
- Mahmassani, H.S., Kim, J., Hou, T., Zockaie, A., Saberi, M., Jiang, L., Verbas, Ö., Cheng, S., Chen, Y., Haas, R., 2012b. Implementation and evaluation of weather responsive traffic estimation and prediction system. United States. Joint Program Office for Intelligent Transportation Systems.
- Mahmassani, H.S., Peeta, S., 1993. Network performance under system optimal and user equilibrium dynamic assignments: implications for ATIS. Transportation Research Board.
- Mahmassani, Hani S., Saberi, M., Zockaie, A., 2013. Urban network gridlock: Theory, characteristics, and dynamics. *Transp. Res. Part C Emerg. Technol.* 36, 480–497. <https://doi.org/10.1016/j.trc.2013.07.002>
- Mahmassani, H.S., Williams, J.C., Herman, R., 1984. Investigation of network-level traffic flow relationships: some simulation results. *Transp. Res. Rec.* 971, 121–130.
- Mariotte, G., Leclercq, L., Laval, J.A., 2017. Macroscopic urban dynamics: Analytical and numerical comparisons of existing models. *Transp. Res. Part B Methodol.* 101, 245–267.
- Maze, T.H., Agarwal, M., Burchett, G., 2006. Whether weather matters to traffic demand, traffic safety, and traffic operations and flow. *Transp. Res. Rec.* 1948, 170–176.
- Mazloumian, A., Geroliminis, N., Helbing, D., 2010. The spatial variability of vehicle densities as determinant of urban network capacity. *Philos. Trans. R. Soc. London A Math. Phys. Eng. Sci.* 368, 4627–4647.
- Metropolis, N., Rosenbluth, A.W., Rosenbluth, M.N., Teller, A.H., Teller, E., 1953. Equation of state calculations by fast computing machines. *J. Chem. Phys.* 21, 1087–1092.
- Mühlich, N., Gayah, V. V, Menendez, M., 2015. Use of microsimulation for examination of macroscopic fundamental diagram hysteresis patterns for hierarchical urban street networks. *Transp. Res. Rec. J. Transp. Res. Board* 117–126.
- Nagle, A.S., Gayah, V. V, 2014. Accuracy of networkwide traffic states estimated from mobile probe data. *Transp. Res. Rec.* 2421, 1–11.
- Nesamani, K.S., Chu, L., McNally, M.G., Jayakrishnan, R., 2007. Estimation of vehicular emissions by capturing traffic variations. *Atmos. Environ.* 41, 2996–3008. <https://doi.org/10.1016/j.atmosenv.2006.12.027>
- Niemeier, U., Granier, C., Kornbluh, L., Walters, S., Brasseur, G.P., 2006. Global impact of

road traffic on atmospheric chemical composition and on ozone climate forcing. *J. Geophys. Res.* 111, D09301. <https://doi.org/10.1029/2005JD006407>

- Noland\*, R.B., Ochieng, W.Y., Quddus, M.A., North, R.J., Polak, J.W., 2004. The vehicle emissions and performance monitoring system: analysis of tailpipe emissions and vehicle performance. *Transp. Plan. Technol.* 27, 431–447.
- Ntziachristos, L., Gkatzoflias, D., Kouridis, C., Samaras, Z., 2009. COPERT: A European Road Transport Emission Inventory Model, in: Athanasiadis, I.N., Rizzoli, A.E., Mitkas, P.A., Gómez, J.M. (Eds.), *Information Technologies in Environmental Engineering: Proceedings of the 4th International ICSC Symposium Thessaloniki, Greece, May 28-29, 2009*. Springer Berlin Heidelberg, Berlin, Heidelberg, pp. 491–504. [https://doi.org/10.1007/978-3-540-88351-7\\_37](https://doi.org/10.1007/978-3-540-88351-7_37)
- Ntziachristos, L., Samaras, Z., 2000. COPERT II Computer Programme to calculate Emissions from Road Transport, In Practice.
- Ortigosa, J., Menendez, M., Tapia, H., 2014. Study on the number and location of measurement points for an MFD perimeter control scheme: a case study of Zurich. *EURO J. Transp. Logist.* 3, 245–266.
- Putha, R., Quadrifoglio, L., 2010. Using ant colony optimization for solving traffic signal coordination in oversaturated networks.
- Qi, Y., Teng, H., Yu, L., 2004. Microscale Emission Models Incorporating Acceleration and Deceleration. *J. Transp. Eng. - J TRANSP ENG-ASCE* 130.
- Qu, X., Zhang, J., Wang, S., 2017. On the stochastic fundamental diagram for freeway traffic: model development, analytical properties, validation, and extensive applications. *Transp. Res. part B Methodol.* 104, 256–271.
- Rakha, H., Farzaneh, M., Arafeh, M., Sterzin, E., 2008. Inclement weather impacts on freeway traffic stream behavior. *Transp. Res. Rec.* 2071, 8–18.
- Ramezani, M., Haddad, J., Geroliminis, N., 2015. Dynamics of heterogeneity in urban networks: aggregated traffic modeling and hierarchical control. *Transp. Res. Part B Methodol.* 74, 1–19.
- Richardson, A.J., Taylor, M.A.P., 1978. Travel time variability on commuter journeys. *High Speed Gr. Transp. J.* 12.
- Robertson, D.I., Bretherton, R.D., 1991. Optimizing networks of traffic signals in real time-the SCOOT method. *IEEE Trans. Veh. Technol.* 40, 11–15.

- Saberi, M., Mahmassani, H., Hou, T., Zockaie, A., 2014a. Estimating network fundamental diagram using three-dimensional vehicle trajectories: extending edie's definitions of traffic flow variables to networks. *Transp. Res. Rec. J. Transp. Res. Board* 12–20.
- Saberi, M., Mahmassani, H., Hou, T., Zockaie, A., 2014b. Estimating Network Fundamental Diagram Using Three-Dimensional Vehicle Trajectories. *Transp. Res. Rec. J. Transp. Res. Board* 2422, 12–20. <https://doi.org/10.3141/2422-02>
- Saberi, M., Mahmassani, H.S., 2012. Exploring properties of networkwide flow–density relations in a freeway network. *Transp. Res. Rec.* 2315, 153–163.
- Saberi, M., Mahmassani, H.S., Zockaie, A., 2014c. Network capacity, traffic instability, and adaptive driving: findings from simulated urban network experiments. *EURO J. Transp. Logist.* 3, 289–308. <https://doi.org/10.1007/s13676-013-0040-2>
- Saedi R, Saeedmanesh M, Zockaie A, Saberi M, Geroliminis N, Mahmassani HS. Improving Network Travel Time Reliability Estimation with Network Partitioning. Transportation Research Board 97th Annual Meeting, Washington, D.C., January 7-11, 2018.
- Saedi R, Saeedmanesh M, Zockaie A, Saberi M, Geroliminis N, Mahmassani HS, 2020. Estimating Network Travel Time Reliability with Network Partitioning. Transportation Research Part C: Emerging Technologies. <https://doi.org/10.1016/j.trc.2020.01.013>
- Saedi, R., Verma, R., Zockaie, A., Ghamami, M., Gates, T.J., 2020. Comparison of Support Vector and Non-Linear Regression Models for Estimating Large-Scale Vehicular Emissions, Incorporating Network-Wide Fundamental Diagram for Heterogeneous Vehicles. *Transportation Research Record.* 0361198120914304.
- Saedi R, Khademi N, 2019. Travel Time Cognition: Exploring the Impacts of Travel Information Provision Strategies. *Travel Behaviour and Society.* <https://doi.org/10.1016/j.tbs.2018.09.007>
- Saedi R, Khademi N. Exploring the Impact of Travel Information Provision Strategies on Travel Time Cognition. Transportation Research Board 98th Annual Meeting, Washington, D.C., January 13-17, 2019.
- Saedi R, Verma R, Zockaie A, Ghamami M, Gates TJ. A Framework for Incorporating the Network-Wide Fundamental Diagram into Large-Scale Emission Estimation. International Conference on Transport & Health, Mackinac Island, MI, June 24-27, 2018.
- Saeedmanesh, M., Geroliminis, N., 2017. Dynamic clustering and propagation of congestion in heterogeneously congested urban traffic networks. *Transp. Res. part B Methodol.* 105, 193–211.

- Saeedmanesh, M., Geroliminis, N., 2016. Clustering of heterogeneous networks with directional flows based on “Snake” similarities. *Transp. Res. Part B Methodol.* 91, 250–269.
- Saeedmanesh, M., Kouvelas, A., Geroliminis, N., 2019. A real-time state estimation approach for multi-region MFD traffic systems based on extended Kalman filter, in: *2019 TRB Annual Meeting: Compendium of Papers*. The National Academies of Sciences, Engineering, and Medicine, pp. 19–2756.
- Saneinejad, S., Roorda, M.J., Kennedy, C., 2012. Modelling the impact of weather conditions on active transportation travel behaviour. *Transp. Res. part D Transp. Environ.* 17, 129–137.
- Shabihkhani, R., Gonzales, E.J., 2013. Analytical model for vehicle emissions at signalized intersection: Integrating traffic and microscopic emissions models.
- Sims, A.G., 1979. The Sydney coordinated adaptive traffic system, in: *Engineering Foundation Conference on Research Directions in Computer Control of Urban Traffic Systems, 1979*, Pacific Grove, California, USA.
- Smola, A.J., Schölkopf, B., 2004. A tutorial on support vector regression. *Stat. Comput.* 14, 199–222.
- Stapleton SY, Gates TJ, Avelar R, Geedipally SR, Saedi R, 2019. Safety Performance Functions for Low-Volume Rural Stop-Controlled Intersections. *Transportation Research Record*. <https://doi.org/10.1177/0361198119840348>
- Sun, Z., Hao, P., Ban, X. (Jeff), Yang, D., 2015. Trajectory-based vehicle energy/emissions estimation for signalized arterials using mobile sensing data. *Transp. Res. Part D Transp. Environ.* 34, 27–40. <https://doi.org/10.1016/j.trd.2014.10.005>
- Suykens, J.A.K., Vandewalle, J., 1999. Least squares support vector machine classifiers. *Neural Process. Lett.* 9, 293–300.
- User’s Guide to MOBILE6.1 and MOBILE6.2: Mobile Source Emission Factor Model, EPA420-R-0 ed, 2002. . U.S. Environmental Protection Agency, Ann Arbor, Michigan.
- Van Laarhoven, P.J.M., Aarts, E.H.L., 1987. Simulated annealing, in: *Simulated Annealing: Theory and Applications*. Springer, pp. 7–15.
- Verma R, Saedi R, Zockaie A, Gates T, 2019. Behavioral Analysis of Drivers Following Winter Maintenance Trucks Enabled with Collision Avoidance System. *Transportation Research Record*. <https://doi.org/10.1177/0361198119850131>
- Williams, J.C., Mahmassani, H.S., Herman, R., 1995. Sampling strategies for two-fluid model

- parameter estimation in urban networks. *Transp. Res. Part A Policy Pract.* 29, 229–244.
- Williams, J.C., Mahmassani, H.S., Herman, R., 1985. ANALYSIS OF TRAFFIC NETWORK FLOW RELATIONS AND TWO-FLUID MODEL PARAMETER SENSITIVITY. *Transp. Res. Rec.* 95–106.
- Williams, J.C., Mahmassani, H.S., Iani, S., Herman, R., 1987. Urban Traffic Network Flow Models. *Transp. Res. Rec.* 1112, 78–88.
- Yagar, S., Dion, F., 1996. Distributed approach to real-time control of complex signalized networks. *Transp. Res. Rec. J. Transp. Res. Board* 1–8.
- Yang, K., Zheng, N., Menendez, M., 2017. Multi-scale perimeter control approach in a connected-vehicle environment. *Transp. Res. procedia* 23, 101–120.
- Yildirimoglu, M., Ramezani, M., Geroliminis, N., 2015a. Equilibrium analysis and route guidance in large-scale networks with MFD dynamics. *Transp. Res. Procedia* 9, 185–204.
- Yildirimoglu, M., Ramezani, M., Geroliminis, N., 2015b. Equilibrium analysis and route guidance in large-scale networks with MFD dynamics. *Transp. Res. Part C Emerg. Technol.* 59, 404–420.
- Zegeye, S.K., De Schutter, B., Hellendoorn, J., Breunese, E.A., Hegyi, A., 2013. Integrated macroscopic traffic flow, emission, and fuel consumption model for control purposes. *Transp. Res. Part C Emerg. Technol.* 31, 158–171. <https://doi.org/10.1016/j.trc.2013.01.002>
- Zhang, L., Garoni, T.M., de Gier, J., 2013. A comparative study of macroscopic fundamental diagrams of arterial road networks governed by adaptive traffic signal systems. *Transp. Res. Part B Methodol.* 49, 1–23.
- Zheng, N., Aboudolas, K., Geroliminis, N., 2013. Investigation of a city-scale three-dimensional macroscopic fundamental diagram for bi-modal urban traffic, in: 16th International IEEE Conference on Intelligent Transportation Systems (ITSC 2013). IEEE, pp. 1029–1034.
- Zheng, N., Waraich, R.A., Axhausen, K.W., Geroliminis, N., 2012. A dynamic cordon pricing scheme combining the Macroscopic Fundamental Diagram and an agent-based traffic model. *Transp. Res. Part A Policy Pract.* 46, 1291–1303.
- Zhong, R.X., Chen, C., Huang, Y.P., Sumalee, A., Lam, W.H.K., Xu, D.B., 2017. Robust perimeter control for two urban regions with macroscopic fundamental diagrams: a control-lyapunov function approach. *Transp. Res. Part B Methodol.*
- Zhou, X., Tanvir, S., Lei, H., Taylor, J., Liu, B., Roupail, N.M., Frey, H.C., 2015. Integrating a

simplified emission estimation model and mesoscopic dynamic traffic simulator to efficiently evaluate emission impacts of traffic management strategies. *Transp. Res. Part D Transp. Environ.* 37, 123–136. <https://doi.org/10.1016/j.trd.2015.04.013>

Zhou, Z., Lin, S., Xi, Y., Li, D., Zhang, J., 2016. A hierarchical urban network control with integration of demand balance and traffic signal coordination. *IFAC-PapersOnLine* 49, 31–36.

Zockaie, A., R. Saedi, T. Gates, P. Savolainen, B. Schneider, M. Ghamami, R. Verma, F. Fakhroosavi, M. Kavianipour, and M. S. Shojaei. Evaluation of a Collision Avoidance and Mitigation System (CAMS) on Winter Maintenance Trucks. 2018. Final Report. U.S. Department of Transportation, Michigan. [https://www.michigan.gov/documents/mdot/SPR-1677-Evaluation\\_of\\_CAMS\\_on\\_Winter\\_Maintenance\\_Trucks\\_635271\\_7.pdf](https://www.michigan.gov/documents/mdot/SPR-1677-Evaluation_of_CAMS_on_Winter_Maintenance_Trucks_635271_7.pdf)

Zockaie, A., Aashtiani, H.Z., Ghamami, M., Nie, Y., 2016. Solving detour-based fuel stations location problems. *Comput. Civ. Infrastruct. Eng.* 31, 132–144.

Zockaie, A., Chen, Y., Mahmassani, H.S., 2014a. Adaptive drivers and time-dependent origin-destination demand estimation: methodology and application to large-scale network.

Zockaie, A., Mahmassani, H., Saberi, M., Verbas, Ö., 2014b. Dynamics of urban network traffic flow during a large-scale evacuation. *Transp. Res. Rec. J. Transp. Res. Board* 21–33.

Zockaie A, Saberi M, Saedi R, 2018. A Resource Allocation Problem to Estimate Network Fundamental Diagram in Heterogeneous Networks: Optimal Locating of Fixed Measurement Points and Sampling of Probe Trajectories. *Transportation Research Part C: Emerging Technologies*. <https://doi.org/10.1016/j.trc.2017.11.017>

Zockaie A, Saberi M, Saedi R. Optimal Locating of Fixed Measurement Points and Sampling of Probe Trajectories to Estimate Network Fundamental Diagram in Heterogeneous Networks. *Transportation Research Board 97th Annual Meeting, Washington, D.C., January 7-11, 2018*.